

On Various Questions in Nonequilibrium  
Statistical Mechanics Relating to Swarms and  
Fluid Flow

Russell Kim Standish

October 30, 1997

Chapters 1 and 5 review the field to set the context of the work. Except where stated, all other chapters report my own original work.

Russell Standish

# Acknowledgements

I wish to thank Denis Evans for the supervision of the work in this thesis, Brian Robson for his continuing support, Robert Robson for his encouragement and advice, Leo Brewin for his comprehensive knowledge of the MSP operating system, and Bill Alford for his advice on T<sub>E</sub>X related matters, without which this thesis would have been much more difficult to write. I would also like to thank all the staff and students of the Department of Theoretical Physics, who have over the years provided much stimulating conversation and ideas. Last, but not least, I would like to thank my dearest friend Kim Crichton for her unwavering support throughout this thesis.

Much of the computation described here was performed on the Fujitsu VP100 of the Australian National University Supercomputer Facility.

I gratefully acknowledge the financial assistance of a Commonwealth Postgraduate Research Award.

This thesis has been typeset by the author using L<sup>A</sup>T<sub>E</sub>X, a macro package written by Leslie Lamport for Donald Knuth's T<sub>E</sub>X typesetting system. The source was typed on a MacIntosh, using a macro package written by the author for Matthias Aebi's MEdit text editor. Andrew Trevorrow's OzT<sub>E</sub>X, a public domain MacIntosh version of L<sup>A</sup>T<sub>E</sub>X, was used to preview the document whereas the final version was produced using a Vax. The figures were produced using a picture macro package written by Brendan McKay, the Vax installation of which was done by Bill Alford. Figures 4.3 to 4.6 were produced by Arnstein Pritz's FPLoT program, and the plates produced using Uniras.

# Publications

This thesis is based in part on the following publications:

**Standish RK (1987)**, “Nonhydrodynamic Contributions to End Effects in Time of Flight Swarm experiments”, *Aust J Phys*, **40**, 519-525

**Standish RK and Kumar K (1987)**, “End Effects in Time of Flight Experiments”, proc. 5th Intl Swarm Seminar, Birmingham, p104-107

**Evans D and Standish RK (1990)**, “Non-equilibrium Statistical Mechanics and Molecular Dynamics Calculations” in *Computer Modelling of Fluids, Polymers and Solids* CRA Catlow *et al.* (eds.) p125-154

**Standish RK (1989)** “Motion of Charged Particles in a Homogeneous Reacting Medium with a One-dimensional Geometry”, *Aust J Phys*, **42**, 223-232

**Standish RK and Evans DJ (1990)**, “On the Nonlinear Burnett Coefficients”, to be published in *Phys. Rev. A*.

## Abstract

The cutting edge of nonequilibrium statistical mechanics has for some time now been concerned with the question of relaxing the approximations used to generate the hydrodynamic equations. In particular, we are interested in form and effects of the Burnett, or higher order transport coefficients, and also in short timescale effects. The motivation for studying these phenomena in swarms comes from the desire for accurate transport data, which is approaching the level of accuracy where these effects are significant. The motivation for studying these effects in high density fluids comes from understanding the behaviour of non-Newtonian fluids.

In this thesis, the theory of nonhydrodynamic phenomena is developed within the framework of the linear Boltzmann equation, and applied to several experimental configurations used in swarm physics. The latter part of the thesis develops fluctuation expressions for the nonlinear Burnett coefficients similar to the Green-Kubo expressions used for linear transport coefficients. A numerical simulation of a simple fluid is used to test these expressions.

# Contents

<b>1</b>	<b>Introduction</b>	<b>1</b>
1.1	Continuity Relations . . . . .	2
1.2	Constitutive Relations . . . . .	3
1.3	Burnett Coefficients . . . . .	5
1.4	Boltzmann Equation . . . . .	6
1.5	Chapman-Enskog Solution . . . . .	8
1.6	Nonhydrodynamic Behaviour . . . . .	9
<b>2</b>	<b>The Linear Boltzmann Equation</b>	<b>11</b>
2.1	Time Dependent Transport Coefficients . . . . .	13
2.2	Projection Operator . . . . .	14
2.3	Formal Solution of the Boltzmann Equation . . . . .	15
2.4	The nature of the Spectrum and the Runaway Phenomenon . . . . .	16
2.5	Klein-Kramers Model . . . . .	17
<b>3</b>	<b>End Effects in Time of Flight Experiments</b>	<b>22</b>
3.1	Time of Flight Experiments . . . . .	22
3.2	Lithium ion - Helium Experiment . . . . .	23
3.3	Nonhydrodynamic Contributions to End-Effects in Time-of-Flight Swarm Experiments . . . . .	25
3.4	Model Calculation . . . . .	26
3.5	Peak Arrival Time . . . . .	27
3.6	Pressure Dependencies of Non-hydrodynamic and Higher Order Diffusion Effects . . . . .	31
3.7	Separation of the Different End Effects. . . . .	32
3.8	Boundaries and Field Inhomogeneities . . . . .	33

<b>4</b>	<b>Non-hydrodynamic effects in Parallel Plane Steady State Townsend Experiments</b>	<b>35</b>
4.1	Steady State Townsend Experiments . . . . .	35
4.2	Conventional Theories . . . . .	36
4.3	Numerical Studies of the Klein-Kramers model . . . . .	38
4.4	Asymptotic behaviour for large times and distances . . . . .	48
4.5	Discussion . . . . .	52
<b>5</b>	<b>Nonequilibrium Molecular Dynamics Simulation</b>	<b>54</b>
5.1	Thermostatted Equations of Motion . . . . .	54
5.2	Formal Solution of Liouville's Equation . . . . .	56
5.3	Nonlinear Response Theory . . . . .	58
5.4	Models of Nonequilibrium Steady States . . . . .	61
5.4.1	Planar Couette Flow . . . . .	61
5.4.2	Colour Current . . . . .	63
<b>6</b>	<b>Nonlinear Burnett Coefficients</b>	<b>65</b>
6.1	Equations of Motion . . . . .	66
6.2	Relation between canonical and $\Delta J$ ensemble . . . . .	69
6.3	Equilibrium Simulation . . . . .	70
6.4	Numerical Evaluation of Burnett Coefficients . . . . .	71
<b>7</b>	<b>Conclusion</b>	<b>78</b>
<b>A</b>	<b>Perturbation of the eigenfunctions for small <math>k</math></b>	<b>80</b>
A.1	Recursion relations in Component Form . . . . .	81
A.2	Consistency with Biorthonormality . . . . .	84
A.3	Invariance of $\Psi_j(\mathbf{c}, i\mathbf{k})\Phi_j(\mathbf{c}', i\mathbf{k})$ . . . . .	85
<b>B</b>	<b>Calculation of the end-effects due to peak collector current measurements</b>	<b>87</b>
<b>C</b>	<b>Numerical Studies of the Klein-Kramers Model</b>	<b>90</b>
<b>D</b>	<b>Isotropic Tensors</b>	<b>97</b>
<b>E</b>	<b>System Size Dependence of a Product of Intensive Phase Variables</b>	<b>105</b>

<b>F</b>	<b>Nonlinear Burnett Coefficients Calculation</b>	<b>107</b>
F.1	Design Considerations . . . . .	107
F.2	Parameters . . . . .	108
F.3	Equations of Motion . . . . .	109
F.4	The Integrator . . . . .	111
F.5	Periodic Boundary Conditions . . . . .	113
F.6	Forces . . . . .	114
F.7	Miscellany . . . . .	116
F.8	Analysis of Data . . . . .	119
F.9	Putting it all Together . . . . .	121
	<b>Bibliography</b>	<b>125</b>
	<b>Mathematical Notation</b>	<b>132</b>
	Conventions . . . . .	132
	Vectors and Tensors . . . . .	132
	Differentiation and Integration . . . . .	132
	Other Conventions . . . . .	133
	List of Symbols . . . . .	134
	<b>Index</b>	<b>137</b>

# List of Figures

2.1	Evolution of the one dimensional Klein-Kramers equation showing non-hydrodynamic effects at large times . . . . .	21
3.1	Bradbury-Nielsen shutter . . . . .	23
3.2	Time of flight experiment with shutters. A typical arrival time spectrum is shown . . . . .	24
4.1	Parallel Plane Steady State Townsend Experiment . . . . .	36
4.2	Townsend-Huxley Diffusion Experiment. Ratio of currents received by sections A and B are measured. . . . .	36
4.3	Density for $\nu = 0$ . . . . .	39
4.4	Density for $\nu = -0.01$ . . . . .	40
4.5	Density for $\nu = 0.01$ . . . . .	41
4.6	ln Density for $\nu = 1$ . . . . .	42
4.7	Logarithmic plot of the steady state density for the case $\nu = -0.01$ . . . . .	43
4.8	Logarithmic plot of the steady state density for the case $\nu = 0.01$ . . . . .	44
4.9	Sketch of the density with the important features labelled . . . . .	49
4.10	Singularity structure of $s_n(c, ik)/\omega_n(ik)$ for the Klein-Kramers model . . . . .	51
4.11	Contour used for the large $z$ asymptotic argument. . . . .	51
5.1	Lees-Edwards Periodic Boundary Conditions for Planar Couette Flow . . . . .	62
6.1	Linear response for colour conductivity . . . . .	73
6.2	Third order nonlinear response for colour conductivity . . . . .	74
6.3	Linear response for planar Couette flow . . . . .	75

6.4	Third order nonlinear response for planar couette flow . . . . .	76
F.1	Internal format of <b>GAMMA</b> . . . . .	108

# Chapter 1

## Introduction

This is a thesis in two parts, both of which fit firmly in the framework of non-equilibrium statistical mechanics. When referring to atoms or molecules at sufficiently low density that collisions in the system are dominated by few body interactions, so that the mesoscopic picture applies (see page 7) this is sometimes called kinetic theory.

The first part of the thesis relates to the kinetic theory of swarms. A swarm is a collection of charged particles moving through a neutral background gas. Typically, these may be electrons inside a discharge tube, or within a gaseous state laser. The prime application of the work here are swarm experiments, whereby atomic collision cross sections are obtained by using kinetic theory to calculate various macroscopic properties from a “trial” cross-section, which can in turn be compared with experimental measurement. This is clearly an ambiguous process, but experiments can be done with sufficient precision to extract reasonable cross-sections. The main advantage of this method over its main competitor, namely beam experiments<sup>1</sup>, is that the low energy regime can be studied, where beams are difficult to focus. Recent developments in the beam technique have blurred the distinction between these two methods, particularly in electrons, however, swarm methods still have a rôle to play with measurements involving more complex ions and molecules.

The second part of this thesis relates to fluid flow. Here the interest is in

---

<sup>1</sup>In these experiments, two beams of particles are crossed and the collision cross section determined by measuring the angular and energy distributions of the products. These measure the cross-sections directly.

understanding how fluids respond to a stress which caused the fluid to depart from equilibrium. For instance, we may wish to understand the behaviour of oil in a bearing, where oil is constantly shearing due to the influence of two surfaces moving past each other. Here, the idea would be to take data on the way that the molecules interact<sup>2</sup>, and predict how the fluid would behave under these situations.

Both the theories of swarms and of fluid flow have a common origin within the atomic theory of matter. However, at an early stage, the theories diverge. Swarms are generally so dilute that the interactions between the charged particles are negligible in comparison with interactions between charged and neutral particles. The resulting theory is therefore linear in regard to the density of the charged particles. By contrast, in fluid flow the interactions involve many particles, and consequently the theory is highly non-linear in the density.

## 1.1 Continuity Relations

The starting point for both theories are the microscopic conservation laws that are obeyed by the particles under observation. These are typically conservation of mass, charge, momentum and energy. For each microscopic conservation law, there is a corresponding macroscopic continuity equation, which basically states that within a volume of a fluid, the influx of each conserved quantity must be balanced by a corresponding outflow of that quantity. By taking these fluid volumes sufficiently small that the macroscopic variables are constant across the volume, yet still large enough for the atomic nature not to manifest itself (coarse graining), these continuity equations may be cast in differential form.

For example, the mass continuity equation is

$$\frac{\partial \rho}{\partial t} = -\nabla \cdot (\rho \mathbf{u}) + S(\mathbf{r}, t), \quad (1.1)$$

where  $\rho$  is the mass density,  $\mathbf{u}$  the streaming velocity of the fluid,  $S$  the source term, and  $t$  is time [de Groot and Mazur (1962)]. Similarly, the momentum

---

<sup>2</sup>This data could come from atomic and molecular experiments, such as those mentioned above, or from molecular modelling which takes configurational information about how the atoms are arranged within the molecule, and derives the forces acting between the molecules.

continuity equation may be written:

$$\rho \frac{d\mathbf{u}}{dt} = -\nabla \cdot \mathbf{P} + \mathbf{a}\rho, \quad (1.2)$$

where  $\mathbf{P}$  is the pressure tensor<sup>3</sup>,  $\mathbf{a}$  is the acceleration of the fluid particles due to an external field and  $d/dt$  is the total derivative given by  $\partial/\partial t + \mathbf{u} \cdot \nabla$ .

## 1.2 Constitutive Relations

The non-equilibrium part of the pressure tensor  $\mathbf{\Pi}$  is called the viscous pressure tensor

$$\mathbf{\Pi} = \mathbf{P} - p_{\text{eq}}\mathbf{1}. \quad (1.3)$$

Two centuries ago Newton realised that  $\mathbf{\Pi}$ , which is zero at equilibrium, can be driven by the strain rate tensor  $\nabla\mathbf{u}$ . For atomic fluids close to equilibrium, the most general linear relation between the viscous pressure tensor and the strain rate tensor is

$$\mathbf{\Pi} = -\mathbf{L}^{(4)} : \nabla\mathbf{u}. \quad (1.4)$$

The fourth rank transport tensor  $\mathbf{L}^{(4)}$  is a function of the thermodynamic state of the system  $(\rho, T)$ . It is independent of the strain rate  $\nabla\mathbf{u}$ . In fluids with no external field applied,  $\mathbf{L}^{(4)}$  must be isotropic, i.e. rotationally invariant.

There are three independent isotropic rank four tensors, [see Temple (1960)] defined by the possible multilinear invariants of four vectors  $\mathbf{u}$ ,  $\mathbf{v}$ ,  $\mathbf{w}$  and  $\mathbf{x}$ :

$$\begin{aligned} \mathbf{l}_1^{(4)} :: \mathbf{u}\mathbf{v}\mathbf{w}\mathbf{x} &= (\mathbf{u} \cdot \mathbf{v})(\mathbf{w} \cdot \mathbf{x}), \\ \mathbf{l}_2^{(4)} :: \mathbf{u}\mathbf{v}\mathbf{w}\mathbf{x} &= (\mathbf{u} \cdot \mathbf{w})(\mathbf{v} \cdot \mathbf{x}), \\ \mathbf{l}_3^{(4)} :: \mathbf{u}\mathbf{v}\mathbf{w}\mathbf{x} &= (\mathbf{u} \cdot \mathbf{x})(\mathbf{v} \cdot \mathbf{w}). \end{aligned}$$

In atomic fluids, the force acting between atoms is parallel to the displacement between the atoms, *i.e.* a central force. This implies that  $\mathbf{P}$  is

---

<sup>3</sup> $\mathbf{P}$  may be defined by considering the infinitesimal force  $d\mathbf{F}$  exerted by the fluid across a surface element  $d\mathbf{S}$ . This force need not be aligned with the normal to the area element, so the most general relationship is given as  $d\mathbf{F} = -\mathbf{P} \cdot d\mathbf{S}$ , where  $\mathbf{P}$  is a rank two tensor.

symmetric<sup>4</sup>, and so (1.4) becomes

$$\begin{aligned}\mathbf{\Pi} &= \left[ -\eta \left( \mathbf{I}_2^{(4)} + \mathbf{I}_3^{(4)} - \frac{2}{3} \mathbf{I}_1^{(4)} \right) - \eta_v \mathbf{I}_1^{(4)} \right] : \nabla \mathbf{u} \\ &= 2\eta \text{Traceless, symmetrized part of } \nabla \mathbf{u} - \eta_v (\nabla \cdot \mathbf{u}) \mathbf{1},\end{aligned}$$

where  $\eta$  is the shear viscosity and  $\eta_v$  is the bulk viscosity. In molecular fluids, the intermolecular forces do not necessarily act parallel to the displacement between the molecules and the pressure is not necessarily symmetric, so a further term, vortex viscosity [de Groot and Mazur (1962)] must be introduced.

The continuity relation (1.2) gives an exact relationship between the velocity field and the pressure tensor. The Newtonian constitutive relation gives a relation between the pressure tensor and the velocity field which is a good approximation for fluids close to equilibrium. By combining the continuity and Newtonian constitutive relations, we obtain the Navier-Stokes equation of hydrodynamics:

$$\rho \frac{d\mathbf{u}}{dt} = -\nabla p + \left( \eta_v + \frac{\eta}{3} \right) \nabla (\nabla \cdot \mathbf{u}) + \eta \nabla^2 \mathbf{u}. \quad (1.5)$$

In swarm physics, the only conserved quantity is mass (or equivalently charge), and even then only in the absence of reactions. The mass continuity equation is (1.1) with an additional term of  $\nu\rho$  on the right hand side representing the net production of swarm particles due to reactions with the background gas. A momentum continuity equation would need to take into account the dynamics of the background gas, and so is not a useful relation for the theory. In this case, the constitutive relation must contain a constant term representing the average streaming velocity due to the electric field, as well as the term proportional to the gradient of  $\rho$ :

$$\rho \mathbf{u} = \rho \boldsymbol{\omega}^{(1)} - \boldsymbol{\omega}^{(2)} \cdot \nabla \rho. \quad (1.6)$$

---

<sup>4</sup>In microscopic terms [Evans and Standish (1990)], the pressure tensor can be written as:

$$\mathbf{P} = \frac{1}{2V} \left( \sum_{i,j=1}^N \mathbf{F}_{ij} \mathbf{q}_{ji} + \sum_{j=1}^N \frac{\mathbf{p}_j^2}{m} \right),$$

where  $\mathbf{F}_{ij}$  is the force acting between particles  $i$  and  $j$ , and  $\mathbf{q}_{ij}$  is their relative displacement.

Upon substituting (1.6) into (1.1), we obtain the diffusion equation:

$$\frac{\partial \rho}{\partial t} = \omega^{(0)} \rho - \boldsymbol{\omega}^{(1)} \cdot \nabla \rho + \boldsymbol{\omega}^{(2)} : \nabla^2 \rho + S(\mathbf{r}, t). \quad (1.7)$$

The transport coefficients  $\omega^{(0)}$ ,  $\boldsymbol{\omega}^{(1)}$  and  $\boldsymbol{\omega}^{(2)}$  can be identified with the reaction rate  $\nu$ , the system drift velocity and the coefficient of diffusion respectively. In free space, the transport coefficients of the swarm must satisfy cylindrical symmetry with the major axis in the direction of the electric field. The only vectors with this property must be proportional to the electric field  $\mathbf{E}$ , and that any second rank tensor must be a linear combination of the unit tensor, and of the dyad  $\hat{\mathbf{E}}\hat{\mathbf{E}}$ . This means that the transport coefficients can be represented by three parameters: the drift velocity  $v_{\text{dr}} = |\boldsymbol{\omega}^{(1)}|$  and the two components of the diffusion coefficient, namely that which is aligned with the field,  $D_L$ , and that which is transverse to the field  $D_T$ . We have  $\boldsymbol{\omega}^{(2)} = D_T \mathbf{1} + (D_L - D_T) \hat{\mathbf{E}}\hat{\mathbf{E}}$ . An alternative parameter to the drift velocity is the mobility:  $\mu = v_{\text{dr}}/E$ .

### 1.3 Burnett Coefficients

When we wish to generalize the linear constitutive relations, swarm theories and dense fluid theories depart rapidly from each other. The most obvious way to generalize the Newtonian constitutive relation is to write the viscous pressure tensor as an arbitrary analytic function of the strain rate:

$$\boldsymbol{\Pi} = -\mathbf{L}^{(4)} : (\nabla \mathbf{u}) + \mathbf{L}^{(6)} :: (\nabla \mathbf{u})^2 + \dots \quad (1.8)$$

Here  $\mathbf{L}^{(6)}$  is a rank six tensor that is clearly symmetric with respect to interchanges of the 3<sup>rd</sup> and 5<sup>th</sup>, and of the 4<sup>th</sup> and 6<sup>th</sup> indices. An arbitrary isotropic 6<sup>th</sup> rank tensor has 15 independent components [Eu (1979)], which is reduced to 7 components when the above symmetries are taken into account (see Appendix D). If we further suppose that the fluid is monatomic, then  $\boldsymbol{\Pi}$  must be symmetric, and the number of independent components reduces to 5, of which two are diagonal in the first two indices, and three are traceless. So at second order in the strain rate, there are five transport coefficients, two of which refer to bulk properties, and the other three which describe shearing properties. Similarly, at the next order in strain rate, there will be 22 transport coefficients.

Burnett (1935) developed a form of hydrodynamics that was more accurate than Navier-Stokes hydrodynamics by applying the Chapman-Enskog procedure to the Boltzmann equation. [See Chapter 7 and 15 of Chapman and Cowling (1970) for a discussion]. This introduced 19 transport coefficients of which the 8 bulk coefficients are zero for a dilute gas. This left 6 coefficients for the correction to the viscous pressure tensor, and 5 for the thermal flux term. The constitutive relation (1.8) refers to a situation where there are no thermal or pressure gradients, and so the three shear components of  $\mathbf{L}^{(6)}$  can be identified with the remaining three Burnett coefficients in equation (15.3,8) of Chapman and Cowling (1970). More will be said of the non-linear Burnett coefficients in chapter 6, where tractable expressions are developed relating the coefficients to equilibrium correlation functions.

The generalization of the constitutive relation (1.6) for swarms is different in that linearity in the swarm density must be preserved:

$$\rho \mathbf{u} = \sum_{l=1}^{\infty} \boldsymbol{\omega}^{(l)} \odot (-\nabla)^{l-1} \rho.$$

Here the generalized transport coefficients  $\boldsymbol{\omega}^{(l)}$  are rank  $l$  tensors, and  $\odot$  indicates the  $(l - 1)$ -fold scalar product.

A fully consistent derivation of this relation based on a Chapman-Enskog-like solution of the linear Boltzmann equation can be found in Kumar *et al.* (1980). It is thought that the higher order transport coefficients  $\boldsymbol{\omega}^{(l)}$ , with  $l \geq 3$ , play a role only where the density gradients are not small, such as near the boundary of the apparatus containing the swarm. However, at large density gradients, this whole approach is doubtful, as non physical behaviour results [see (1974)]. Analogous problems occur with Burnett and Super-Burnett level hydrodynamics in the theory of neutral gases [see (1983)]. More will be discussed on the subject of higher-order transport coefficients in chapter 3, where certain experimental effects can be explained in terms of these coefficients.

## 1.4 Boltzmann Equation

So far, we have discussed the behaviour of fluids in terms of density and flow fields that are functions of position  $\mathbf{r}$  and time  $t$ . This is a macroscopic, or hydrodynamic, picture of the fluid, where microscopic details such as

the atomic nature of matter, and the fluctuations of molecular velocities are washed out of the picture. At the other extreme is the microscopic picture, in which one follows the trajectories of each individual molecule. This is described by means of the Liouville equation, which in the case of an isolated system, generates Newton's laws of motion for each molecule. More will be said on this in section 5.7. The third picture, called the mesoscopic picture, [Serra *et al.* (1986)] treats the velocity fluctuations by a phase-space distribution function  $f(\mathbf{r}, \mathbf{c}, t)$  that depends on position  $\mathbf{r}$  and velocity  $\mathbf{c}$  at time  $t$ , where  $f(\mathbf{r}, \mathbf{c}, t)d\mathbf{r}d\mathbf{c}$  is the number of particles contained in the phase space volume element  $d\mathbf{r}d\mathbf{c}$ . The rate of change of the distribution function is made up of a streaming term due to particles entering and leaving the volume  $d\mathbf{r}$ , another term due to collisions between particles, and in the presence of an external field, an acceleration term describing the particle flux in the volume  $d\mathbf{c}$ . Symbolically, this reads

$$\partial_t f = \underbrace{-\mathbf{c} \cdot \partial_{\mathbf{r}} f}_{\text{streaming term}} - \underbrace{\mathbf{a} \cdot \partial_{\mathbf{c}} f}_{\substack{\text{acceleration term, } \mathbf{a} \text{ is} \\ \text{the acceleration due to} \\ \text{field}}} - \underbrace{\mathcal{J}(f)}_{\text{collision term}}.$$

When Boltzmann first derived this equation, he considered a dilute gas in which only two gas molecules at a time are involved in the collisions. This implies that  $\mathcal{J}$  is a quadratic operator, and this equation is known as the Boltzmann equation. For a more detailed discussion on the form of  $\mathcal{J}$ , and a derivation, see Dorfman and van Beijeren (1977). Attempts have been made to generalize the Boltzmann equation to handle denser gases by including collisions involving three or more bodies. The simplest and clearest formulation was given by Bogolubov in 1945 [see Cohen (1962)]. However, in the middle of the 1960s, it was discovered that Bogolubov's generalization of the Boltzmann equation could not be correct, since the fourth and all higher order collision terms diverged. In two dimensions, even the third order term diverges. It is believed that the higher order collision operators may be resummed to obtain convergent collision integrals. See Cohen (1983) and references therein for a discussion.

Since the mesoscopic approach fails for fluids of high density, a different approach is required for computing the transport coefficients from details of the microscopic interactions. A method was pioneered by Green and Kubo [see Zwanzig (1965)], which relates the transport coefficients to certain time correlation functions that can be computed by simulating the motion of the

molecules due to their interactions. This expression is exact for arbitrary density, but is limited to the linear coefficients such as the  $\mathbf{L}^{(4)}$  in (1.8). Recently, Evans and Lynden-Bell (1988) have produced expressions for the non-linear Burnett coefficients. The work in this thesis implements the calculation for the simple model of electrical conductivity outlined in that paper.

In swarm physics, the swarm is dilute in comparison with the background neutral gas. The collisions between the charged particles and the neutral gas dominate over the collisions of the charged particles amongst themselves. This leads to a modelling of swarm physics by the linear Boltzmann equation, where  $\mathcal{J}$  is taken to be a linear operator acting on  $f$ . This allows us to make use of the vast array of techniques available for linear operators.

## 1.5 Chapman-Enskog Solution

The Chapman-Enskog procedure alluded to earlier provides a way of passing from the mesoscopic picture of the Boltzmann equation to the hydrodynamic picture. In the theory of neutral gases, there are two timescales, the first being the mean free time between collisions, and the second a macroscopic time which depends on the size of the system under consideration. This macroscopic time might be, for example, the time taken for a gas to equalize its pressure after being let into an empty box. The approach to equilibrium occurs in two stages. The first stage is the approach to a local thermal equilibrium on a timescale of the order of the mean free time. The distribution function approaches that of a local Maxwellian,

$$f(\mathbf{r}, \mathbf{c}, t) \approx n(\mathbf{r}, t) \left( \frac{m}{2\pi k_B T(\mathbf{r}, t)} \right)^{\frac{3}{2}} \exp \left( -\frac{m}{2k_B T(\mathbf{r}, t)} [\mathbf{c} - \mathbf{u}(\mathbf{r}, t)]^2 \right),$$

where  $n$  is the local gas number density,  $T$  the local temperature,  $\mathbf{u}$  the local velocity field,  $k_B$  Boltzmann's constant and  $m$  the molecular mass. The second stage, occurring on a macroscopic timescale, is described by the relaxation of the functions  $n$ ,  $T$ , and  $\mathbf{u}$  to their uniform equilibrium values.

The Chapman-Enskog solution of the Boltzmann equation uses the smallness of the mean free time as a perturbation parameter. On successive iterations of this perturbation, one obtains the Euler, Navier-Stokes, Burnett and Super-Burnett hydrodynamics respectively. See Chapman and Cowling (1970).

In swarm physics, the linear Boltzmann equation has an analogous solution. There are two timescales, a mean free time, and a macroscopic time which is usually the drift time. Since energy is constantly being extracted from the electric field, there is no approach to equilibrium. However, after several collision times, the velocity distribution will relax to a “local steady state”, in which the energy being extracted from the field by the swarm is removed by collisions with the background gas. This state is called the hydrodynamic regime by analogy with the hydrodynamics of neutral gas theory.

Instead of the five fields ( $n$ ,  $T$ , and the three components of  $\mathbf{u}$ ) of the neutral gas theory, the space-time dependence of a swarm in the hydrodynamic regime is carried by the density alone:

$$f(\mathbf{c}, \mathbf{r}, t) = \sum_{j=0}^{\infty} \mathbf{f}^{(j)}(\mathbf{c}) \odot (-\boldsymbol{\partial}_{\mathbf{r}})^j n(\mathbf{r}, t). \quad (1.9)$$

Here the  $\mathbf{f}^{(j)}(\mathbf{c})$  are rank  $j$  tensor functions of  $\mathbf{c}$ .

It should be noted that equation (1.9) is the complete description of the hydrodynamic regime. By contrast, the hydrodynamic regime of the neutral gas problem is described by a coupled set of equations in the five fields ( $n$ ,  $T$  and  $\mathbf{u}$ ). The Chapman-Enskog method constructs these equations at successive levels of approximation (Euler, Navier-Stokes etc.). Similarly, a coupled set of equations can be derived for  $\mathbf{f}^{(j)}$  with the operator  $\mathcal{M} = \mathbf{a} \cdot \boldsymbol{\partial}_{\mathbf{c}} + \mathcal{J}$  playing a rôle similar to the rôle that the linearized collision operator plays in neutral gas theory.

## 1.6 Nonhydrodynamic Behaviour

If the timescale of one’s interest is of comparable size to the mean free time, or if the length scale is of the order of the mean free path, then the assumptions involved in the Chapman-Enskog procedure break down. Examples of where this is the case include the behaviour of the fluid near the boundary, or the short-time evolution of the fluid in an arbitrary initial configuration. Even if the timescale of interest is large in comparison with the mean free time, then the hydrodynamic trajectory that the system follows is not identical to the hydrodynamic trajectory that passes through the system’s initial point. As we shall see in the case of swarms in chapter 3, this difference has a long range persistence, and can be quite significant on hydrodynamic timescales.

A further example where the assumptions of the Chapman-Enskog method break down is where the mean free time of the system becomes infinite. This might occur if the collision frequency diminishes sufficiently rapidly with increasing energy, leading to a runaway effect of the fluid becoming increasingly hotter in time [see Waldman and Mason (1981) for a discussion]. This effect has been observed experimentally in swarms [Howorka *et al.* (1979), Morruzzi and Kondo (1980)], and has been reviewed by Kumar (1984).

The operator  $\mathcal{M}$  introduced earlier controls the decay of the velocity distribution to its hydrodynamic distribution  $f_0(\mathbf{c})$ . In this thesis,  $\mathcal{M}$  is assumed to have a discrete spectrum, so we can identify the ground eigenstate of  $\mathcal{M}$  with the hydrodynamic distribution  $f_0(\mathbf{c})$ . The presence of field inhomogeneities and boundary processes in which particles are being absorbed, (and perhaps re-emitted with different energies,) may be represented by an operator  $\mathcal{B}$ , which is localized in position, in the Boltzmann equation. This operator is unlikely to commute with  $\mathcal{M}$ , so it will have the effect of mixing the eigenstates in this region, producing a non-hydrodynamic velocity distribution.

## Chapter 2

# The Linear Boltzmann Equation

The theory of swarm physics starts with the linear Boltzmann equation

$$[\partial_t + \mathbf{c} \cdot \boldsymbol{\partial}_{\mathbf{r}} + \mathbf{a} \cdot \boldsymbol{\partial}_{\mathbf{c}} + \mathcal{J}] f(\mathbf{c}, \mathbf{r}, t) = S(\mathbf{c}, \mathbf{r}, t), \quad (2.1)$$

where the various terms have been introduced in section 1.4. The state of the art of swarm theory, as far as analysis of experiments is concerned is expounded in Huxley and Crompton (1974). This is based on the diffusion equation

$$[\partial_t - \boldsymbol{\omega}^{(2)} : \boldsymbol{\partial}_{\mathbf{r}}^2 + \boldsymbol{\omega}^{(1)} \cdot \boldsymbol{\partial}_{\mathbf{r}} - \omega^{(0)}] n(\mathbf{r}, t) = S(\mathbf{r}, t), \quad (2.2)$$

where  $\omega^{(0)}$  is the total reaction rate,  $\boldsymbol{\omega}^{(1)}$  the drift velocity, and  $\boldsymbol{\omega}^{(2)}$  the diffusion tensor. This equation is exactly solvable, whose solution for an initial delta function pulse  $S(\mathbf{r}, t) = \delta(\mathbf{r})\delta(t)$  is a displaced Gaussian

$$n(\mathbf{r}, t) = (4\pi t)^{-\frac{3}{2}} [\det(\boldsymbol{\omega}^{(2)})]^{-\frac{1}{2}} \exp[-(\mathbf{r} - \boldsymbol{\omega}^{(1)}t)^2 : (4\boldsymbol{\omega}^{(2)}t)^{-1}]. \quad (2.3)$$

The hydrodynamic assumption (1.9) leads to the transport equation

$$\left[ \partial_t - \sum_{k=0}^{\infty} \boldsymbol{\omega}^{(k)} \odot (-\boldsymbol{\partial}_{\mathbf{r}})^k \right] n(\mathbf{r}, t) = S(\mathbf{r}, t), \quad (2.4)$$

which is a generalization of the diffusion equation. This follows from (2.1) if we identify the transport coefficients  $\omega^{(k)}$  with

$$\omega^{(0)} = - \int \mathcal{J} f^{(0)} d\mathbf{c},$$

$$\omega^{(k)} = \int \mathbf{c} \mathbf{f}^{(k-1)}(\mathbf{c}) d\mathbf{c} - \int \mathcal{J} \mathbf{f}^{(k)}(\mathbf{c}) d\mathbf{c}.$$

That hydrodynamic transport should be governed by the infinite multipole transport equation (2.4) and that the diffusion equation was but an approximation truncated at second order, was pointed out by Kumar and Robson (1973). Skullerud (1974) developed the transport equation into a theory that explained anisotropies observed earlier in Monte Carlo experiments [MacIntosh (1974)].

The first steps beyond the hydrodynamic assumption (1.9) were taken by such people as MacIntosh (1974) who studied the effect of initial value conditions by Monte Carlo techniques, and Skullerud (1974; 1977) who used numerical solutions to the Boltzmann equation. A significant improvement in technique came with the introduction of time dependent transport coefficients [Tagashira et al. (1977), Tagashira (1981)]. These workers have suggested that different transport coefficients are applicable to the different type of swarm experiments. This debate has largely been settled by expressing the various transport coefficients in terms of the time of flight parameters [Blevin and Fletcher (1984)].

The next major step in the development of a non-hydrodynamic theory comes with Kumar (1981), who relates the characteristic time of the approach to the hydrodynamic regime to the inverse of a gap in the spectrum of  $\mathcal{M} = \mathbf{a} \cdot \partial_{\mathbf{c}} + \mathcal{J}$  between the lowest eigenvalue, and the rest of the spectrum. Kondo (1987) introduced a projection operator which projected out the hydrodynamic solution. This work is a restatement of adiabatic elimination methods [Marchesoni and Grigolini (1985)] in a swarm context. Kondo's paper is general, and the formal nature of the work does not properly address the conditions under which the hydrodynamic regime might exist, or what the timescales of the approach to the hydrodynamic regime might be. We can answer some of these questions by making the simplifying assumption that the spectrum of  $\mathcal{M}$  is discrete, and that the set of eigenfunctions is complete in the space of all velocity distributions, and that one eigenvalue

has smaller real part than all the others. This work has been published as Standish (1987).

## 2.1 Time Dependent Transport Coefficients

By integrating the Boltzmann equation over  $\mathbf{c}$ , we obtain the continuity equation

$$\partial_t n(\mathbf{r}, t) + \omega^{(0)}(t)n(\mathbf{r}, t) + \nabla \cdot \mathbf{j}(\mathbf{r}, t) = S(\mathbf{r}, t).$$

We can write the Fourier transform of the current  $\mathbf{j}$  as a product  $\tilde{\mathbf{j}}(\mathbf{k}, t) = \mathbf{j}_0(\mathbf{k}, t)\tilde{n}(\mathbf{k}, t)$ . If  $\mathbf{j}_0$  is analytic, we can write

$$\mathbf{j}_0(\mathbf{k}, t) = \sum_{l=0}^{\infty} \omega^{(l+1)}(t) \odot (-i\mathbf{k})^l \quad (2.5)$$

which defines the time dependent transport coefficients  $\omega^{(l)}(t)$ . Upon substituting this back into the continuity equation, we obtain a generalization of the transport equation (2.4) having time dependent transport coefficients:

$$\sum_{l=0}^{\infty} \omega^{(l)}(t) \odot (-\partial_{\mathbf{r}})^l n = \partial_t n. \quad (2.6)$$

Taking the Fourier transform of this equation, and dividing by  $\tilde{n}$ , the Fourier transform of  $n$ , one gets

$$\sum_{l=0}^{\infty} \omega^{(l)}(t) \odot (-i\mathbf{k})^l = \partial_t \ln \tilde{n}(\mathbf{k}, t).$$

The individual transport coefficients can be extracted from this power series by taking the  $l$ th derivative of this at the origin of  $k$ -space. Defining the operation

$$\Omega^{(l)} = \lim_{k \rightarrow 0} \frac{(i\partial_{\mathbf{k}})^l}{l!},$$

the transport coefficients can be expressed as

$$\omega^{(l)}(t) = \Omega^{(l)} \partial_t \ln \tilde{n}(\mathbf{k}, t). \quad (2.7)$$

In Kumar *et al.* (1980), these coefficients are identified with the time derivatives of certain correlation functions. In particular,  $\omega^{(0)}(t)$  is the logarithmic time derivative of the number of charged particles, and  $\omega^{(1)}(t)$  is the velocity of the centroid of the swarm.

## 2.2 Projection Operator

Since we are interested in obtaining  $\tilde{n}(\mathbf{k}, t)$  for small values of  $\mathbf{k}$ , it is reasonable to assume that  $i\mathbf{c} \cdot \mathbf{k} + \mathcal{M}$  also admits a complete set of eigenfunctions, at least for sufficiently small  $\mathbf{k}$ . The adjoint operator  $i\mathbf{c} \cdot \mathbf{k} + \tilde{\mathcal{M}}$  will then admit a complete set of eigenfunctions that are biorthogonal with those of  $i\mathbf{c} \cdot \mathbf{k} + \mathcal{M}$ :

$$(i\mathbf{c} \cdot \mathbf{k} + \mathcal{M})\Psi_j(\mathbf{c}, i\mathbf{k}) = -\omega_j(i\mathbf{k})\Psi_j(\mathbf{c}, i\mathbf{k}) \quad (2.8)$$

$$(i\mathbf{c} \cdot \mathbf{k} + \tilde{\mathcal{M}})\Phi_j(\mathbf{c}, i\mathbf{k}) = -\omega_j(i\mathbf{k})\Phi_j(\mathbf{c}, i\mathbf{k})$$

$$\int \Psi_j(\mathbf{c}, i\mathbf{k})\Phi_l(\mathbf{c}, i\mathbf{k})d\mathbf{c} = \delta_{jl}. \quad (2.9)$$

These eigenfunctions may be used as a basis set for finding the solution function  $\tilde{f}(\mathbf{c}, \mathbf{k}, t)$ , as in equation (2.14).

The index  $j$  takes values from a set  $\sigma$ , which is isomorphic to the natural numbers, as the spectrum is assumed discrete. Let the index 0 denote the eigenvalue of  $-\mathcal{M}$  with largest real value, *i.e.*  $\text{Re}(\omega_0(0)) > \text{Re}(\omega_j(0))$  for every other  $j \in \sigma$ . Then, we define a projection operator  $P_k$ , which projects out the hydrodynamic (long time) part of the Fourier transform of a phase space distribution  $\tilde{f}(\mathbf{c}, \mathbf{k}, t)$  by

$$P_k \tilde{f}(\mathbf{c}, \mathbf{k}, t) = \Psi_0(\mathbf{c}, i\mathbf{k}) \int \Phi_0(\mathbf{c}', i\mathbf{k}) \tilde{f}(\mathbf{c}', i\mathbf{k}, t) d\mathbf{c}'.$$

The  $k$ -space density function can now be split into a hydrodynamic part

$$\tilde{n}_0(\mathbf{k}, t) = \int P_k \tilde{f}(\mathbf{c}, \mathbf{k}, t) d\mathbf{c} \quad (2.10)$$

and a non-hydrodynamic part

$$x(\mathbf{k}, t) = \frac{\tilde{n}(\mathbf{k}, t) - \tilde{n}_0(\mathbf{k}, t)}{\tilde{n}_0(\mathbf{k}, t)}. \quad (2.11)$$

The Taylor series coefficients of  $x(\mathbf{k}, t)$  are denoted by

$$\mathbf{x}^{(l)}(t) = \boldsymbol{\Omega}^{(l)} x(\mathbf{k}, t).$$

These can be computed from the Taylor coefficients  $\boldsymbol{\Psi}_j^{(l)}$ ,  $\boldsymbol{\Phi}_j^{(l)}(\mathbf{c})$ , which can be computed from the eigenfunctions of  $\mathcal{M}$  by means of a recursion method

(see Appendix A). Substituting  $\tilde{n} = \tilde{n}_0(1+x)$  into (2.7), the time dependent transport coefficients become

$$\begin{aligned}\omega^{(l)}(t) &= \Omega^{(l)}\partial_t\{\ln\tilde{n}_0 + \ln(1+x)\} \\ &= \Omega^{(l)}\{\partial_t\ln\tilde{n}_0 + \partial_t x(1-x+x^2-\dots)\}.\end{aligned}\quad (2.12)$$

## 2.3 Formal Solution of the Boltzmann Equation

The Fourier transform of (2.1) with an initial distribution  $S(\mathbf{c}, \mathbf{r}, t) = \delta(t)f_i(\mathbf{c}, \mathbf{r})$  is

$$(\partial_t + i\mathbf{c} \cdot \mathbf{k} + \mathcal{M})\tilde{f}(\mathbf{c}, \mathbf{k}, t) = \delta(t)\tilde{f}_i(\mathbf{c}, \mathbf{k}),$$

and has the formal solution

$$\tilde{f}(\mathbf{c}, \mathbf{k}, t) = \Theta(t)\exp\{-(i\mathbf{c} \cdot \mathbf{k} + \mathcal{M})t\}\tilde{f}_i(\mathbf{c}, \mathbf{k}).\quad (2.13)$$

Equation (2.13) can be expressed in terms of the complete basis defined by equations (2.8) as

$$\tilde{f}(\mathbf{c}, \mathbf{k}, t) = \Theta(t)\sum_{j \in \sigma} \exp(\omega_j(i\mathbf{k})t)\Psi_j(\mathbf{c}, i\mathbf{k}) \int \Phi_j(\mathbf{c}', i\mathbf{k})\tilde{f}_i(\mathbf{c}', i\mathbf{k})d\mathbf{c}'.\quad (2.14)$$

Substituting this into equations (2.10), (2.11) we see that

$$\tilde{n}_0(\mathbf{k}, t) = \Theta(t)\exp\{\omega_0(i\mathbf{k})t\}\tilde{n}_0(\mathbf{k}, 0),\quad (2.15)$$

$$\begin{aligned}\tilde{n}_0(\mathbf{k}, 0)x(\mathbf{k}, t) &= \Theta(t)\sum_{j \neq 0} \exp[\{\omega_j(i\mathbf{k}) - \omega_0(i\mathbf{k})\}t] \times \\ &\int \Psi_j(\mathbf{c}, i\mathbf{k})d\mathbf{c} \int \Phi_j(\mathbf{c}', i\mathbf{k})\tilde{f}_i(\mathbf{c}, i\mathbf{k})d\mathbf{c}'\end{aligned}\quad (2.16)$$

and so  $\mathbf{x}^{(l)}$  is going to be of the form

$$\sum_{\substack{j \in \sigma \\ j \neq 0}} \mathbf{p}_j^{(l)}(t)\exp\{-(\omega_0(0) - \omega_j(0))t\}$$

where  $\mathbf{p}_j^{(l)}(t)$  is an  $l$ th order polynomial in  $t$ , with rank  $l$  tensor coefficients.

For  $t \gg \tau = \{\min_j \operatorname{Re}(\omega_0(0) - \omega_j(0))\}^{-1}$ , all the moments of  $x$ , and their time derivatives will become vanishingly small. So, we have

$$\omega^{(l)}(t) \longrightarrow \Omega^{(l)} \partial_t \ln \tilde{n}_0 = \Omega^{(l)} \omega_0(i\mathbf{k}) \equiv \omega_0^{(l)},$$

thus establishing the existence of a hydrodynamic regime, where the time development of swarms is characterized by constant transport coefficients.

If the total number of particles is conserved, then  $\omega^{(0)}(t) = 0$  at all times. This means from equation (2.12) that  $\partial_t x^{(0)} = 0$ , so that  $x^{(0)}$  is constant. Since for large times,  $x^{(0)} \longrightarrow 0$ , this means that  $x^{(0)}(t) = 0$  at all times.

## 2.4 The nature of the Spectrum and the Run-away Phenomenon

Very little is known about the nature of the spectrum of  $\mathcal{M}$  for collision operators corresponding to real interactions. The main features of the spectrum of  $\mathcal{J}$ , but not all of its detailed properties are known for the hard sphere potential, and for  $r^{-s}$  potentials [Grad (1963), Dorfman (1963), Kušcer and Williams (1967), Yan and Wannier (1968) and Pao (1974)]. The spectrum for Maxwell molecules ( $r^{-4}$  potential) is the only potential for which the spectrum is known completely [see preceding refs]. Almost nothing is known for the potentials having an attractive component.

We have chosen a discrete spectrum because our exactly solvable model has this structure, and we wish to understand the features of this model in the first instance, and also because the mathematics of discrete spectra is vastly simpler to that of continuous spectra. (This is why the theory of compact operators, and of bounded self-adjoint operators is so much more developed than the case of general linear operators.) However, the existence of runaway [Howorka et al. (1979), Moruzzi and Kondo (1980)] shows that there are circumstances where this assumption fails. In this phenomenon, there are regions of the parameter  $E/N$  for which the transport coefficients are not well defined. The motion of the centroid is reminiscent of acceleration rather than that of a steady drift velocity. The arguments in the previous section rule out the possibility of runaway arising when the spectrum is discrete. Consequently, we can say that a necessary condition for runaway is that the spectrum must have continuous or residual components.

Cavalleri and Pavari-Fontana (1972) give as sufficient condition for runaway to occur that the integral  $\int_0^\infty \nu(c)dc$  of the velocity dependent collision frequency should exist. This collision frequency is defined by

$$\nu(c) = \int |\mathbf{c} - \mathbf{c}'| \sigma(|\mathbf{c} - \mathbf{c}'|) f_0(c') d\mathbf{c}'$$

where  $f_0(c)$  is the background gas distribution function, and  $\sigma(c)$  is the total scattering cross section. Since necessity and sufficiency are often closely connected conditions in mathematics, one may speculate that there is a strong connection between the asymptotic form of  $\nu(c)$  for large  $c$ , and the structure of the spectrum of  $\mathcal{J}$ .

## 2.5 Klein-Kramers Model

As a way of obtaining insight into how the behaviour of swarms are related to various mathematical features of the Boltzmann equation, it is useful to have an exactly solvable model. The models most often employed in transport theory are briefly reviewed in section 13 of Kumar *et al.* (1980). The model that reflects best the theory developed so far is the Rayleigh gas model, which describes Brownian motion.

Brownian motion may be considered to be a limiting case of swarms in which the diffusing particle is very much more massive than the background fluid molecules. This phenomenon is described in stochastic theory by the master equation, which is an integral equation, and an equivalence with a differential form, known as the Kramers-Moyal expansion. This expansion is often truncated at second order, where it is known as the Fokker-Planck equation, which is essentially exact for Brownian motion. A general introduction to this subject can be found by Risken (1984), and in a kinetic theory context by Braglia (1980).

The analogy of Brownian motion and swarm physics suggests that a differential form of the collision operator can be found in which the ratio  $M/(m + M)$  plays the part of a small expansion parameter, where  $M$  is the background gas molecule mass, and  $m$  the charged particle mass. Kumar *et al.* (1980) develop this expansion, which they call the Fokker-Planck expansion, and another expansion valid when  $m/(m + M)$  is small.

If we make the approximation of the background gas molecule velocities being much larger than the charged particle velocities, and truncate the

Fokker-Planck expansion at second order, we obtain the Klein-Kramers equation:

$$\begin{aligned} \partial_t f + \mathbf{c} \cdot \partial_{\mathbf{r}} f + \mathbf{a} \cdot \partial_{\mathbf{c}} f - \nu_1 \partial_{\mathbf{c}} \cdot (\mathbf{c} f) - \nu_2 \partial_{\mathbf{c}}^2 f + \nu f = \\ (\partial_t + \mathbf{c} \cdot \partial_{\mathbf{r}} + \mathcal{M}) f(\mathbf{c}, \mathbf{r}, t) = S(\mathbf{c}, \mathbf{r}, t). \end{aligned} \quad (2.17)$$

The reaction rate  $\nu$  is positive when ionization occurs. The coefficients  $\nu_1$  and  $\nu_2$  are related to physical quantities by

$$\nu_1 = m\nu_c/M, \quad \nu_2 = k_B T \nu_c/M,$$

where  $k_B$  is Boltzmann's constant and  $T$  the background gas temperature. The collision frequency  $\nu_c$  is approximately the product of the swarm drift velocity, the background gas number density, and the collision cross section.

We look for a solution to the Klein-Kramers equation in the form  $f(\mathbf{c}, \mathbf{r}, t) = \int G(\mathbf{c}, \mathbf{r}, t; \mathbf{c}', \mathbf{r}', t') S(\mathbf{c}', \mathbf{r}', t') d\mathbf{c}' d\mathbf{r}' dt'$  where the Greens function  $G$  satisfies

$$(\partial_t + \mathbf{c} \cdot \partial_{\mathbf{r}} + \mathcal{M}) G(\mathbf{c}, \mathbf{r}, t; \mathbf{c}', \mathbf{r}', t') = \delta(t - t') \delta(\mathbf{c} - \mathbf{c}') \delta(\mathbf{r} - \mathbf{r}'). \quad (2.18)$$

Taking the Fourier transform of (2.18) with respect to position, we find:

$$[\partial_t + i\mathbf{c} \cdot \mathbf{k} + \mathcal{M}] \tilde{G}(\mathbf{c}, \mathbf{k}, t; \mathbf{c}', \mathbf{r}', t') = \delta(t - t') \delta(\mathbf{c} - \mathbf{c}') e^{-i\mathbf{k} \cdot \mathbf{r}'}$$

The operator  $i\mathbf{c} \cdot \mathbf{k} + \mathcal{M}$  can be transformed into a hermitian operator by means of the similarity transformation  $\mathcal{H}_{\mathbf{k}} = [w(\mathbf{c})]^{-1} (i\mathbf{c} \cdot \mathbf{k} + \mathcal{M}) w(\mathbf{c})$ , where  $w(\mathbf{c}) = \exp(-(\nu_1 \mathbf{c} - \mathbf{a}^2/4\nu_1\nu_2))$ . This has a discrete spectrum with a complete set of eigenfunctions:

$$\mathcal{H}_{\mathbf{k}} \Xi_n(\mathbf{c}, \mathbf{k}) = -\omega_n(i\mathbf{k}) \Xi_n(\mathbf{c}, \mathbf{k}). \quad (2.19)$$

The Green's function can then be written using a spectral expansion

$$\begin{aligned} \tilde{G}(\mathbf{c}, \mathbf{k}, t; \mathbf{c}', \mathbf{r}', t') = \\ \Theta(t - t') \sum_n w(\mathbf{c}) \Xi_n(\mathbf{c}, \mathbf{k}) \exp[\omega_n(i\mathbf{k})(t - t')] [w(\mathbf{c}')]^{-1} \Xi_n(\mathbf{c}', \mathbf{k}) e^{-i\mathbf{k} \cdot \mathbf{r}'}. \end{aligned} \quad (2.20)$$

Making the change of variables  $\mathbf{g} = (-\nu_1 \mathbf{c} + \mathbf{a} - 2\nu_2 i\mathbf{k}/\nu_1) / (2\nu_1 \nu_2)^{\frac{1}{2}}$  the eigenvalue equation (2.19) for  $\mathcal{H}_{\mathbf{k}}$  is transformed to the harmonic oscillator problem familiar from quantum mechanics:

$$\left\{ \partial_{\mathbf{g}}^2 - g^2 + 3 + \left( -\frac{2\omega_n(i\mathbf{k})}{\nu_1} - \frac{2k^2\nu_2}{\nu_1^3} - \frac{2i\mathbf{a} \cdot \mathbf{k}}{\nu_1^2} - 6 + \frac{2\nu_0}{\nu_1} \right) \right\} \Xi_n(\mathbf{g}) = 0.$$

This equation is separable in cartesian coordinates  $g_1, g_2, g_3$  and has solutions in terms of Hermite polynomials [Abramowitz and Stegun (1965) 22.6.20]:

$$\Xi_n(\mathbf{g}) = e^{-g^2/2} H_{n_1}(g_1) H_{n_2}(g_2) H_{n_3}(g_3) \quad (2.21)$$

$$\omega_n(i\mathbf{k}) = -\nu_1(n_1 + n_2 + n_3) + \nu - \frac{i\mathbf{a} \cdot \mathbf{k}}{n_1} - \frac{\nu_2}{\nu_1^2} k^2, \quad (2.22)$$

where  $n_1, n_2$  and  $n_3$  are whole numbers, and  $n$  is the cartesian triple  $(n_1, n_2, n_3)$ . These solutions can also be expressed in spherical coordinates by means of Burnett functions [Kumar (1980)]. In one dimension, the result is identical except that  $g$  is now a scalar, and the index set  $\{n\}$  is the set of whole numbers.

The Greens function may now be evaluated by substituting (2.21) and (2.22) into (2.20):

$$\begin{aligned} \tilde{G}(\mathbf{c}, \mathbf{k}, t; \mathbf{c}', \mathbf{r}', t') = & \\ & \Theta(t - t') \frac{w(\mathbf{c})}{w(\mathbf{c}')} \exp\left(-\frac{g^2}{2} - \frac{g'^2}{2} + \left[\nu - \frac{i\mathbf{a} \cdot \mathbf{k}}{\nu_1} - \frac{\nu_2}{\nu_1^2} k^2\right] [t - t']\right) \times \\ & \prod_{j=1}^3 \sum_{n=0}^{\infty} \frac{\exp(-\nu_1 n [t - t'])}{2^n n!} H_n(g_j) H_n(g'_j). \end{aligned}$$

The sum over  $n$  may be evaluated using a generating function for Hermite polynomials [Erdélyi (1954) 10.13.22]:

$$\sum_{n=0}^{\infty} \frac{(z/2)^n}{n!} H_n(x) H_n(y) = (1 - z^2)^{-\frac{1}{2}} \exp\left(\frac{2xy - (x^2 + y^2)z^2}{1 - z^2}\right).$$

Thus we obtain

$$\begin{aligned} \tilde{G}(\mathbf{c}, \mathbf{k}, t; \mathbf{c}', \mathbf{r}', t') = & (1 - \exp[2\nu_1(t - t')])^{-3/2} \times \\ & \Theta(t - t') \frac{w(\mathbf{c})}{w(\mathbf{c}')} \exp\left(-\frac{g^2}{2} - \frac{g'^2}{2} + \left[\nu - \frac{i\mathbf{a} \cdot \mathbf{k}}{\nu_1} - \frac{\nu_2}{\nu_1} k^2\right] [t - t']\right) \times \\ & \exp\left(-\mathbf{g} \cdot \mathbf{g}' \operatorname{cosech}(\nu_1 [t - t']) + \frac{1}{2} (g^2 + g'^2) \{\coth(\nu_1 [t - t']) + 1\}\right). \end{aligned}$$

The inverse Fourier transform of  $\tilde{G}$  is a Gaussian integral, so we obtain

$$G(\mathbf{c}, \mathbf{r}, t; \mathbf{c}', \mathbf{r}', t') = \Theta(t - t') \left[(1 - z^2)A\right]^{-3/2} \exp(C - B^2/4A) \quad (2.23)$$

where  $z = e^{-\nu_1 t}$  and

$$A = \frac{1}{2}\nu_1 t - \tanh \frac{\nu_1 t}{2},$$

$$\mathbf{B} = \sqrt{\frac{\nu_1}{2\nu_2}} \left\{ \nu_1 \mathbf{r} - \mathbf{a}t - (\mathbf{c} + \mathbf{c}' - 2\frac{\mathbf{a}}{\nu_1}) \tanh \frac{\nu_1 t}{2} \right\},$$

$$C = -\frac{\nu_1}{\nu_2} \frac{|(\mathbf{c} - \mathbf{a}/\nu_1) - (\mathbf{c}' - \mathbf{a}/\nu_1)z|^2}{1 - z^2}.$$

In one dimension, the exponent on the second factor in (2.23) is  $-\frac{1}{2}$ , *i.e.*

$$G(c, r, t; c', r', t') = \Theta(t - t') \left[ (1 - z^2)A \right]^{-\frac{1}{2}} \exp(C - B^2/4A). \quad (2.24)$$

Figure (2.1) shows the one dimensional density distribution plotted at successive values of  $t$ , from an initial delta function pulse, *i.e.*

$$n(r, t) = \int_{-\infty}^{\infty} G(c, r, t; 0, 0, 0) dc.$$

In the  $r$ - $t$  plane, the path that the centroid traces out is plotted (dotted curve) and can be compared with the path expected if the system were hydrodynamic with a constant drift velocity (dashed curve). Non-hydrodynamic effects manifest themselves within time  $1/\nu_1$  of the origin, with a residual constant retardation of the swarm at large times. This was an effect first observed by Harris (1981), who noted the “non-diffusive” nature of the Klein-Kramers equation at large times. Titulaer (1983) explained the phenomenon using a detailed analysis of the Klein-Kramers equation. This effect has been discovered a number of times in different contexts, for example Robson (1975) noted the effect in the BGK model. However, it was generally ignored as not having physical consequences. I rediscovered this phenomenon independently, and showed that it should occur under quite general circumstances and have measurable consequences for swarm experiments. More will be said on this in chapter 3.

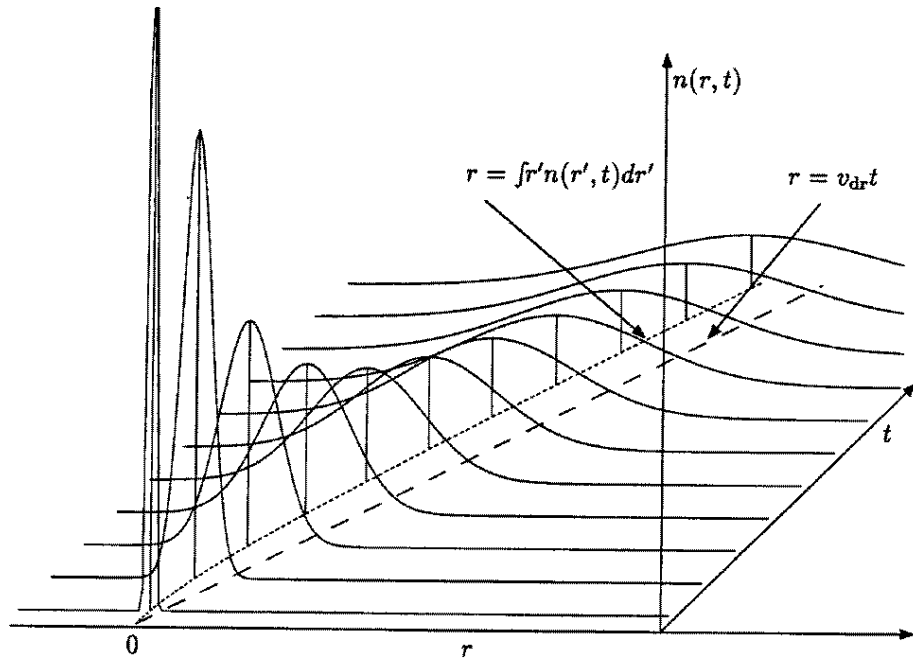


Figure 2.1: Evolution of the one dimensional Klein-Kramers equation showing non-hydrodynamic effects at large times

## Chapter 3

# End Effects in Time of Flight Experiments

### 3.1 Time of Flight Experiments

The general principle of this experiment is that a narrow pulse of charged particles is injected into the drift region, and the resulting distribution of charged particles is observed at some time later. By taking the final observation at different times, a picture can be built up of how a pulse evolves in time. The drift velocity is usually calculated by finding the time that the swarm's peak takes to traverse a certain distance.

Many methods have been used to measure drift velocities, but this thesis will only be concerned with the electrical shutter method. The shutters usually consist either of a pair of wire gauzes, as in the Tyndell-Powell method, or of a grid of wires of alternating polarity as in the more accurate Bradbury-Nielson method (see fig.3.1). The first shutter opens to let the swarm into the drift region. The particles then drift and diffuse in a uniform electric field to a second shutter which samples the charged particle flux at some time after the pulse was transmitted through the first shutter (see fig. 3.2). The distance between the shutters may be varied to measure the swarm density as a function of distance, as well as time. The shutters are usually operated by applying either a sine or square wave of variable frequency. The arrival time spectrum is obtained by measuring the current as a function of the shutter frequency. This consists of a series of peaks at frequencies,  $f_n$ ,

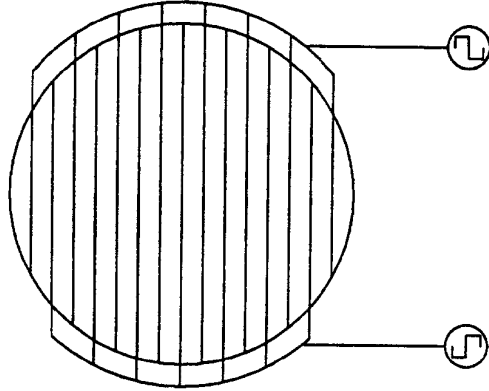


Figure 3.1: Bradbury-Nielsen shutter

which in the case of the Tyndell-Powell method satisfy the relation

$$\frac{f_n}{n} \approx \frac{v_{dr}}{d}$$

where  $n$  is an integer,  $v_{dr}$  the drift velocity, and  $d$  the distance between the shutters. In the Bradbury-Nielsen technique, the frequencies are effectively doubled, as the shutter is open when the shutter control signal passes through zero, and closed when a voltage of either polarity is applied to the shutter.

## 3.2 Lithium ion - Helium Experiment

The transport properties of  $\text{Li}^+$  ions in helium have received much interest owing to the relative simplicity of this particular ion-atom system, which has allowed the calculation of highly accurate ab initio interaction potentials. These can be used in conjunction with transport theory to give “ab initio” transport coefficients, which can be compared directly with experiment.

However the results from experiment were confusing. Skullerud *et al.* (1986) measured the ratio of  $D_T/\mu$  of transverse diffusion to mobility, and found that their data is in significant disagreement with values of  $D_T/\mu$  calculated from the potential of Viehland (1983), which was based on the data

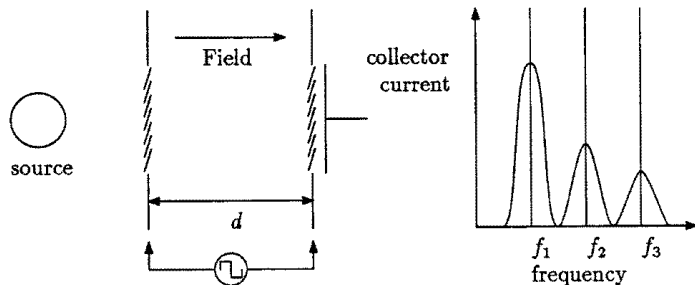


Figure 3.2: Time of flight experiment with shutters. A typical arrival time spectrum is shown

of Gatland *et al.*(1977). Furthermore, a highly accurate ab initio potential calculation by Senff and Burton (1986) yielded  $D_T/\mu$  values that agrees with the measured values within the stated uncertainty of 2%.

Furthermore, there was considerable discrepancy amongst the mobility values of Takata (1975), Gatland *et al.* (1977) and Cassidy and Elford (1985), even allowing for the slightly different experimental conditions under which the experiments were performed. The differing data were finally reconciled by explicitly recognizing the possibility that the experiments were no longer described by a second order diffusion equation of the form (2.2). Two different ad hoc methods of eliminating the effects due to the breakdown of this description were applied by England and Elford (1987) and Løvaas *et al.* (1988), and yielded transport data in agreement with the ab initio calculations. These effects are known as end-effects, because the diffusion equation is expected to hold in the bulk of a homogeneous neutral gas, with a uniform field, and any departures from this state occur at the ends of the apparatus.

England and Elford (1987) assume that the end effects in time of flight mobility measurements take the form of a power series in the inverse of the drift length. By fitting this power series to their mobility measurements at different drift distances, they eliminated the end effects by extrapolating to infinite drift distance.

Løvaas *et al.* (1988) assume that the end effects induce a distortion to the basic gaussian solution (2.3) that can be written as a series in Hermite

polynomials, similar to the solution of the transport equation (2.4) given by Skullerud (1974). By truncating the series at third order, they obtain expressions for the mean and variance of the drift time. By comparing these values at different drift distances, they can obtain values for the transport coefficients.

In the case of lithium ions in helium, the transport properties are now considered to be well understood. However, it has highlighted a deficiency in the conventional transport theory based on the diffusion equation (1.7), which needs to be overcome if the correction methods employed are to be understood. In this chapter, I develop a non-hydrodynamic theory of time-of-flight experiments which provides theoretical underpinning to the methods of England and Elford, and to those of Løvaas *et al.*. These results have been reported in Standish (1987) However, I have not treated the effects due to the distortion of the field near the shutter, nor the effects of absorption onto the apparatus, which are considered to be a significant contribution to the total end-effect. Much work remains to be done in this area before there is full understanding of end-effects.

### 3.3 Nonhydrodynamic Contributions to End-Effects in Time-of-Flight Swarm Experiments

Let us consider an experiment where the time at which the centroid arrives at the collector is measured. This is not the same thing as measuring the time at which the peak collector current occurs. We will deal with the experiment in which the peak collector current is measured in the next section.

The distance travelled by the centroid in time  $t$  can be found by integrating  $\omega^{(1)}(t)$ :

$$\begin{aligned}
 \mathbf{d} = \int_0^t \omega^{(1)}(t') dt' &= \omega_0^{(1)} t - \frac{\mathbf{x}^{(1)}(0)}{1 + x^{(0)}(0)} + \frac{\mathbf{x}^{(1)}(t)}{1 + x^{(0)}(t)} \\
 &= \omega_0^{(1)} t - \mathbf{x}^{(1)}(0) + \mathbf{x}^{(1)}(t) \text{ for the non-reactive case.} \\
 &\longrightarrow \omega^{(1)} t - \mathbf{x}^{(1)}(0) \text{ as } t \longrightarrow \infty
 \end{aligned} \tag{3.1}$$

If we measure the times  $t_1$  and  $t_2$  at two different drift distances  $d_1$  and  $d_2$ , and then extract the drift velocity from the ratio  $(d_1 - d_2)/(t_1 - t_2)$ , as

Løvaas *et al.* (1988) do, then the non-hydrodynamic effects are completely eliminated. However, if we just take the ratio of drift length to drift time, then a correction needs to be made to take into account the  $\mathbf{x}^{(1)}(0)$  term. Inverting (3.1) to get  $t$  as a function of  $\mathbf{d}$ , the measured value of the drift velocity is obtained by dividing  $\mathbf{d}$  by the time (since all vectors in the system must be proportional to  $\mathbf{a}$  we can treat them as scalar quantities):

$$v_{\text{dr}} = \omega_0^{(1)} \left( 1 - \frac{x^{(1)}(0)}{d + x^{(1)}(0)} \right). \quad (3.2)$$

England and Elford (1987) supposed that the correction due to all the end effects is a power series in  $1/d$ :

$$v_{\text{dr}} = \omega_0^{(1)} \left( 1 + \sum_{i=1}^{\infty} \alpha_i d^{-i} \right). \quad (3.3)$$

Equation (3.2) is exactly this form, the correction being just the sum of a geometric series:

$$v_{\text{dr}} = \omega_0^{(1)} \left\{ 1 + \sum_{i=1}^{\infty} \left( -\frac{x^{(1)}(0)}{d} \right)^i \right\}.$$

### 3.4 Model Calculation

To compute  $\mathbf{x}^{(1)}(0)$  for the Klein-Kramers model, we need to make some assumptions about the initial phase space distribution. The swarm is collected in a potential well formed by the electric shutter, before being released into the drift tube. For calculational simplicity, we assume that the initial velocity distribution is a Gaussian. Thus, we have

$$\tilde{f}_i(\mathbf{c}, \mathbf{k}) = (\sigma/\pi)^{\frac{3}{2}} \exp(-\sigma \mathbf{c}^2).$$

Substituting this into (2.10), we get

$$\begin{aligned} \tilde{n}_0(\mathbf{k}, 0) &= \exp \left\{ \frac{\nu_2 k^2}{2\nu_1^3} \left( 3 - \frac{\nu_1}{2\nu_2\sigma} \right) + \frac{i\mathbf{a} \cdot \mathbf{k}}{\nu_1^2} \right\}, \\ \mathbf{x}^{(1)}(0) &= \boldsymbol{\Omega}^{(1)} \left( \frac{1 - \tilde{n}_0(\mathbf{k}, 0)}{\tilde{n}_0(\mathbf{k}, 0)} \right) = \frac{\mathbf{a}}{\nu_1^2} = \frac{v_{\text{dr}}}{\nu_1}. \end{aligned} \quad (3.4)$$

England and Elford (1987) have measured the mobility of  $\text{Li}^+$  ions in helium at various distances, and fitted the experimental data to equation (3.3), truncating the series at  $\alpha_2$ . Their fitted values for  $\alpha_1$  ranged from 0.5 to 2 mm, as a function of electric field strength. It is of interest to compare this value of  $\alpha_1$ , which is the combined error due to all end effects, with the numerical value for  $\mathbf{x}^{(1)}(0)$  obtained by substituting the experimental parameters into equation (3.4). Even though the Klein-Kramers model is not really applicable to lithium in helium, where the ions and neutrals have nearly the same mass, the result should indicate whether non-hydrodynamic effects are a significant proportion of the total end effect.

The experiment was performed with a neutral gas pressure of 50 Pa and a temperature of 300 K. Using the ideal gas equation of state, this corresponds to a number density of  $10^{22}$  particles per  $\text{m}^3$ . The measured drift velocity was  $4 \times 10^3 \text{ms}^{-1}$ . From Viehland (1982), the cross section at this kinetic energy ( $\frac{1}{2}m_{\text{Li}}v_{\text{dr}}^2$ ) is about  $20a_0^2 = 5 \times 10^{-20} \text{m}^2$ , where  $a_0$  is the Bohr radius. This figure is very similar to  $4\pi a_0^2$  obtained by considering the collision of two spheres of radius  $a_0$ . From this, we can conclude that the collision frequency will be of the order of  $500v_{\text{dr}}$ , or  $\nu_1 \approx 870v_{\text{dr}}$ . Upon substituting this into equation (3.4), the value of  $\mathbf{x}^{(1)}(0)$  is found to be of the order of 1 mm, to be compared with the typical drift distance of 100mm.

While experimental corrections must include other end effects, as discussed by England and Elford (1987), we can conclude that non-hydrodynamic effects are a significant contribution to experimental end effects.

### 3.5 Peak Arrival Time

Consider now an experiment such as that of England and Elford (1987), where the time at which the peak collector current occurs is taken as the drift time. A brief summary of the results to be presented in the rest of this chapter has been reported in Standish and Kumar (1987). We will assume that the swarm is described by the free space solution at large times (2.15):

$$n(\mathbf{r}, t) = (2\pi)^{-\frac{3}{2}} \int \exp(i\mathbf{k} \cdot \mathbf{r} + \omega_0(i\mathbf{k})t - \ln(1 + x(\mathbf{k}, 0)))\tilde{n}(\mathbf{k}, 0)d\mathbf{k}. \quad (3.5)$$

In the following analysis, we will assume a delta function initial pulse  $\tilde{n}(\mathbf{k}, 0) = 1$ , and that the velocity distribution of the source has cylindrical symmetry

about the axis defined by the field. Choose cylindrical coordinates  $k_\perp$ ,  $k_\theta$  and  $k_z$ . All quantities in this system must satisfy cylindrical symmetry, *i.e.* depend only on  $k_\perp^2$  and  $k_z$ , so that

$$\omega_0(i\mathbf{k}) = \sum_{j,l} \omega_{2j,l} (-k_\perp^2)^j (ik_z)^l$$

and

$$\ln(1 + x(\mathbf{k}, 0)) = \sum_{j,l} \xi_{2j,l} (-k_\perp^2)^j (ik_z)^l.$$

Note that  $\xi_{01} = x^{(1)}(0)$  when the swarm is conserved. Then equation (3.5) may be written [Skullerud (1974)]:

$$\begin{aligned} n(\rho_\perp, \rho_z, t) = & (4\pi)^{-\frac{3}{2}} (\omega_{02}t - \xi_{02})^{-\frac{1}{2}} (\omega_{20}t - \xi_{20})^{-1} \times \\ & \exp\left(\sum_{2i+j>2} (\omega_{2i,j}t - \xi_{2i,j}) 2^{-2i} (\omega_{20}t - \xi_{20})^{-i} (-2)^{-j} (\omega_{02}t - \xi_{02})^{-\frac{j}{2}} \partial_{\rho_\perp}^{2i} \partial_{\rho_z}^j\right) \times \\ & \exp(-\rho_\perp^2 - \rho_z^2) \end{aligned} \quad (3.6)$$

where  $\rho_\perp = r_\perp/2(\omega_{20}t - \xi_{20})^{\frac{1}{2}}$  and  $\rho_z = (z - \omega_{01}t + \xi_{01})/2(\omega_{02}t - \xi_{02})^{\frac{1}{2}}$ .

If the total number of charged particles is conserved, the continuity equation for the current density is:

$$\partial_t n + \nabla \cdot \mathbf{j} = 0.$$

Substituting the time dependent transport equation (2.6), we get:

$$\nabla \cdot \mathbf{j} = - \sum_{l=1}^{\infty} \boldsymbol{\omega}^{(l)}(t) \odot (-\nabla)^l n. \quad (3.7)$$

The total current passing through an infinite plane electrode located at  $d$  is:

$$i(d, t) = \int_{\text{electrode}} \mathbf{j} \cdot d\mathbf{S} = \int_{\substack{\text{half space} \\ \text{left of elec-} \\ \text{trode}}} \nabla \cdot \mathbf{j} d\mathbf{r} = \int_{\text{electrode}} \sum_{l=0}^{\infty} \boldsymbol{\omega}^{(l)}(t) \odot (-\nabla)^{(l-1)} n d\mathbf{S}, \quad (3.8)$$

where use has been made of the divergence theorem to substitute equation (3.7).

To calculate the peak arrival time, we differentiate the above expression for the collector current and solve. Since we are interested in drift times much larger than the non-hydrodynamic relaxation time  $\tau$ , the transport coefficients can be replaced by their constant values, so that the required condition is

$$\int \sum_{l=1}^{\infty} \boldsymbol{\omega}_0^{(l)} \odot (-\nabla)^{l-1} \partial_t n d\mathbf{S} = 0.$$

Substitute for  $\partial_t n$  using the transport equation, and the integral

$$\int_{\text{infinite plane}} \nabla_{\perp}^i \exp(-\rho_{\perp}^2) d\mathbf{S} = 4\pi(\omega_{20}t_m - \xi_{20})\delta_{i0}$$

and we find:

$$\begin{aligned} 0 &= \int \sum_{l=1}^{\infty} \sum_{m=1}^l \boldsymbol{\omega}_0^{(m)} \boldsymbol{\omega}_0^{(l-m+1)} \odot (-\nabla)^l n d\mathbf{S} \\ &= 4\pi(\omega_{20}t_m - \xi_{20}) \sum_{l=1}^{\infty} \sum_{m=1}^l \omega_{0m} \omega_{0,l-m+1} (-2)^l (\omega_{02}t_m - \xi_{02})^{-\frac{l}{2}} \times \\ &\quad \partial_{\rho_z}^l \exp\left(\sum_{j=3}^{\infty} (\omega_{0j}t_m - \xi_{0j}) (-2)^{-j} (\omega_{02}t_m - \xi_{02})^{-\frac{j}{2}} \partial_{\rho_z}^j\right) \exp(-\rho_z^2). \end{aligned}$$

Expanding the exponential differential operator, collecting terms in powers of  $\partial_{\rho_z}$ , and using Rodrigues' formula [Abramowitz and Stegun (1965), 22.11.7] to express it in terms of Hermite polynomials, we find:

$$\begin{aligned} 0 &= 4\pi(\omega_{20}t_m - \xi_{20}) \exp(-\rho_z^2) \times \\ &\quad \sum_{l=1}^{\infty} \left( \sum_{m=1}^l \omega_{0m} \omega_{0,l-m+1} + \sum_{k=1}^{[(l-1)/3]} \sum_{j=3}^{[(l-1)/k]} \sum_{m=1}^{l-jk} \omega_{0m} \omega_{0,l-jk-m+1} (\omega_{0j}t_m - \xi_{0j})^k / k! \right) \times \\ &\quad 2^{-l} (\omega_{02}t_m - \xi_{02})^{-\frac{l}{2}} H_l(\rho_z) \end{aligned} \tag{3.9}$$

where  $[n]$  denotes the greatest integer less than or equal to  $n$ . If we assume that the sum over  $l$  is appropriately convergent, then  $t_m$  is a power series in the inverse drift length. In particular, we expect that the measured drift velocity found by dividing the drift length by the drift time is given by the

true drift velocity plus corrections that decay as a power series in  $1/d$ . So we assume that

$$\frac{d}{t_m} = \omega_{01} + \sum_{l=1}^{\infty} a_l d^{-l}. \quad (3.10)$$

This power series can be inverted to obtain a power series for  $t_m$  [Knopp (1951), 4.3(20)]:

$$t_m = \frac{d}{\omega_{01}} \left( 1 - \frac{\omega_{01}}{a_1} d^{-1} + \dots \right).$$

Substituting this into  $\rho_z$ , one obtains:

$$\rho_z = \frac{1}{2} \left( \frac{\omega_{02} d}{\omega_{01}} \right)^{-\frac{1}{2}} \left( \left[ \xi_{01} + \frac{a_1}{\omega_{01}} \right] + \text{terms of order } d^{-1} \right).$$

The leading power of the Hermite polynomials at large drift distances will be given by the constant or linear term of the polynomial, for even and odd polynomials respectively. So

$$\begin{aligned} H_l(\rho_z) &\sim (-1)^{[l/2]} \frac{l!}{[l/2]!} \begin{cases} 1 & l \text{ even} \\ 2\rho_z & l \text{ odd} \end{cases} \\ &\sim (-1)^{[l/2]} \frac{l!}{[l/2]!} \begin{cases} 1 & l \text{ even} \\ \left( \frac{\omega_{02} d}{\omega_{01}} \right)^{-\frac{1}{2}} \left( \xi_{01} + \frac{a_1}{\omega_{01}} \right) & l \text{ odd} \end{cases}. \end{aligned}$$

Substituting this into equation (3.9), we get

$$\begin{aligned} \sum_{l=1}^{\infty} \left( \sum_{m=1}^l \omega_{0m} \omega_{0,l-m+1} + \sum_{k=1}^{[(l-1)/3]} \sum_{j=3}^{[(l-1)/k]} \sum_{m=1}^{l-jk} \omega_{0m} \omega_{0,l-jk-m+1} (\omega_{0j} d / \omega_{01} - \xi_{0j})^k / k! \right) \times \\ 2^l (\omega_{02} d / \omega_{01})^{-[(l+1)/2]} (-1)^{[l/2]} \frac{l!}{[l/2]!} \begin{cases} 1 & l \text{ even} \\ \xi_{01} + \frac{a_1}{\omega_{01}} & l \text{ odd} \end{cases}. \end{aligned}$$

The leading power of  $d$  will be the one that maximizes  $k - [(l+1)/2]$ . As  $k$  increases proportionally to  $l/3$ , this will happen for low values of  $l$ . In particular, the leading term will have contributions from  $l = 1, 2$  and  $4$ , and  $k = [(l-1)/3]$ . Setting the leading term to zero yields a linear equation for the unknown  $a_1$ , to which the solution is:

$$a_1 = -\omega_{01} \xi_{01} + 2\omega_{02} - \frac{3\omega_{03}\omega_{01}}{2\omega_{02}} \quad (3.11)$$

The three terms in this expression can be identified. The first is just the non-hydrodynamic term discussed in the previous section. The second is the effect of diffusion over a plane electrode [Huxley and Crompton (1974), §(5.8)] and the third is the contribution from higher order transport effects.

Similarly, the next term in the series (3.10) can be calculated. This was done using a computer algebra package (see Appendix B), the result being

$$\begin{aligned}
a_2 = & \frac{27\omega_{03}}{4} + \frac{9\omega_{01}\omega_{04}}{2\omega_{02}} - \frac{117\omega_{01}\omega_{03}^2}{8\omega_{02}^2} + \frac{15\omega_{01}^2\omega_{05}}{4\omega_{02}^2} + \frac{3\omega_{01}^2\xi_{03}}{2\omega_{02}} \\
& + \frac{423\omega_{01}^2\omega_{03}^3}{32\omega_{02}^4} + \frac{3\omega_{01}\omega_{03}\xi_{01}}{\omega_{02}} - \frac{3\omega_{01}\omega_{03}\xi_{02}}{2\omega_{02}^2} + \omega_{01}\xi_{01}^2 - 4\omega_{02}\xi_{01} \quad (3.12)
\end{aligned}$$

### 3.6 Pressure Dependencies of Non-hydrodynamic and Higher Order Diffusion Effects

In classical transport theory, the transport coefficients have a simple dependence upon the pressure of the neutral gas if the ratio of the electric field to neutral gas density is kept constant. The presence of end effects introduces anomalous pressure dependencies in the experimental data. It is therefore of interest to calculate the pressure dependence of the two end effects discussed here. This is done by dimensional analysis on the Boltzmann equation.

Introduce a parameter  $\nu$  which scales proportionally with the neutral gas density, and, since  $\mathbf{a}/n_0$  is constant, the field. As the collision operator  $\mathcal{J}$  is proportional to the neutral gas density, the scaled operator is  $i\mathbf{c} \cdot \mathbf{k} + \nu\mathbf{a} \cdot \partial_{\mathbf{c}} + \nu\mathcal{J}$  and has eigenvectors  $\Psi_j(\nu; \mathbf{c}, \mathbf{k}) = \Psi_j(1; \mathbf{c}, \mathbf{k}/\nu)$  with eigenvalues  $\omega_j(\nu; i\mathbf{k}) = \nu\omega_j(1; i\mathbf{k}/\nu)$ . Upon identifying the transport coefficients with the multipole coefficients of the lowest eigenvalue, we see that  $\omega^{(l)} \sim \nu^{-l+1}$ .

The non-hydrodynamic part of the density is given explicitly by (2.16). For a delta function initial pulse, the initial Fourier transformed phase space distribution does not depend on  $\mathbf{k}$ , and so  $x(\nu; \mathbf{k}, t) = x(1; \mathbf{k}/\nu, t)$  or  $\mathbf{x}^{(l)} \sim \nu^{-l}$ . Substituting these relations into equation (3.5), we can obtain the scaling for the spatial density function  $n(\nu; \mathbf{r}, t) = \nu^3 n(1; \nu\mathbf{r}, \nu t)$  and similarly, the collector current scaling  $i(\nu; d, t) = \nu i(1; \nu d, \nu t)$ . If we differentiate this

expression with respect to  $t$ , and solve for  $t_m$ , we find

$$\frac{d}{t_m}(\nu) = \omega_{01} + \sum_{l=1}^{\infty} a_l(1)(\nu d)^{-l}$$

and so the end effects scale as  $a_l \sim \nu^{-l}$ . This property is obeyed by equation (3.11) and (3.12) for  $a_1$  and  $a_2$ .

The experimental data of England and Elford (1987) for  $a_1$  (called  $\alpha_1$  in their paper) seem to indicate that  $a_1$  is almost independent of pressure. This discrepancy is surprising in view of the clear nature of the pressure dependence derived in this section. One must conclude that other effects must play a significant rôle in the total end-effect. One such effect might be an error in the initial position of the swarm. For example, a delta function pulse of the form  $n(z, 0) = \delta(z - \epsilon)$ , where  $\epsilon$  is the true centroid of the initial pulse, will give rise to a pressure independent component of  $\xi_{01}$ .

### 3.7 Separation of the Different End Effects.

In this section, we propose an answer to an idealized problem: Given that the only source of end effects are those discussed so far, how might one disentangle these two different effects from experimental data? This is tantamount to asking how the drift time for the centroid of the swarm might be measured, as (from eq. 4) this measurement is influenced only by the non-hydrodynamic process.

We assume that the collector current can be recorded as a function of drift length and time, and that the drift velocity  $\omega_{01}$  and the diffusion coefficient  $\omega_{02}$  are known for the system (presumably by extrapolating the data to infinite drift lengths). Then taking the first moment of the current, we have

$$\begin{aligned} \int_{-\infty}^{\infty} zi(z, t)dz &= \int z \sum_{j=1}^{\infty} \omega_{0j} (-\partial_z)^{j-1} n d\mathbf{r} \\ &= \omega_{01} \int z n d\mathbf{r} - \omega_{02} \int n d\mathbf{r} \\ &= \omega_{01} \bar{z}(t) - \omega_{02} \end{aligned}$$

where  $\bar{z}(t)$  is the position of the centroid at time  $t$ , and in the last line,  $n$  has been normalized. At large times, according to (3.1), this should become

linear in  $t$  with slope  $\omega_{01}$ . The intercept of this line with the  $t = 0$  axis will give the value of  $\xi_{01}$ .

### 3.8 Boundaries and Field Inhomogeneities

England and Elford (1987) discuss the end-effects in mobility measurements under five headings; those of contact potentials, non-hydrodynamic effects, higher-order diffusion effects, field interpenetration and boundary effects. The first effect is simply an error in the measured value of the drift potential, which introduces an uncertainty proportional to  $1/d$  in the the electric field. In this chapter, I have examined the second two effects, and showed that they give rise to corrections in the form of a power series in  $1/d$  of about the same magnitude as observed in experiment.

The final two effects are due to inhomogeneities in the field caused by the shutters being imperfect, and those due to the selective removal of particles incident on the boundaries of the apparatus. The theory is formally the same, and it would appear that either effect is quite difficult to describe. Formally we would include these effects into the Boltzmann equation by writing an additional operator  $\mathcal{B}$  which represents the loss of particles to the boundary or the scattering of particles on a field inhomogeneity. This operator is localized, and may be idealized as being proportional to a surface delta function.

If one has the free space Greens function  $G_0$  (e.g. eq (2.23)), then one can write the complete Greens function in the presence of a boundary as a Dyson equation: [Kumar (1984)]

$$G = G_0 \sum_{n=0}^{\infty} (\mathcal{B}G_0)^n. \quad (3.13)$$

If we consider an operator  $\mathcal{B}$  representing a completely impenetrable barrier, then the two regions must be causally unconnected, i.e.  $G(\mathbf{r}, \mathbf{r}') = 0$  where  $\mathbf{r}$  and  $\mathbf{r}'$  lie on opposite sides of the barrier. However, this would imply that  $G$  is not an analytic function, and so that the approximation (3.13) in terms of analytic functions is doomed at best to be slowly convergent. Furthermore, the correction terms to the free space Greens function must be of infinite range.

Another method, in which the corrections to the free space solution are localized around the boundary, involves taking linear combinations of free

space solutions valid in half spaces on either side of the boundary, and requiring them to satisfy some auxiliary condition at the boundary. A lot of work has been done with this method considering a one-dimensional Klein-Kramers equation with an absorbing or reflecting barrier at the origin. See Selinger and Titulaer (1984) for a review. Even in this simple case, the method is said to be slowly convergent owing to the problems of approximating non-analytic functions. It may be more feasible to consider a leaky barrier, or a field inhomogeneity where presumably this is not a problem, and then to extrapolate the results to an impenetrable barrier. Furthermore, the analytic result of Marshall and Watson (1987) may provide some insight on this particular problem.

As to the original problem of how the boundaries affect swarm measurements, these methods prove to be intractable owing to the complex geometries found inside a typical drift tube. What is needed is a new paradigm in which the form of the boundary effects is independent of the specific details of shutter design etc., in much the same way as thermodynamics is independent of the specific details of molecular motion. Without this, one cannot be satisfied that we completely understand how to correct the swarm data in spite of the successes of the empirical methods used to date.

## Chapter 4

# Non-hydrodynamic effects in Parallel Plane Steady State Townsend Experiments

### 4.1 Steady State Townsend Experiments

In these experiments, the source of charged particles is constant in time [Huxley and Crompton(1974)]. The usual transport coefficients measured by this technique are the first Townsend ionization coefficient, and diffusion perpendicular to the field (lateral diffusion). The ionization coefficient is measured in a parallel plane apparatus where the variation of the source in the radial direction can be ignored (figure 4.1).

The current obtained at the collector is measured as a function of the distance  $d$  between the electrodes. If charged particles are ionizing the background gas, then the density of charged particles in the drift region is found to vary exponentially as  $n \sim \exp(\alpha_T d)$ , where  $\alpha_T$  is known as the first Townsend ionization coefficient.

Lateral diffusion is measured by means of a split collector (fig 4.2). In this case, the source has small diameter compared with the dimensions of the apparatus (idealized as a point source). The diffusion perpendicular to the field is extracted from the ratio of currents measured on section A and B. Before 1967, it was assumed that diffusion had the same value in all directions. That this is not the case was shown by Wagner, Davis and Hurst

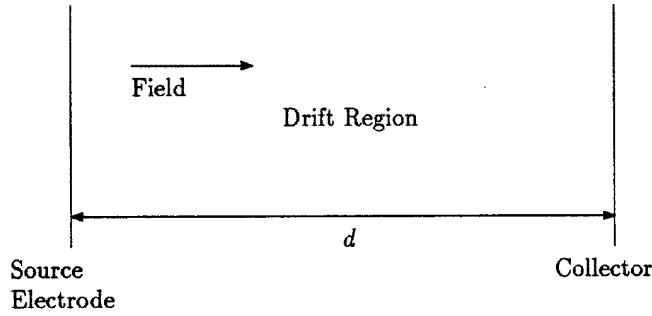


Figure 4.1: Parallel Plane Steady State Townsend Experiment

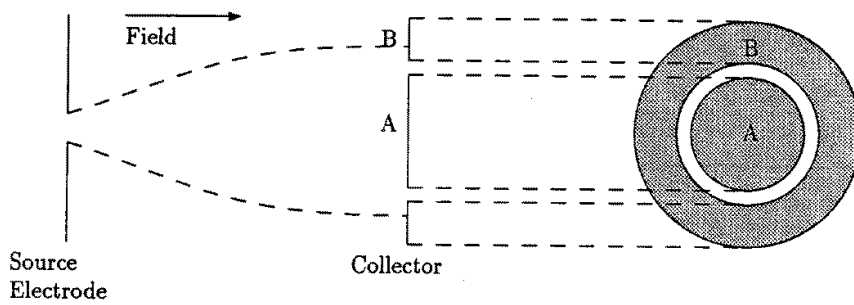


Figure 4.2: Townsend-Huxley Diffusion Experiment. Ratio of currents received by sections A and B are measured.

(1967) who from time of flight experiments obtained coefficients of diffusion parallel to the field direction that were different to those obtained by the Townsend-Huxley method.

## 4.2 Conventional Theories

In the previous chapters, I have developed a theory on the form of non-hydrodynamic effects in time of flight experiments. The obvious extension to this work is to develop such a theory for the other main classes of

swarm experiments, namely the Steady State Townsend experiments and the Pulsed Townsend experiment. In this chapter, I develop a theory of the parallel plane experiment. The generalization to the Townsend-Huxley experiment, involving as it does elements of multivariable complex analysis, is not straightforward, and so little will be said in this case.

In the conventional theory of steady state experiments, the diffusion equation (2.2) is solved with the time derivative set to zero. The homogeneous equation gives rise to solutions in terms of modified Bessel functions of half integer order, which are merely polynomials in the inverse distance from the source, multiplied by an exponential of this distance. At large distances, the dominant term from a compact source is  $n \propto \rho^{-1} \exp(\omega_{01}z/2\omega_{02} - 2\delta\rho)$ , where  $\rho^2 = (x^2 + y^2)/4\omega_{20} + z^2/4\omega_{02}$  and  $\delta = (\omega_{01}^2/4\omega_{02} - \omega_{00})^{1/2}$ . For a planar source, as in the parallel plane experiment, the dominant term is  $n \propto \exp([\omega_{01} - \sqrt{\omega_{01}^2 - 4\omega_{02}\omega_{00}}]z/2\omega_{02})$ , which as noted in the previous section, is seen experimentally. The remaining terms, in the case of a compact source, arise from the structure of the source. These decay polynomially with respect to the dominant mode, away from the source. Since these effects are clustered near the source, a full theory should also include a description of the relaxation to local thermal equilibrium of the particles as they leave the source. This requires a theory based on the Boltzmann equation.

The usual technique for analysing the parallel plane experiment by means of the Boltzmann equation was first developed by Thomas (1969), and subsequently used by many authors. This involves assuming the solution has an exponential dependence on distance. The Boltzmann equation with one spatial dimension is solved by solutions of the form

$$\exp(q_n^r z) \Psi_n(\mathbf{c}, q_n^r), \quad (4.1)$$

where the  $q_n^r$  are the roots of  $\omega_n(q_n^r) = 0$ , where  $r$  indexes the roots of  $\omega_n$ . It might be supposed that only solutions (4.1) are needed for the general solution:

$$f(\mathbf{c}, z) = \sum_{n,r} a_n^r \exp(q_n^r z) \Psi_n(\mathbf{c}, q_n^r). \quad (4.2)$$

Since it is known experimentally that the distribution function varies exponentially as a function of the distance from the source, one might assume that there is a root whose real part is larger than all the others, and so contributes dominantly to the distribution function at large distances from the source. If this is the case, then we can identify this root with  $\alpha_T$ .

For the one dimensional Klein-Kramers model, one can readily solve  $\omega_n(q_n^r) = 0$  from the one dimensional version of (2.22). In the following, we will use dimensionless units, in which  $\nu_1 = 1$  and  $\nu_2 = \frac{1}{2}$ . In these units, the mean free time of the charged particle is  $\frac{m}{M}$  and the mean free path is  $\frac{1}{2} \left(\frac{m}{M}\right)^3$ . From the usual quadratic formula, the roots of  $\omega_n(q_n^\pm)$  are easily found to be

$$q_n^\pm = a \pm \left[ a^2 + 2(n - \nu) \right]^{\frac{1}{2}}. \quad (4.3)$$

The first Townsend ionization coefficient can be identified with the largest root of the negative branch  $q_0^-$ . [Blevin and Fletcher (1984)] There are an infinite number of positive branch roots that one would expect to dominate over the  $q_0^-$  term in (4.2), and so (4.2) does not in this case agree with what one expects to see physically. This raises the question of why only the negative branch roots contribute to the solution, and of what role the positive branch roots play. To get some insight into the problem, the number density was computed numerically for the Klein-Kramers model. This work has been reported as Standish (1989).

### 4.3 Numerical Studies of the Klein-Kramers model

We numerically computed the number density  $\int_{-\infty}^{\infty} f(c, z) dc$  as a function of  $z$ , and the reaction rate  $\nu$ . In these computations charged particles are injected at a constant rate into the drift region with velocity equal to the drift velocity,  $a$ , which is set to unity. The computations were carried out using the exact form of the Greens function (2.24).

The phase space distribution may be found by integrating the Greens function over source times  $0 \leq t' \leq t$ :

$$\begin{aligned} f(c, z, t) &= \int_0^t \int_{-\infty}^{\infty} \int_{-\infty}^{\infty} G(c, z, t; c', z', t') S(c', z', t') dc' dz' dt' \\ &= \int_0^t G(c, z, t; a, 0, t') dt'. \end{aligned} \quad (4.4)$$

Firstly the integration over  $c$  to find the number density was performed analytically, and then the time integration was performed numerically using an

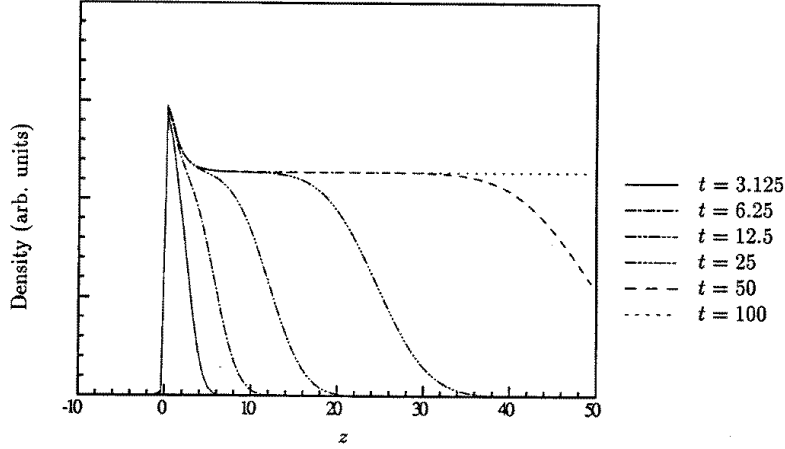


Figure 4.3: Density for  $\nu = 0$ . In the following four figures the curves shown are at successively greater times after the source is switched on.

adaptive integrator. Plates 1 to 3 show  $f(c, z, t)$  at times  $t = 6$ ,  $t = 25$ , and  $t = 100$  respectively, for the reactionless case  $\nu = 0$ .

Figures 4.3 to 4.6 show the effect of varying the reaction rate  $\nu$ . In the cases where  $\nu < a^2/2$ , the distribution builds up to a steady state distribution. Non-hydrodynamic effects manifest themselves in a neighbourhood of size  $(q_0^- - q_1^-)^{-1}$  ( $= 1.374, 1.366$  and  $0.995$  for  $\nu = -0.01, 0$  and  $0.01$ ) around the origin. Outside this region, the non-hydrodynamic modes ( $n \neq 0$ ) are damped exponentially with respect to the hydrodynamic mode ( $n = 0$ ), and it is here that we see exponential behaviour governed by the Townsend ionization coefficient. In figures 4.7 and 4.8, the steady state distribution is plotted on a logarithmic plot. It can be seen that the density behaves exponentially in  $z$  far from the source. The slopes at either extremity give  $q_0^-$  downstream of the source, and  $q_0^+$  upstream. This is evidence that the positive branch roots control the spatial decay of particles diffusing against the electric field.

In figure 4.6, the reaction rate has been increased to larger than  $a^2/2$ . In this case, no steady state is seen to occur. Rather, the density of charged particles increases exponentially in time. Physically this can be understood as the electric field not being strong enough to remove at a sufficiently rapid

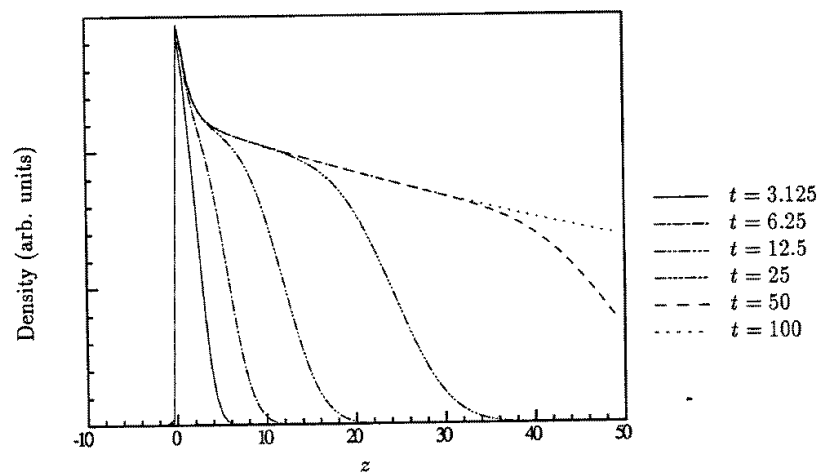


Figure 4.4: Density for  $\nu = -0.01$ .

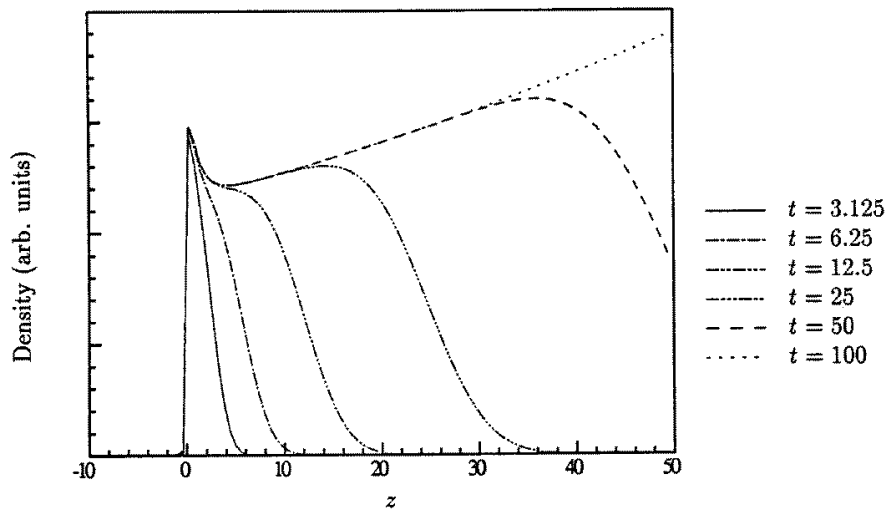


Figure 4.5: Density for  $\nu = 0.01$ .

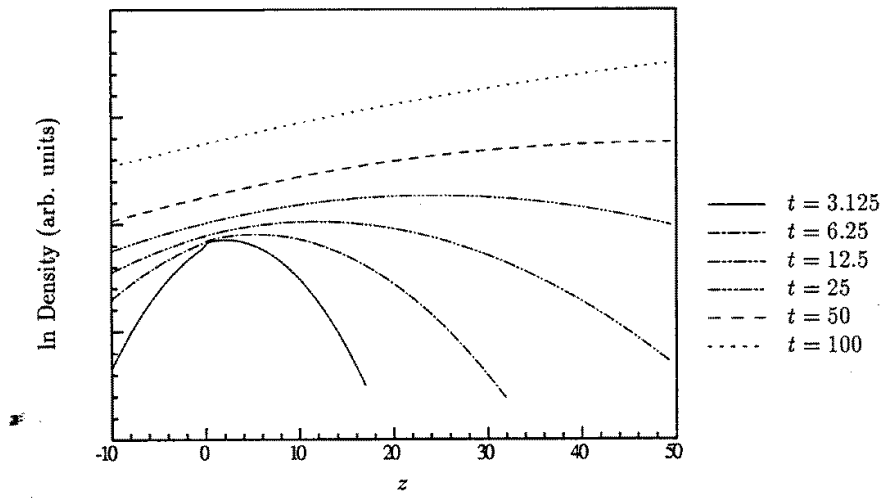


Figure 4.6: ln Density for  $\nu = 1$ .

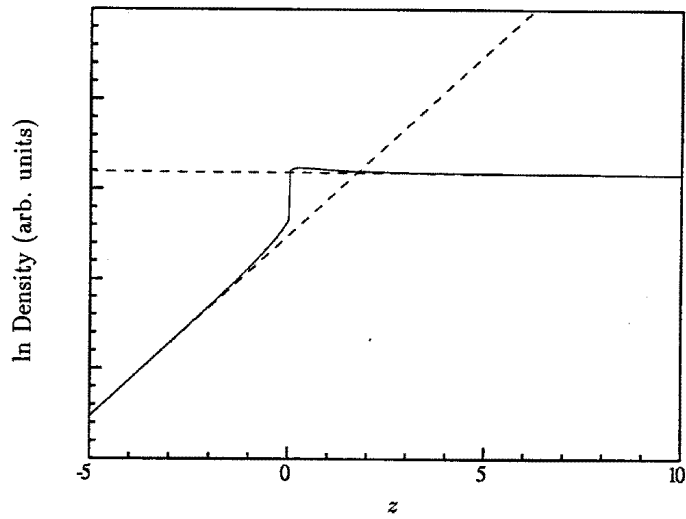


Figure 4.7: Logarithmic plot of the steady state density for the case  $\nu = -0.01$ . Lines fitted to the tails of the distribution have slopes corresponding to  $q_0^+ = 2.01$  and  $q_0^- = -0.01$  respectively.

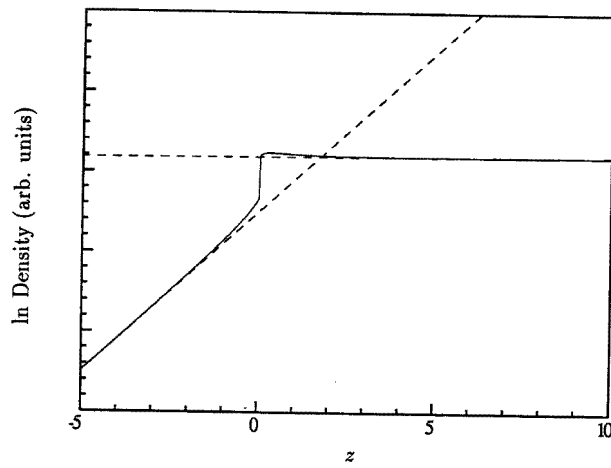


Figure 4.8: Logarithmic plot of the steady state density for the case  $\nu = 0.01$ . Lines fitted to the tails of the distribution have slopes corresponding to  $q_0^+ = 1.98$  and  $q_0^- = 0.01$  respectively.

rate the charged particles created by ionization. This effect will be seen to arise out of the analysis in the next section.

## 4.4 Asymptotic behaviour for large times and distances

In the previous section, we examined a model in which there were an infinite number of roots  $q_n^r$  of either sign. The numerical work indicates that the root  $q_0^-$  controls the asymptotic exponential behaviour downstream from the source, and that  $q_0^+$  controls the behaviour upstream. In this section, we discuss the time dependence analytically, and show how the steady state solution is established. It will be seen that the positive and negative branches of the roots control the swarm behaviour upstream and downstream of the source respectively.

Let us initially model the situation with a one dimensional time dependent diffusion equation with a constant source switched on at time  $t = 0$ :

$$\partial_t n - \omega_{02} \partial_z^2 n + \omega_{01} \partial_z n - \omega_{00} n = \Theta(t).$$

The solution can be found by integrating the shifted Gaussian solution (2.3) with respect to time [Abramowitz and Stegun (1965) 7.4.33]:

$$\begin{aligned} n(z, t) &= (4\pi\omega_{02})^{-\frac{1}{2}} \int_0^t t'^{-\frac{1}{2}} \exp\left(\frac{\omega_{01}}{2\omega_{02}}z - \delta^2 t' - \frac{z^2}{4\omega_{02}t'}\right) dt' \\ &= (4\delta)^{-1} \omega_{02}^{-\frac{1}{2}} \exp\left(\frac{\omega_{01}}{2\omega_{02}}z\right) \left[ \exp\left(-\delta z \omega_{02}^{-\frac{1}{2}}\right) \operatorname{erfc}\left(z(4\omega_{02}t)^{-\frac{1}{2}} - \delta t^{\frac{1}{2}}\right) - \right. \\ &\quad \left. \exp\left(\delta z \omega_{02}^{-\frac{1}{2}}\right) \operatorname{erfc}\left(z(4\omega_{02}t)^{-\frac{1}{2}} + \delta t^{\frac{1}{2}}\right) \right]. \end{aligned}$$

The error functions are nearly constant over most of the real line, but change sharply from one value to another near the origin. The effect is of wave fronts in the form of error functions propagating at velocity  $\delta$  leaving exponential functions in their wake, as shown in figure 4.9.

This model gives us the dynamical picture. We now must turn to a full Boltzmann equation theory to determine how non-hydrodynamic modes enter

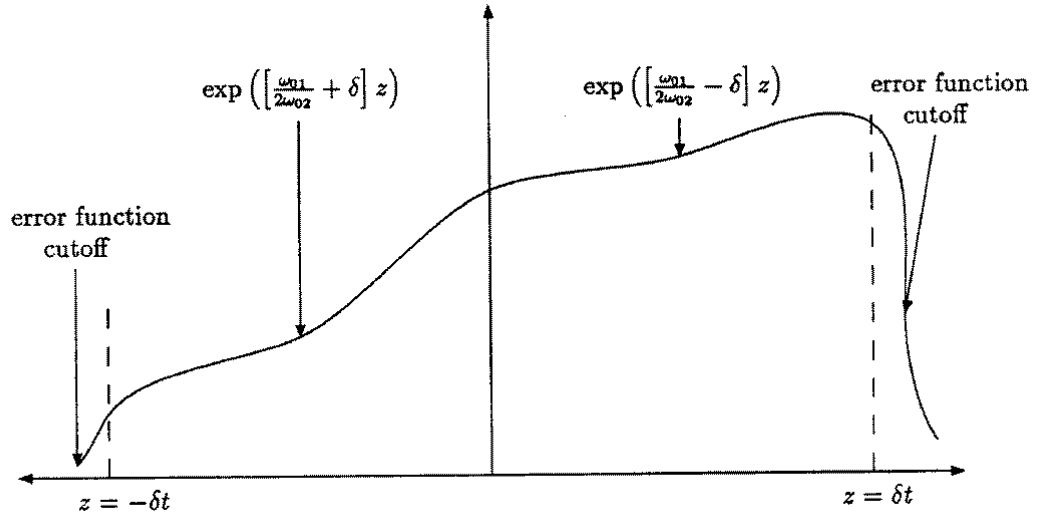


Figure 4.9: Sketch of the density with the important features labelled

this picture. We start with the spatially one dimensional time dependent Boltzmann equation for a steady source  $S(\mathbf{c}, z)$  switched on at  $t = 0$ .

$$(\partial_t + c_z \partial_z + a \partial_c + \mathcal{J}) f(\mathbf{c}, z, t) = S(\mathbf{c}, z) \Theta(t). \quad (4.5)$$

This may be formally solved by means of the assumption of a discrete spectrum [eq. (2.8)] to give

$$f(\mathbf{c}, z, t) = \sum_n f_n(\mathbf{c}, z, t) \equiv \sum_n \int_{-\infty}^{\infty} \frac{s_n(\mathbf{c}, ik)}{\omega_n(ik)} \exp(ikz) \{1 - \exp(\omega_n(ik)t)\} dk \quad (4.6)$$

where

$$s_n(\mathbf{c}, ik) = \frac{1}{2\pi} \Psi(\mathbf{c}, ik) \iint \exp(-ikz') \Phi_n(\mathbf{c}', ik) S(\mathbf{c}', z') d\mathbf{c}' dz'. \quad (4.7)$$

We assume that the source has been chosen in such a way that the integral over  $k$  in (4.6) is well defined. For example, with the Klein-Kramers model we may choose a Gaussian source located at  $z = 0$ :

$$S(\mathbf{c}, z) = \exp(-\sigma c^2) \delta(z). \quad (4.8)$$

Upon substituting (2.21) and (4.8) into (4.7), we find

$$s_n(c, ik) = \frac{\left(1 - \frac{1}{\sigma}\right)^{\frac{n}{2}}}{\sigma^{\frac{1}{2}} 2^n n!} \exp\left(\left(1 - \frac{1}{4\sigma}\right)k^2 - (c - 2a)ik - (c - a)^2\right) \times \\ \text{H}_n\left(\frac{ik\left(1 - \frac{1}{2\sigma}\right) - a}{\left(1 - \frac{1}{\sigma}\right)^{\frac{1}{2}}}\right) \text{H}_n(c - a + ik). \quad (4.9)$$

To get  $s_n$  to vanish fast enough as  $k \rightarrow \pm\infty$  for (4.6) to be convergent, we must choose  $\sigma < \frac{1}{4}$ .

Assuming  $s_n$  and  $\omega_n$  are analytic functions of  $k$ , the integrand in (4.6) is analytic. Also,  $s_n(c, ik) \rightarrow 0$  as  $\text{Re}(k) \rightarrow \pm\infty$ , and so the contour of integration in (4.6) may be translated by an arbitrary amount. In particular, we may move the contour so that it passes through the saddle point  $-iQ_n$  of  $\omega_n(ik)$ , which in the Klein-Kramers case is  $-ai$ . We may then use the method of steepest descent [Jeffreys (1961)] to evaluate the time dependent portion of the integral at large times:

$$f_n(\mathbf{c}, z, t) \sim \int_{-\infty+Q_n i}^{\infty+Q_n i} \frac{s_n(\mathbf{c}, ik) \exp(ikz)}{\omega_n(ik)} dk \\ - \exp(\omega_n(Q_n)t) \left(\frac{2\pi}{t}\right)^{\frac{1}{2}} \frac{s_n(\mathbf{c}, Q_n) \exp(Q_n z)}{\omega_n(Q_n) (-\omega_n''(Q_n))}. \quad (4.10)$$

The behaviour of  $f$  in time will depend critically upon the signs of  $\omega_n(Q_n)$ . If  $\omega_n(Q_n)$  is positive for any  $n$ , then the time dependent part will grow exponentially, and the system will not approach a steady state. On the other hand, if  $\omega_n(Q_n)$  is negative for all  $n$ , then the time dependent term is exponentially damped, and a steady state is reached. In the Klein-Kramers case,

$$\omega_n(Q_n) = \nu - n - a^2/2. \quad (4.11)$$

If  $\nu > a^2/2$ , then there is no steady state approached (figure 4.6), otherwise the system does approach a steady state (figs 4.3 to 4.5).

Let us consider a system satisfying  $\omega_n(Q_n) < 0$  for all  $n$ . The steady state term is given by the integral in (4.10). Since  $s_n$  and  $\omega_n$  are analytic, the only singularities of the integrand occur at the zeros of  $\omega_n$ . In the Klein-Kramers case, there are only two singularities as shown in fig 4.10. The contour of

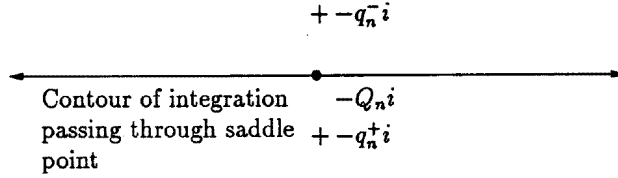


Figure 4.10: Singularity structure of  $s_n(c, ik)/\omega_n(ik)$  for the Klein-Kramers model. There are two simple poles at  $-q_n^\pm i$ , and a saddle point at  $-Q_n i = -(q_n^+ + q_n^-)i$ . The fact that the contour of integration must lie between the poles determines that the negative branch controls downstream behaviour, and that the positive branch determines upstream behaviour.

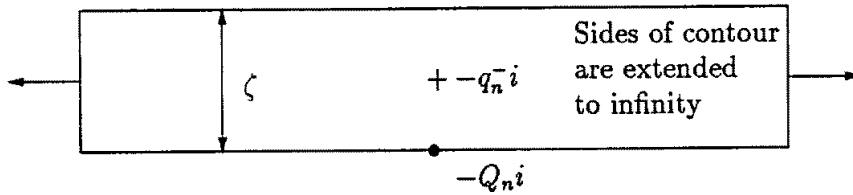


Figure 4.11: Contour used for the large  $z$  asymptotic argument.

integration must lie between the poles  $q_n^+$  and  $q_n^-$  for the time dependent term to approach zero according to (4.10). As we shall see, this leads to the term proportional to  $\exp(q_n^+ z)$  not contributing to the distribution at positive  $z$  and similarly the  $\exp(q_n^- z)$  term not contributing to the distribution at negative  $z$ .

Since in general, as in the Klein-Kramers model,  $s_n$  grows much faster than any exponential as  $k \rightarrow \pm i\infty$ , it is not possible to evaluate the integral in (4.10) by completing the contour around the positive imaginary half plane for positive  $z$ , and around the negative half plane for negative  $z$ . Instead, we must use a large  $z$  asymptotic argument that is similar to the method described in section 2.6 of Jeffreys (1961). In this, we complete the contour

in the fashion shown in fig 4.11, with  $\zeta$  an arbitrarily large positive but finite value. We may now apply Cauchy's residue theorem to obtain

$$f_n(\mathbf{c}, z, \infty) = \int_{-\infty+Q_n i}^{\infty+Q_n i} \frac{s_n(\mathbf{c}, ik) \exp(ikz)}{\omega_n(ik)} dk = \quad (4.12)$$

$$2\pi i \exp(q_n^- z) \text{Res} \left( \frac{s_n(\mathbf{c}, ik)}{\omega_n(ik)}, iq_n^- \right) + \int_{-\infty+(Q_n+\zeta)i}^{\infty+(Q_n+\zeta)i} \frac{s_n(\mathbf{c}, ik) \exp(ikz)}{\omega_n(ik)} dk.$$

But the absolute value of the second term is

$$\left| \int_{-\infty+(Q_n+\zeta)i}^{\infty+(Q_n+\zeta)i} \frac{s_n(\mathbf{c}, ik) \exp(ikz)}{\omega_n(ik)} dk \right|$$

$$\leq \exp(-[\zeta + Q_n]z) \int_{-\infty+(Q_n+\zeta)i}^{\infty+(Q_n+\zeta)i} \left| \frac{s_n(\mathbf{c}, ik)}{\omega_n(ik)} \right| dk.$$

Since  $\zeta$  may be chosen arbitrarily large, the second term must vanish faster than any exponential as a function of  $z$ , and so

$$f_n(\mathbf{c}, z, \infty) \sim 2\pi i \exp(q_n^- z) \text{Res} \left( \frac{s_n(\mathbf{c}, ik)}{\omega_n(ik)}, iq_n^- \right) \text{ as } z \rightarrow \infty. \quad (4.13)$$

By taking  $\zeta$  negative, one can similarly show that

$$f_n(\mathbf{c}, z, \infty) \sim 2\pi i \exp(q_n^+ z) \text{Res} \left( \frac{s_n(\mathbf{c}, ik)}{\omega_n(ik)}, iq_n^+ \right) \text{ as } z \rightarrow -\infty. \quad (4.14)$$

In general, we may state the selection principle thus: the contour passing through the saddle point of  $\text{Re}(\omega_n(ik))$  divides the complex plane; those roots of  $\omega_n$  that lie above this contour contribute to the asymptotic behaviour of  $f_n$  downstream of the source, and those that lie below contribute to the asymptotic behaviour upstream of the source.

## 4.5 Discussion

In this chapter, a non-hydrodynamic theory of the parallel plane steady state Townsend experiment is developed relating the asymptotic properties of the steady state solution to the distribution of zeros of the eigenvalues  $\omega_n(ik)$  of the inhomogeneous Boltzmann operator  $ick + a\partial_c + \mathcal{J}$ . It was found

that non-hydrodynamic effects are clustered around the source, and decay exponentially away from the source.

The spectrum of  $ick + a\partial_c + \mathcal{J}$  was taken to be discrete and the eigenvalues and eigenfunctions taken to be analytic functions of  $k$ . These assumptions were chosen to make the theory simple, and are sufficient for understanding the simple model used in this work. However, in general, the situation may be more complex. Consider what would happen if  $s_n$  from equation (4.9) is not analytic everywhere, but has a singularity at say  $ik_0$ . If this singularity is a pole, then the effect is of an additional term that behaves like  $\exp(k_0z)$  in the steady state solution. If, however, the singularity is part of a branch cut, then there is an additional term whose form is not generally exponential, but will be bounded asymptotically by  $\exp(k_0z)$ .

A similar situation arises if the spectrum contains a continuous portion. Here we might expect that the sum over  $n$  is replaced by the integration over a continuous parameter  $\lambda$ :

$$f_{\text{cont}}(\mathbf{c}, z, \infty) \sim 2\pi i \int \exp(q_\lambda z) \text{Res} \left( \frac{s_\lambda(\mathbf{c}, ik)}{\omega_\lambda(ik)}, iq_\lambda \right) d\lambda.$$

If  $\text{Re}(q_\lambda)$  is always less than some value  $Q$ , then  $f_{\text{cont}}$  will be bounded by an exponential of the form  $\exp(Qz)$ . Needless to say, the formal theory of continuous spectra is beyond the scope of this work. The purpose of mentioning it here is to point out how this work might be generalized to handle these cases.

# Chapter 5

## Nonequilibrium Molecular Dynamics Simulation

### 5.1 Thermostatted Equations of Motion

Consider a classical system of  $N$  particles. The state of the system is uniquely specified by the  $3N$  spatial co-ordinates  $q_{ix}, q_{iy}, q_{iz}$  and the  $3N$  momentum co-ordinates  $p_{ix}, p_{iy}, p_{iz}$ . The  $6N$  dimensional vector  $\Gamma$  consisting of the positions and momenta for all particles is a point in the phase space of the system. The dynamics of the system evolving in time is described by the trajectory of the phase point through phase space. The trajectory is given by Hamilton's equations:

$$\dot{\mathbf{q}}_j = \frac{\partial H}{\partial \mathbf{p}_j}, \quad \dot{\mathbf{p}}_j = -\frac{\partial H}{\partial \mathbf{q}_j}. \quad (5.1)$$

Linear transport coefficients, (e.g.  $\eta$  and  $\eta_v$ ) can be calculated from computer simulations of molecules obeying eq. (5.1) by means of the Green-Kubo relations. These have proved to be of enormous value in experimental and theoretical applications. If we wish to extend the theory to non-linear steady states, then we are faced with two problems; one being the inclusion of higher order terms in the perturbation due to the external field, and the other due to thermostating. In a dissipative process, such as shear flow, the temperature would rise in the system if the heat generated is not removed by a heat sink. This effect is second order in the small field limit ( $\dot{H} = -JF_e = LF_e^2$ ,

with  $L$  being the linear transport coefficient relating  $F_e$  to  $J$ ), and can be ignored in the linear theory, but needs to be included in non-linear theories.

The most obvious way of modelling the non-equilibrium steady state is to include the interactions of the system with the outside world. This method is impractical owing to the high complexity of these interactions, and the large surface effects inherent in modelling small systems (computer simulations typically involve  $10^2$  to  $10^5$  molecules). It turns out that the heat sink can be modelled by means of a friction-like term, which acts as a thermostat, and that provided the dissipation is not too large, the Transient Time Correlation Functions we will derive are independent of what model thermostat is used [Evans and Morriss (1984), Evans and Holian (1985)].

The thermostatted equations of motion are

$$\begin{aligned}\dot{\mathbf{q}}_i &= \frac{\mathbf{p}_i}{m} \\ \dot{\mathbf{p}}_i &= \mathbf{F}_i - \alpha \mathbf{p}_i,\end{aligned}\tag{5.2}$$

where  $\mathbf{F}_i$  describes the force on molecule  $i$  due to all the other molecules. The momenta in this equation are *peculiar*, *i.e.* measured with respect to the motion of the centre of mass so that  $\sum_i \mathbf{p}_i = 0$ . The first model thermostat is produced by requiring that the kinetic energy be a constant of motion:

$$\sum_i \mathbf{p}_i \cdot \dot{\mathbf{p}}_i = 0 \implies \alpha = \frac{\sum_i \mathbf{F}_i \cdot \mathbf{p}_i}{\sum_i p_i^2}\tag{5.3}$$

This is known as the Gaussian thermostat, after Gauss's principle of least constraint [Hoover *et al.* (1982), Evans (1983)]. This feedback mechanism does not constrain the *actual* value of the kinetic energy required, it only constrains the time derivative to be zero. This implies that the propagator (to be defined in the next section) will commute with the operation of differentiation with respect to temperature, allowing equilibrium fluctuation expressions for the second order, or derived thermodynamic quantities, such as specific heats. Such a thermostat is called *differential*. The equilibrium distribution in this case is given by

$$f_K(\Gamma) = \frac{\delta(K - K_0)e^{-\beta\Phi(\mathbf{q})}}{\int \delta(K - K_0)e^{-\beta\Phi(\mathbf{q})}d\Gamma},\tag{5.4}$$

where  $\mathbf{F}_i = -\partial_{\mathbf{q}_i}\Phi$ ,  $K = \sum_i \frac{p_i^2}{2m}$ ,  $K_0 = \frac{3}{2}N\beta^{-1} = \frac{3}{2}Nk_B T$ . This distribution is called the isokinetic distribution.

The other common thermostating method was first proposed by Nosé (1984a; 1984b). The original formulation by Nosé involved a cumbersome external reservoir and a non-linear time transformation. Hoover (1985) made significant simplifications to the method, which has since become known as the Nosé-Hoover thermostat. The basic idea is to extend phase space by adding the variable  $\alpha$ , whose equation of motion is given by

$$\dot{\alpha} = (K - K_0)/Q. \quad (5.5)$$

Thus  $\alpha$  acts to keep the kinetic energy fluctuating about the target value  $K_0$ , with the timescale of the fluctuations being proportional to  $Q$ . The parameter  $Q$  is arbitrary, but the  $Q = 0$  case, which corresponds to the kinetic energy being rigidly constrained, has infinitely stiff equations of motion. In practice, its value is determined from numerical experiments. The equilibrium distribution generated by the Nosé-Hoover equations of motion is canonical:

$$f_c(\mathbf{\Gamma}) = \frac{\exp(-\beta[H_0 + Q\alpha^2/2])}{\int \exp(-\beta[H_0 + Q\alpha^2/2])d\mathbf{\Gamma}}, \quad (5.6)$$

where  $H_0 = \sum_i \frac{p_i^2}{2m} + \Phi(\mathbf{q})$ . In contrast to the former thermostat, this is an integral thermostat, with the value of  $\alpha$  depending on all past states of the system.

## 5.2 Formal Solution of Liouville's Equation

We may also consider an ensemble of such systems for which there are well defined macroscopic properties. This can be described by means of a distribution function  $f(\mathbf{\Gamma}, t)$  of phase space points within the ensemble. By considering the number of phase points entering and leaving an infinitesimal volume of phase point [Tolman (1962)], we get a generalized form of Liouville's equation:

$$\frac{\partial f(\mathbf{\Gamma}, t)}{\partial t} = -\frac{\partial}{\partial \mathbf{\Gamma}} \cdot (\dot{\mathbf{\Gamma}} f(\mathbf{\Gamma}, t)) \equiv -i\mathcal{L}f(\mathbf{\Gamma}, t). \quad (5.7)$$

The operator  $\mathcal{L}$  is called the f-Liouvillean. Equation (5.7) can be solved formally by integrating with respect to  $t$ :

$$f(\mathbf{\Gamma}, t) = \exp(-i\mathcal{L}t)f(\mathbf{\Gamma}, 0).$$

We can also consider the time dependence of a phase variable  $B$  as we follow a phase point through its trajectory:

$$\frac{dB}{dt} = \dot{\Gamma} \cdot \frac{\partial B}{\partial \Gamma} \equiv iLB(\Gamma).$$

The operator  $L$  is called the p-Liouvillean. This equation can be solved formally to give

$$B(\Gamma(t)) = \exp(iLt)B(\Gamma(0)).$$

The exponential of a Liouvillean is called a propagator. From now on, the abbreviation  $B(t) \equiv B(\Gamma(t))$  will be used.

The p-Liouvillean and the f-Liouvillean are hermitian adjoints of each other:

$$\begin{aligned} \int B(-i\mathcal{L})f d\Gamma &= \int B \left( -\frac{d}{d\Gamma} \cdot (\dot{\Gamma}f) \right) d\Gamma \\ &= \int \dot{\Gamma} \cdot \frac{\partial B}{\partial \Gamma} f d\Gamma = \int (iLB)f d\Gamma. \end{aligned} \quad (5.8)$$

If the system were described by a Hamiltonian, such as in equation (5.1), then Liouville's theorem,  $(\partial/\partial\Gamma) \cdot \Gamma = 0$ , would hold, and equation (5.7) takes the form of the usual Liouville equation. The existence of a Hamiltonian is sufficient, but not necessary for this condition to hold. In this case, the p- and f-Liouvilleans are identical and self adjoint. Since we wish to describe systems in a nonequilibrium steady state, the presence of dissipative terms implies distinct p- and f-Liouvilleans, and the general equation (5.7).

Macroscopic quantities are computed from microscopic quantities by means of phase averages, for example the temperature of the system ensemble (in equilibrium at least) is given by

$$T = \left\langle \sum_i \frac{p_i^2}{2m} \right\rangle = \int \sum_i \frac{p_i^2}{2m} d\Gamma.$$

We can determine the time evolution of the phase average by propagating the distribution function with the f-propagator, and then forming the phase average over a phase variable  $B$ :

$$\begin{aligned} \langle B(t) \rangle &= \int B(\Gamma) f(\Gamma, t) d\Gamma \\ &= \int B(\Gamma) \exp(-i\mathcal{L}t) f(\Gamma, 0) d\Gamma. \end{aligned} \quad (5.9)$$

By analogy with quantum mechanics, this is called the Schrödinger picture. Alternatively, one may form the phase average by following the phase variable along the trajectories:

$$\begin{aligned} \langle B(t) \rangle &= \int f(\mathbf{\Gamma}) B(t) d\mathbf{\Gamma} \\ &= \int f(\mathbf{\Gamma}) \exp(iLt) B(\mathbf{\Gamma}) d\mathbf{\Gamma}. \end{aligned} \quad (5.10)$$

This is the Heisenberg picture. The equivalence of the two pictures is guaranteed by the adjointness property (5.8).

### 5.3 Nonlinear Response Theory

In this section, a derivation of an expression for phase averages as they evolve after an external field is switched on is given. At the time  $t = 0$ , the distribution function is given by the equilibrium distribution,  $f(\mathbf{\Gamma}, 0) = f_{\text{eq}}(\mathbf{\Gamma})$ . Consider the impact of a steady external field,  $F_e$ , on the distribution. A discussion for the case where the external field has an arbitrary time dependence is much more complex [Evans and Morriss (1988)], and will not be given here. The external field  $F_e$  is switched on at  $t = 0$ , and changes the dynamics to

$$\begin{aligned} \dot{\mathbf{q}}_i &= \frac{p_i}{m} + \mathbf{C}_i F_e \\ \dot{\mathbf{p}}_i &= \mathbf{F}_i + \mathbf{D}_i F_e - \alpha \mathbf{p}_i, \end{aligned} \quad (5.11)$$

where  $\mathbf{C}_i$  and  $\mathbf{D}_i$  are phase variables determined by the system under study. In this derivation we will take the thermostating to be Nosé-Hoover, so the equilibrium distribution will be  $f_{\text{eq}} = f_c$ . The same argument can also be applied to the Gaussian thermostat, or to any other type, with identical results. In writing these equations, we are assuming that the momenta are measured with respect to the local streaming velocity of the fluid, hence the term ‘peculiar momenta’. At low Reynolds number, this presents no major difficulties, but in the turbulent flow regime new methods have to be applied [Evans and Morriss (1986)].

We assume that the external force  $F_e$  is properly conservative, so that in the absence of thermostating ( $\alpha = 0$ ), Liouville’s theorem holds. This

assumption is known as adiabatic incompressibility of phase space, or AIF for short. We can of course pursue the theory without invoking this assumption, but it has proven unnecessary to do so. With AIF, we can compute the phase space compressibility  $\Lambda = \frac{\partial}{\partial \Gamma} \cdot \dot{\Gamma} = -\frac{1}{f} \frac{\partial f}{\partial t}$  from (5.11):

$$\Lambda = \frac{\partial}{\partial \Gamma} \cdot \dot{\Gamma} = -3N\alpha(\Gamma).$$

The time evolution of  $f(\Gamma, t)$  from its initial state  $f_c(\Gamma)$  can now be computed using Morriss's lemma, [Morriss and Evans (1985)] which states:

$$\exp(i\mathcal{L}t) = \exp\left(\int_0^t \Lambda(s) ds\right) \exp(iLt). \quad (5.12)$$

The proof of this uses Dyson's equation [see Evans and Standish (1990)]:

$$e^{iLt} = e^{iL_0t} + \int_0^t e^{iL(t-s)} i\Delta L e^{iL_0s} ds, \quad (5.13)$$

where  $\Delta L = L - L_0$ .

The time evolution is given by

$$f(\Gamma, t) = e^{-i\mathcal{L}t} f_c(\Gamma) \quad (5.14)$$

$$= \exp\left(-\int_0^t \Lambda(s) ds\right) e^{-iLt} e^{-\beta(H_0 + Q\alpha^2/2)} \quad (5.15)$$

$$= \exp\left(\int_0^t 3N\alpha(-s) ds\right) e^{-\beta[H(-s) + Q\alpha(-s)^2/2]}. \quad (5.16)$$

The exponent  $H + Q\alpha^2/2$  can be expressed in terms of its time derivative:

$$H(-t) + Q\alpha(-t)^2/2 = H(0) - \int_0^t \dot{H}(-s) + Q\alpha(-s)\dot{\alpha}(-s) ds.$$

Upon substituting this, we get

$$f(\Gamma, t) = \exp\left[\int_0^t 3N\alpha(-s) + \beta[\dot{H}(-s) + [K - K_0]\alpha(-s)] ds\right] f_c(\Gamma). \quad (5.17)$$

Now we can write

$$\dot{H} = \dot{H}^{\text{ad}} - \alpha K$$

where  $\dot{H}^{\text{ad}}$  is the rate of change of internal energy with the thermostating turned off. This is related to dissipative flux  $J(\Gamma)$  through

$$J = -\dot{H}^{\text{ad}}/F_e. \quad (5.18)$$

Substituting this into (5.17) gives

$$f(\Gamma, t) = f_c(\Gamma) \exp \left[ -\beta \int_0^t J(-s) F_e ds \right]. \quad (5.19)$$

This is the Kawasaki distribution function [Yamada and Kawasaki (1967), Morriss and Evans (1985)], which describes the phase space distribution that has evolved under the influence of a dissipative force  $F_e$ , and thermostating has been used to guarantee a steady state. According to the Schrödinger picture, (5.9), we can evaluate Kawasaki phase averages for a typical phase variable  $B$ :

$$\langle B(t) \rangle = \frac{\langle B(\Gamma) \exp \left( -\beta \int_0^t J(-s) F_e ds \right) \rangle_c}{\langle \exp \left( -\beta \int_0^t J(-s) F_e ds \right) \rangle_c}, \quad (5.20)$$

where  $\langle \dots \rangle_c$  means average over phase space distribution  $f_c$ . The time evolution implicit in (5.20) is generated by the full, field dependent, thermostatted equations of motion (5.11).

In the case of the Gaussian thermostat, only equations (5.14) through (5.17) differ. The corresponding equations are

$$\begin{aligned} f(\Gamma, t) &= e^{-i\mathcal{L}t} f_K(\Gamma) \\ &= \exp \left( -\int_0^t \Lambda(s) ds \right) e^{-iLt} \delta(K - K_0) e^{-\beta\Phi} \\ &= \exp \left( \int_0^t 3N\alpha(-s) ds \right) \delta(K - K_0) e^{-\beta\Phi(-s)}. \end{aligned} \quad (5.21)$$

The time derivative of  $\Phi$  is similarly related to the adiabatic heating of the system:  $\dot{\Phi} = \dot{H}^{\text{ad}} - 3N\alpha\beta^{-1}$ . Upon substituting this into (5.21), one obtains the Kawasaki distribution:

$$f(\Gamma, t) = f_K(\Gamma) \exp \left[ -\beta \int_0^t J(-s) F_e ds \right]. \quad (5.22)$$

The phase average (5.20) is difficult to work with owing to the extensive nature of the argument to the exponential. We can cast this phase average

into an easier form to work with by differentiating (5.20) with respect to time:

$$\begin{aligned}
\frac{d}{dt} \langle B(t) \rangle &= \frac{-\beta F_e \langle B(0) J(-t) \exp(-\beta \int_0^t J(-s) F_e ds) \rangle_{\text{eq}}}{\langle \exp(-\beta \int_0^t J(-s) F_e ds) \rangle_{\text{eq}}} \\
&+ \frac{\beta F_e \langle B(0) \exp(-\beta \int_0^t J(-s) F_e ds) \rangle_{\text{eq}} \langle J(-t) \exp(-\beta \int_0^t J(-s) F_e ds) \rangle_{\text{eq}}}{\langle \exp(-\beta \int_0^t J(-s) F_e ds) \rangle_{\text{eq}}^2} \\
&= -\beta F_e \langle B(t) J(0) \rangle_{\text{eq}} + \beta F_e \langle B(t) \rangle_{\text{eq}} \langle J(0) \rangle_{\text{eq}} .
\end{aligned}$$

Now the average dissipation flux at  $t = 0$  is zero, so we get the Transient Time Correlation Function

$$\langle B(t) \rangle_{\text{eq}} = \langle B(0) \rangle_{\text{eq}} - \beta F_e \int_0^t \langle \Delta B(s) \Delta J(0) \rangle_{\text{eq}} ds. \quad (5.23)$$

This relation is exact, regardless of the magnitude of the external field  $F_e$ .

## 5.4 Models of Nonequilibrium Steady States

### 5.4.1 Planar Couette Flow

Planar Couette flow occurs when the steady state streaming velocity,  $\mathbf{u}$ , is a linear function of position  $\mathbf{r}$ . In particular, assume  $u_x = \gamma z$ . Shear flow, like all Navier-Stokes transport processes, is driven by boundary conditions (e.g. moving walls). This is inconvenient for computer simulations because of the huge surface effects that would be induced in the small systems which we are capable of simulating on computers ( $10^2 < N \leq 10^5$ ).

Computer simulation of equilibrium systems has always employed periodic boundary conditions to minimize size dependence effects. Figure 5.1 illustrates a way of adapting periodic boundary conditions to planar Couette flow. The so-called Lees-Edwards periodic boundary conditions [Lees and Edwards (1972)] employ time varying nonorthogonal lattice vectors. The perpendicular height of the cells remains fixed so that the shearing deformation occurs isochorically. Once  $\Theta = 45^\circ$ , it may be reset to  $0^\circ$  without changing the mutual disposition of particles. If a particle exits a cell through a top face, it is replaced by its periodic image which enters at the bottom

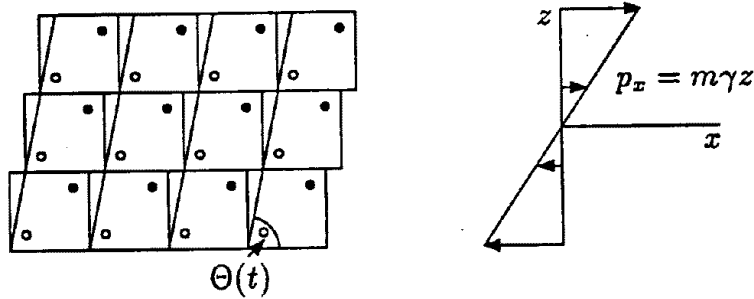


Figure 5.1: Lees-Edwards Periodic Boundary Conditions for Planar Couette Flow

face. This image will be positioned according to the current angle of the slewing lattice vector. The  $x$ -component of its velocity will be the old velocity minus the strain rate multiplied by the perpendicular height of the cell. Its peculiar velocity (*i.e.* relative to the planar velocity profile) is unchanged.

This is all that is really needed to run a molecular dynamics simulation of planar Couette flow at low Reynolds number. The flow of the periodic particles above and below the primitive cell will try to induce a linear velocity profile in the system. One simply solves Newton's equations of motion for the system of  $N$  interacting particles, waits for the initial transients to decay, and then accumulates statistical averages for the shear stress, the energy, etc.

Of course such a system will heat up. It will never achieve a steady state. To remedy this, we may employ a Gaussian or Nosé-Hoover thermostat. We must be careful, however, to ensure that it is the peculiar velocities which are thermostatted, and *not* the laboratory velocities. If the Reynolds number is sufficiently small so that a linear velocity profile is stable, the streaming velocity will be  $\hat{\mathbf{x}}\gamma z$ .

The so-called SLLOD equations provide a more convenient and more elegant set of variables with which to work. The first advantage of the SLLOD equations of motion is that they only involve the coordinates and the *peculiar* momenta of the particles. Since the thermostat, the internal energy and the pressure all involve peculiar, rather than laboratory velocities, this is an advantage.

The second advantage is that SLLOD momenta are continuous as particles leave and enter the primitive cell, as the calculation is more stable than it otherwise might be. The SLLOD equations of motion are:

$$\begin{aligned}\dot{\mathbf{q}}_i &= \frac{\mathbf{p}_i}{m} + \gamma \hat{\mathbf{x}} q_{zi} \\ \dot{\mathbf{p}}_i &= \mathbf{F}_i - \gamma \hat{\mathbf{x}} p_{zi}.\end{aligned}\tag{5.24}$$

Differentiating the  $\dot{\mathbf{q}}$  equation gives:

$$\ddot{\mathbf{q}}_i = \frac{\mathbf{F}_i}{m} + \dot{\gamma} \hat{\mathbf{x}} q_{zi}.$$

Thus, except at  $t = 0$ , when the shear rate is switched on, the SLLOD equations of motion are simply Newton's. Once the shear motion has impulsively started at  $t = 0$ , the Lees-Edwards boundary conditions continue the shear flow motion. The third advantage of the SLLOD equations is that they transform a boundary driven system to one with an external field, which makes the system more amenable to theoretical analysis.

## 5.4.2 Colour Current

The other model system that will be referred to arises from considering models of electrical conductivity within a dense plasma. In this case, we have two species of ion, positive and negative, interacting with a background field. The equations of motion for this system will be

$$\begin{aligned}\dot{\mathbf{q}}_i &= \frac{\mathbf{p}_i}{m_i} - \frac{e_i \sum_j e_j \mathbf{p}_j \cdot \hat{\mathbf{E}}}{m \sum_j \mathbf{F}_i \cdot \hat{\mathbf{E}}} \\ \dot{\mathbf{p}}_i &= \mathbf{F}_i + \mathbf{E} e_i,\end{aligned}\tag{5.25}$$

where  $m_i$  is the mass of each ion,  $e_i$  its charge and  $\mathbf{E}$  the applied electric field. Note that in this equation, the momenta are chosen so that  $\pm$ ve species is carrying  $m_{\mp}/(m_+ + m_-)$  of the current, where  $m_{\mp}$  is the mass of the negative and positive ion respectively. In the particular case of  $m_+ = m_-$ , which we shall discuss henceforth, each species carries half the current. In a real electrical system, the forces  $\mathbf{F}_i$  must be sums of Coulomb terms ( $\mathbf{F}_{ij} = e_i e_j \hat{\mathbf{r}}_{ij}/r_{ij}^2$ ), which is effectively of infinite range, so there will be significant error involved in modelling it with the small systems available with computer

simulations. There is a technique for resumming the electrical forces to take into account the screening effect [Allen and Tildesley (1987)], but since at this stage we are interested in the feasibility of such calculations, rather realistic values, we take a simpler approach of using a short range force, such as the Lennard-Jones force. We call this colour conductivity to distinguish it from electrical conductivity, because we can consider that each molecule has a colour label which interacts with the colour field, but that the Hamiltonian is colour blind. A number of authors have studied this system [Evans and Morriss (1985), Evans *et al.* (1983), Erpenbeck (1987)].

## Chapter 6

# Nonlinear Burnett Coefficients

The nonlinear Burnett Coefficients have already been introduced in section 1.3. Ever since the Green-Kubo formalism for calculating the linear transport coefficients was developed, there has been interest in a corresponding theory for the nonlinear Burnett coefficients. The discovery of long-time tails in the velocity autocorrelation function by Alder and Wainwright (1970) indicated that the hydrodynamic transport coefficients do not exist in two dimensions, but do exist in three dimensions. By applying mode-coupling theories, Ernst *et al.* (1978) showed that the relation between stress and strain rate should be  $P_{xy} = |\gamma| \ln |\gamma|$  for hard disks and  $P_{xy} = -\eta\gamma + c|\gamma|^{\frac{3}{2}}$  for hard spheres, rather than the analytic form suggested by (1.8). This result indicates that the nonlinear Burnett coefficients do not exist at all, so the interest has intensified for a numerical simulation to test the mode-coupling theories.

In a recent paper by Evans and Lynden-Bell (1988), equilibrium fluctuation expressions for inverse Burnett coefficients were derived for the colour conductivity problem. The coefficients,  $B_i$ , give a Taylor series representation of a nonlinear transport coefficient  $L$ , in terms of the thermodynamic force  $F$ . Thus if a thermodynamic flux  $J$  is written in terms of the coefficient's defining constitutive relation as  $\langle J \rangle = L(F)F$ , then the Burnett coefficients are related by  $L(F) = B_0 + B_1F + B_2F^2 + \dots$ . In order to derive closed form expressions for the Burnett coefficients, it was found necessary to work in the Norton ensemble, in which the flux  $J$ , rather than the thermodynamic force  $F$  was the independent variable. The constitutive relation in this case is  $\langle F \rangle = \mathcal{L}(J)J = \mathcal{B}_0 + \mathcal{B}_1J + \dots$ . In the thermodynamic limit, we may write  $\mathcal{L}(J) = L^{-1}(J)$ , and so the non-linear Burnett coefficients can

be computed by inverting the series.

Evans and Lynden-Bell (1988) applied constant current dynamics to a canonical ensemble with the currents distributed about an average current  $J_0$ . This allowed the derivation of a transient time correlation function for the non-equilibrium phase average  $\langle F \rangle$ . It was then a simple matter to compute the derivatives of  $\langle F \rangle$  with respect to the average current  $J_0$ , as the constant current propagator commutes with the derivative operator. However, this method appeared to be limited to colour currents, for which an appropriate canonical distribution could be found. In this chapter, we show that this method can be applied to the situation of an arbitrary thermodynamic flux. This result has been reported by Standish and Evans (1990).

## 6.1 Equations of Motion

The equations of motion used to generate the flux-statted dynamics in general will be of the form

$$\dot{\mathbf{q}}_i = \frac{\mathbf{p}_i}{m} + \mathbf{C}_i \lambda \quad (6.1)$$

$$\dot{\mathbf{p}}_i = \mathbf{F}_i + \mathbf{D}_i \lambda - \alpha \mathbf{p}_i.$$

The intermolecular forces are given by  $\mathbf{F}_i$ . In these equations,  $\lambda$  and  $\alpha$  are computed by a Nosé-Hoover feedback mechanism to keep the flux  $J$ , and the temperature  $T = \sum_i \frac{m\mathbf{p}_i^2}{3Nk_B}$  fluctuating about fixed mean values  $J_0$  and  $T_0$ . Specifically, we have  $\dot{\lambda} = \frac{N}{Q_\lambda}(J - J(t=0))$  and  $\dot{\alpha} = \frac{3Nk_B}{Q_\alpha}(T - T(t=0))$ . The phase variables  $\mathbf{C}_i$  and  $\mathbf{D}_i$  are chosen so that

$$\frac{\dot{H}^{ad}}{\lambda} = \sum_i \left( \frac{\mathbf{p}_i \cdot \mathbf{D}_i}{m} - \mathbf{F}_i \cdot \mathbf{C}_i \right) = NJ. \quad (6.2)$$

For example, in the case of constant colour current dynamics,  $\mathbf{D}_i = e_i \hat{\mathbf{x}}$ , where  $e_i$  is the charge on the ion, and  $\mathbf{C}_i = -\frac{Ne_i \hat{\mathbf{x}} J}{\sum_j F_{xj} e_j}$ . In the case of stress-statted dynamics [Brown and Clarke(1986) , Hood *et al.*(1987)], the flux to be kept constant is the  $xz$  component of the stress tensor, namely

$$J = \frac{V}{N} \sigma_{xz} = -\frac{1}{N} \sum_i \left( \frac{p_{xi} p_{zi}}{m} + q_{xi} F_{zi} \right) \quad (6.3)$$

with  $\mathbf{C}_i$  and  $\mathbf{D}_i$  given by  $\mathbf{C}_i = q_{xi}\hat{\mathbf{z}}$  and  $\mathbf{D}_i = p_{zi}\hat{\mathbf{x}}$ .

Consider an initial ensemble characterized by the distribution function  $f_0$ ,

$$f_0 = \exp(-\beta H + \epsilon J) / \int \exp(-\beta H + \epsilon J) d\Gamma. \quad (6.4)$$

If we assume adiabatic incompressibility of phase space (AIF), then the Kawasaki expression for the average of an arbitrary phase variable,  $B$ , can be derived [Morriss and Evans (1985)]

$$\langle B(t_J) \rangle = \frac{\langle B(0) \exp[\beta N \int_0^{-t} J \lambda(s_J) ds] \rangle}{\langle \exp[\beta N \int_0^{-t} J \lambda(s_J) ds] \rangle}. \quad (6.5)$$

Here the subscript  $J$  denotes that  $\lambda(s)$  is evolved under constant flux dynamics. The ensemble average  $\langle \dots \rangle$  is taken with respect to the distribution function  $f_0$ .

By differentiating and reintegrating (6.5) in the usual way, a transient time correlation function expression for the nonequilibrium phase average is generated. Thus

$$\begin{aligned} \langle B(t_J) \rangle &= \langle B(0) \rangle + \beta N \int_0^t \langle \Delta B(s_J) \lambda(0) J \rangle ds \\ &= \langle B(0) \rangle + \beta N J_0 \int_0^t \langle B(s_J) \lambda(0) \rangle ds \end{aligned} \quad (6.6)$$

in the thermodynamic limit, where  $J_0 = \langle J \rangle$ . Since the flux-statted propagators do not depend on the average flux  $J_0$ , the only dependence on  $J_0$  in the above expression is either explicit, or comes in indirectly through  $f_0$ . By the chain rule,  $\frac{\partial f_0}{\partial J_0} = \frac{d\epsilon}{dJ_0} \frac{\partial f_0}{\partial \epsilon}$ . The first derivative can be evaluated by the inverse function theorem

$$\begin{aligned} 1 / \frac{d\epsilon}{dJ_0} &= \frac{dJ_0}{d\epsilon} \\ &= \frac{d}{d\epsilon} \left[ \int J \exp(-\beta H + \epsilon J) d\Gamma / \int \exp(-\beta H + \epsilon J) d\Gamma \right] \\ &= \frac{\int J^2 \exp(-\beta H + \epsilon J) d\Gamma}{\int \exp(-\beta H + \epsilon J) d\Gamma} - \left( \frac{\int J \exp(-\beta H + \epsilon J) d\Gamma}{\int \exp(-\beta H + \epsilon J) d\Gamma} \right)^2 \\ &= \langle (\Delta J)^2 \rangle, \end{aligned}$$

and the second derivative is simply

$$\frac{\partial f_0}{\partial \epsilon} = \Delta J f_0.$$

So

$$\frac{\partial f_0}{\partial J_0} = \frac{\Delta J}{\langle (\Delta J)^2 \rangle} f_0.$$

The derivatives of (6.6) with respect to  $J_0$  can be easily evaluated around  $J_0 = 0$ , and the first three are:

$$\left. \frac{\partial \langle B(t_J) \rangle}{\partial J_0} \right)_{J_0=0} = \frac{\langle B(0)\Delta J \rangle}{\langle (\Delta J)^2 \rangle} + \beta N \int_0^t \langle B(s_J)\lambda(0) \rangle ds \quad (6.7)$$

$$\begin{aligned} \left. \frac{\partial^2 \langle B(t_J) \rangle}{\partial J_0^2} \right)_{J_0=0} &= \frac{\langle B(0)((\Delta J)^2 - \langle (\Delta J)^2 \rangle) \rangle}{\langle (\Delta J)^2 \rangle^2} \\ &- \frac{\langle B(0)\Delta J \rangle \langle (\Delta J)^3 \rangle}{\langle (\Delta J)^2 \rangle^3} + \frac{2\beta N}{\langle (\Delta J)^2 \rangle} \int_0^t \langle B(s_J)\lambda(0)\Delta J \rangle ds \end{aligned} \quad (6.8)$$

$$\begin{aligned} \left. \frac{\partial^3 \langle B(t_J) \rangle}{\partial J_0^3} \right)_{J_0=0} &= \frac{\langle B(0)(\Delta J)^3 \rangle}{\langle (\Delta J)^2 \rangle^3} - \frac{3 \langle (\Delta J)^3 \rangle}{\langle (\Delta J)^2 \rangle^4} \langle B(0)(\Delta J)^2 \rangle \\ &+ \left( \frac{3 \langle (\Delta J)^3 \rangle^2}{\langle (\Delta J)^2 \rangle^5} - \frac{\langle (\Delta J)^4 \rangle}{\langle (\Delta J)^2 \rangle^4} \right) \langle B(0)\Delta J \rangle + \frac{2 \langle (\Delta J)^3 \rangle}{\langle (\Delta J)^2 \rangle^3} \langle B(0) \rangle \\ &- \frac{3N\beta \langle (\Delta J)^3 \rangle}{\langle (\Delta J)^2 \rangle^3} \int_0^t \langle B(s_J)\lambda(0)\Delta J \rangle ds \\ &+ \frac{3N\beta}{\langle (\Delta J)^2 \rangle^2} \int_0^t \langle B(s_J)\lambda(0)((\Delta J)^2 - \langle (\Delta J)^2 \rangle) \rangle ds. \end{aligned} \quad (6.9)$$

In comparing these results with Evans and Lynden-Bell (1988), it should be noted that one is interested in computing the phase average of the force required to maintain a steady current. This phase variable is antisymmetric with respect to a reflection in space, whereas  $J$  is independent of position, and so all the averages of the form  $\langle B(0)g(\Delta J) \rangle$  will vanish. Similarly,  $\langle (\Delta J)^3 \rangle$  and all odd moments of  $J$  will vanish. The quantity  $\langle (\Delta J)^2 \rangle$  can be evaluated, and is found to be  $\langle (\Delta J)^2 \rangle = (\beta m N)^{-1}$ .

Similar simplifications will also apply with the case of planar Couette flow, where one is attempting to deduce the nonlinear viscosity, defined by

$$\eta(\gamma) \equiv \frac{\langle \sigma(\gamma) \rangle}{\gamma},$$

where  $\sigma_{xz}$  is the shear stress, and  $\gamma$  the strain rate associated with it. Both  $\lambda$  and  $J$  are antisymmetric under a reflection in the  $x$  direction in both position and velocity space ( $q_{xi} \rightarrow -q_{xi}, p_{xi} \rightarrow -p_{xi}$ ), but under a time reversal ( $\mathbf{p}_i \rightarrow -\mathbf{p}_i$ ),  $\lambda$  is antisymmetric, and  $J$  is symmetric. Thus the Burnett coefficients simplify to

$$\begin{aligned} \left. \frac{\partial \langle \gamma \rangle}{\partial S_{xz}} \right|_{S_{xz}=0} &= \beta V \int_0^\infty \langle \gamma(s_\sigma) \gamma(0) \rangle ds \\ \left. \frac{\partial^2 \langle \gamma \rangle}{\partial S_{xz}^2} \right|_{S_{xz}=0} &= \frac{2\beta^2 V^2}{G_\infty} \int_0^\infty \langle \gamma(s_\sigma) \gamma(0) \sigma_{xz} \rangle ds \\ \left. \frac{\partial^3 \langle \gamma \rangle}{\partial S_{xz}^3} \right|_{S_{xz}=0} &= \frac{3\beta^3 V^3}{G_\infty^2} \int_0^\infty \langle \gamma(s_\sigma) \gamma(0) (\sigma_{xz}^2 - \langle \sigma_{xz}^2 \rangle) \rangle ds, \end{aligned}$$

where  $S_{xz} = \langle \sigma_{xz} \rangle$  and  $\langle (\Delta J)^2 \rangle = \frac{V^2}{N^2} \langle \sigma_{xz}^2 \rangle = \frac{V G_\infty}{N^2 \beta}$ , with  $G_\infty$  being the infinite frequency shear modulus [Brown and Clarke (1986)].

## 6.2 Relation between canonical and $\Delta J$ ensemble

The inverse Burnett coefficients are defined in terms of the derivatives with respect to the flux of the average of a thermodynamic force in an ensemble where the flux is fixed value. In this section, we demonstrate the equivalence of this and derivatives with respect to the flux in a canonical ensemble. The subset of the canonical ensemble in which the flux takes on a specific value of  $J$  is called the  $\Delta J$ -ensemble. One may write a phase average  $\langle B \rangle$  as an integration over all possible  $\Delta J$ -ensembles

$$\langle B \rangle = \int f_0(J) \langle B; J \rangle dJ, \quad (6.10)$$

where  $f_0(J)$  is the probability that the flux takes on a specific value  $J$ , and  $\langle B; J \rangle$  is the phase average in the  $\Delta J$ -ensemble.

In the thermodynamic limit,  $f_0(J)$  will be clustered about  $J_0$  with infinitesimal spread, suggesting that we can write a Taylor series expansion of  $\langle B; J \rangle$  about  $J_0$ :

$$\langle B; J \rangle = \langle B; J_0 \rangle + \Delta J \left. \frac{\partial \langle B; J \rangle}{\partial J} \right|_{J=J_0} + \frac{(\Delta J)^2}{2!} \left. \frac{\partial^2 \langle B; J \rangle}{\partial J^2} \right|_{J=J_0} + \dots$$

Substituting this into (6.10), we find that

$$\begin{aligned} \frac{\partial \langle B \rangle}{\partial J_0} &= \left. \frac{\partial \langle B; J \rangle}{\partial J} \right|_{J=J_0} + \frac{\langle (\Delta J)^3 \rangle}{2! \langle (\Delta J)^2 \rangle} \left. \frac{\partial^2 \langle B; J \rangle}{\partial J^2} \right|_{J=J_0} \\ &+ \frac{\langle (\Delta J)^4 \rangle}{3! \langle (\Delta J)^2 \rangle} \left. \frac{\partial^3 \langle B; J \rangle}{\partial J^3} \right|_{J=J_0} + \dots \end{aligned}$$

From Appendix E,  $\langle (\Delta J)^n \rangle$  is of order  $N^{1-n}$  in the large system limit, and so it is clear that the ensemble corrections are of order  $1/N$ .

### 6.3 Equilibrium Simulation

The two time correlation functions in equations (6.7) to (6.9) are averaged over an ensemble of flux-statted trajectories. To calculate this, one would first need to generate the distribution  $f_0$ , using molecular dynamics simulation or Monte Carlo methods. Once an initial phase space configuration  $\Gamma_0$  was produced with probability  $f_0(\Gamma_0)$ , then its evolution under the flux-statted equations of motion (6.1) needs to be followed. If we wish to follow these trajectories for  $n_t$  time steps, then we require  $n_\Gamma n_t$  timesteps to average over  $n_\Gamma$  trajectories. By contrast, the Green-Kubo expressions for the linear transport coefficients involve correlation functions whose propagators are independent of the initial state of the trajectory. We can therefore form the average as

$$\langle A(t)B(0) \rangle = \frac{1}{n_\Gamma} \sum_{j=1}^{n_\Gamma} A(t + j\tau)B(j\tau),$$

with  $\tau$  being the timestep. This clearly requires only  $n_\Gamma + n_t$  timesteps, and so is more efficient by roughly a factor of  $n_t$ . We shall see in this section that the ensemble averages in equations (6.7) to (6.9) can be calculated from a

single equilibrium trajectory, with the consequent improvement in efficiency. Write the flux-statted propagator explicitly as  $e^{iL_J t}$ :

$$\langle A(0)B(t_J) \rangle = \int f_0(J) \langle Ae^{iL_J t} B; J \rangle dJ. \quad (6.11)$$

Now use the Dyson equation (5.13) to expand  $e^{iL_J t}$  in terms of  $e^{iL_{J_0} t}$ :

$$\begin{aligned} \langle Ae^{iL_J t} B; J \rangle &= \langle Ae^{iL_{J_0} t} B; J \rangle \\ &+ \langle A \int_0^t e^{iL_{J_0}(t-s)} i\Delta L e^{iL_{J_0} s} B ds; J \rangle + \dots \end{aligned} \quad (6.12)$$

For  $L_J$  being the flux-statted Liouvillean with Nosé-Hoover feedback mechanism, the difference in operators is contained only in the equation of motion for  $\lambda$ :

$$i\Delta L = \dot{\lambda} \partial_\lambda = \frac{1}{Q_\lambda} \Delta J \partial_\lambda.$$

Now  $B' \equiv \int_0^t e^{iL_{J_0}(t-s)} \partial_\lambda e^{iL_{J_0} s} B ds$  is just another intensive phase variable, so we may write the series (6.12) as

$$\langle B(t_J)A(0); J \rangle = \langle B(t_{J_0})A(0); J \rangle + \langle B' A \Delta J; J \rangle + \dots$$

Using the result of Appendix E, the higher terms will vanish in the thermodynamic limit, and so we may write

$$\langle B(t_J)A(0); J \rangle = \langle B(t_{J_0})A(0); J \rangle.$$

Substituting this into (6.11) reveals

$$\langle B(t_J)A(0) \rangle = \langle B(t_{J_0})A(0) \rangle.$$

Thus the time correlation functions of (6.7... 6.9) are expressed in terms of an average over a single trajectory, provided that the flux-statted propagator generates  $f_0$ . This is the case for the Nosé-Hoover feedback mechanism discussed, for the case  $J_0 = 0$ .

## 6.4 Numerical Evaluation of Burnett Coefficients

In order to establish the feasibility of calculations based on equations (6.9), it was decided to perform a calculation using the colour conductivity model

described in section 5.4.2. The intermolecular potential was taken to be the Lennard-Jones potential, which has an attractive component due to van der Waals interaction, and a repulsive hard core that goes as  $r^{-12}$ :

$$V(r) = 4\varepsilon \left( \left( \frac{\sigma}{r} \right)^{12} - \left( \frac{\sigma}{r} \right)^6 \right).$$

In what follows, every quantity will be given in reduced units, in which  $\varepsilon = \sigma = m = 1$ .

The system consists of 108 particles at a temperature of 1.08 and density of 0.85. This state point was chosen because considerable information was already known about this system at that state point [Evans and Morriss (1985), and references therein].

The equations of motion employed were the Nosé-Hoover feedback mechanism for the Norton ensemble (eq 6.1). The feedback parameter  $Q_\lambda$  was chosen to be of order unity, and  $Q_\alpha$  to be 3.24. The values of these parameters were chosen to give optimal convergence of the linear response function. There is no real reason for them to be optimal for non-linear response functions.

The code used is reported in appendix F. When finally optimized, it executed  $1.2 \times 10^6$  timesteps per hour, or about 75 Mflops on the Fujitsu VP100 computer. Even so, hundreds of hours of CPU time were required to establish reasonable statistics for the response functions. Clearly, computers of one to two orders of magnitude greater power are required for these calculations to be practical. Already, the next generation of supercomputers promise this power.

Figure 6.2 shows  $\frac{\partial^3 \langle \lambda(t) \rangle}{\partial J^3}$  for the system under study for  $Q_\lambda = 1$  and  $Q_\lambda = 2$ . One immediately notices that the non-linear response lasts much longer than the linear case, with the integral converging by a time of 8, compared with unity in the case of the linear response, which is shown in figure 6.1 for the same system. The agreement of these results for different values of  $Q_\lambda$  within statistical uncertainty indicates that a true value has been found for the third order coefficient.

Evans (private communication) has run a similar simulation on a planar Couette flow system, using code that is described in Hood (1989). Figure 6.4 shows the third order response  $\frac{\partial^3 \langle \gamma \rangle}{\partial S_{zz}^3}$  for  $Q_\gamma = 100, 150$  and 200. The linear response for the system is shown in figure 6.3 The good agreement between

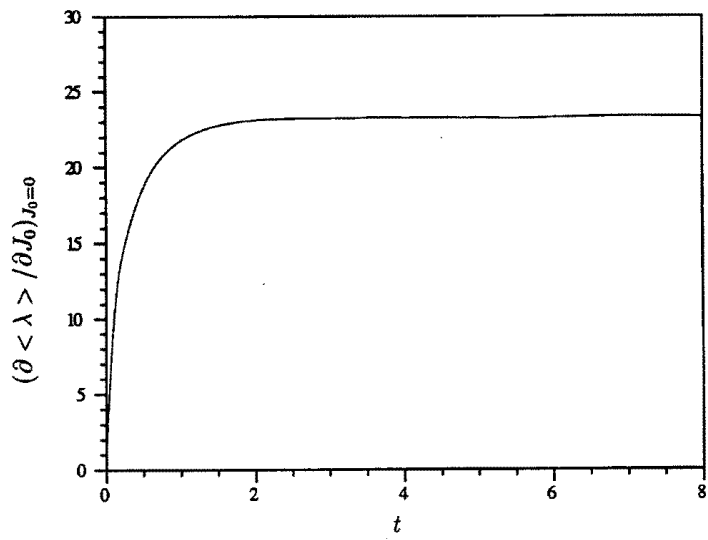


Figure 6.1: Linear response for colour conductivity

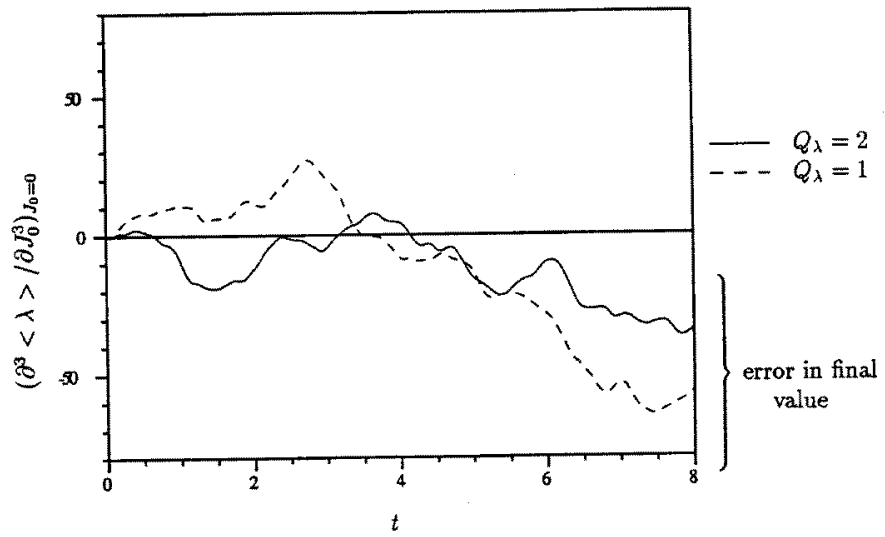


Figure 6.2: Third order nonlinear response for colour conductivity

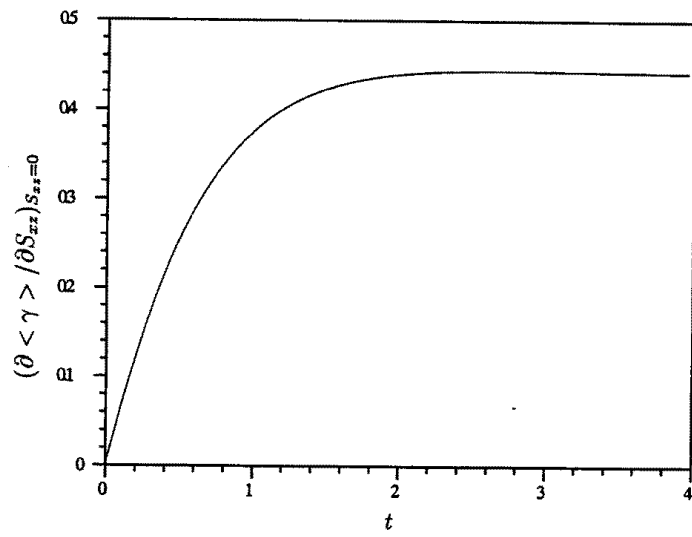


Figure 6.3: Linear response for planar Couette flow

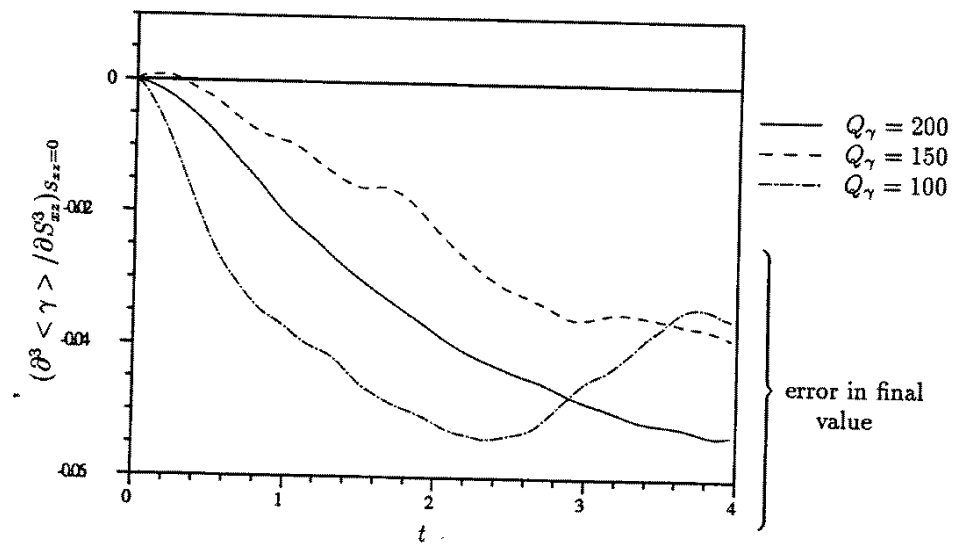


Figure 6.4: Third order nonlinear response for planar Couette flow

these results indicates that the calculation is feasible. Unfortunately, we don't have sufficient evidence to tackle the question of divergences in the Burnett coefficients. It has been suggested [van Beijeren, private communication] that the coefficients may diverge in the thermodynamic limit. To test this hypothesis requires rerunning the code at different system sizes, something that is impractical at current processor speeds.

# Chapter 7

## Conclusion

In this thesis, I have established that if the linear Boltzmann operator  $\mathcal{M}$  has a discrete spectrum, then a hydrodynamic regime occurs after a characteristic time  $\tau$  in which the spatial moments of the density have constant time derivatives. However, in time-of-flight experiments, non-hydrodynamic and higher-order (non-Fickian) diffusion effects are significant at times much greater than  $\tau$ , unless explicitly recognised and accounted for. In parallel plane steady state Townsend experiments, there appears to be no such effects in the drift region away from the electrodes. It would be desirable to establish a non-hydrodynamic theory of the Townsend-Huxley experiment. The obvious way to do this is to generalize the parallel plane theory to two dimensions. The generalization of the saddle point method to higher dimensions goes through in a fairly straight-forward manner [Malgrange (1974), Hamm (1977)], however the asymptotic arguments at large  $z$  and  $r_{\perp}$  are not easy to generalize.

A complete theory of end-effects is not possible until boundary effects have been analysed. This is a difficult problem that people have been tackling for nearly 50 years with marginal success. Another problem this thesis sheds a little light on is the form of the spectrum of the linear Boltzmann operator. Since it is known that a discrete spectrum gives rise to a hydrodynamic regime, runaway must occur only when the spectrum is continuous. However, it is known that runaway occurs when  $\int \nu(c)dc$  converges [Cavalleri and Pavari-Fontana (1972)], so there is a clear link between  $\nu(c)$  and the spectrum.

The final portion of the thesis deals with the non-linear Burnett coeffi-

cients. General fluctuation expressions have been developed for these coefficients, and have been applied to some simple computational models of dense fluids. However, it is still too early to tell whether the non-linear Burnett coefficients actually exist in the thermodynamic limit.

# Appendix A

## Perturbation of the eigenfunctions for small $\mathbf{k}$

If the eigenvalue problem for  $\mathcal{M}$  is solved for a particular form of the collision operator, then it would be useful to have a scheme to compute the derivatives of  $\omega(i\mathbf{k})$ ,  $\Psi(\mathbf{c}, i\mathbf{k})$  and  $\Phi(\mathbf{c}, i\mathbf{k})$  around  $\mathbf{k} = 0$  to compute the nonhydrodynamic effects described by  $\mathbf{x}^{(l)}(t)$ . The scheme one would use for this is similar to the recursion scheme outlined in Kumar *et al.* (1980), that is the swarm theory analogue of the Chapman-Enskog method.

The eigenfunctions and eigenvalues of equation (2.8) are expanded as a power series in  $\mathbf{k}$ :

$$\begin{aligned}\Psi_j(\mathbf{c}, i\mathbf{k}) &= \sum_{n=0}^{\infty} \Psi_j^{(n)} \odot (-i\mathbf{k})^n \\ \Phi_j(\mathbf{c}, i\mathbf{k}) &= \sum_{n=0}^{\infty} \Phi_j^{(n)} \odot (-i\mathbf{k})^n \\ \omega_j(i\mathbf{k}) &= \sum_{n=0}^{\infty} \omega_j^{(n)} \odot (-i\mathbf{k})^n\end{aligned}\tag{A.1}$$

Upon substituting these series into equation (2.8), the following recursion relations for multipole functions  $\Psi_j^{(n)}$ ,  $\Phi_j^{(n)}$  are generated:

$$(\mathcal{M} + \omega_j^{(0)})\Psi_j^{(n)}(\mathbf{c}) = \mathbf{c}\Psi_j^{(n-1)}(\mathbf{c}) - \sum_{m=1}^n \omega_j^{(m)}\Psi_j^{(n-m)}(\mathbf{c})\tag{A.2}$$

$$\begin{aligned}
(\tilde{\mathcal{M}} + \omega_j^{(0)})\Phi_j^{(n)}(\mathbf{c}) &= \mathbf{c}\Phi_j^{(n-1)}(\mathbf{c}) - \sum_{m=1}^n \omega_j^{(m)}\Phi_j^{(n-m)}(\mathbf{c}) \\
\sum_{m=0}^n \int \Psi_j^{(m)}(\mathbf{c})\Phi_k^{(n-m)}(\mathbf{c})d\mathbf{c} &= \delta_{jk}\delta_{n0}
\end{aligned} \tag{A.3}$$

The recursion relations (A.2) define  $\Psi_j^{(n)}(\mathbf{c})$  up to an arbitrary additive term in the kernel of  $\mathcal{M} + \omega_j^{(0)}$ , *i.e.* a term proportional to  $\Psi_j^{(0)}(\mathbf{c})$ . The corresponding additive term for  $\Phi_j^{(n)}$  is then fixed by the normalization (A.3). It will be shown that, whilst the functions  $\Psi_j(\mathbf{c}, i\mathbf{k})$  and  $\Phi_j(\mathbf{c}, i\mathbf{k})$  may be quite different functions with different choices of the arbitrary additive terms, the product  $\Psi_j(\mathbf{c}, i\mathbf{k})\Phi_j(\mathbf{c}', i\mathbf{k})$  is unique. Since these functions enter the Greens function through this product, this means that any physical results are well determined by this method.

## A.1 Recursion relations in Component Form

We will now present formulae for calculating  $\Psi_j^{(n)}$ ,  $\Phi_j^{(n)}$  and  $\omega_j^{(n)}$ . We do this by expanding (2.8) and (A.1) in the  $\Psi_j^{(0)}$  and  $\Phi_j^{(0)}$  basis (zeroth order basis) with the following definition:

$$\Psi_j^{(n)}(\mathbf{c}) = \sum_{k \in \sigma} \mathbf{A}_{jk}^{(n)} \Psi_k^{(0)}(\mathbf{c}), \quad \Phi_j^{(n)}(\mathbf{c}) = \sum_{k \in \sigma} \mathbf{B}_{jk}^{(n)} \Phi_k^{(0)}(\mathbf{c}).$$

We now define an operator  $\mathcal{L}_j$  so that

$$\mathcal{L}_j(\mathcal{M} + \omega_j^{(0)}) = (\mathcal{M} + \omega_j^{(0)})\mathcal{L}_j = \mathcal{P}_j$$

where  $\mathcal{P}_j$  is the projection onto the orthogonal complement of  $\mathcal{M} + \omega_j^{(0)}$ . In other words, if the domain of  $\mathcal{M} + \omega_j^{(0)}$  is restricted to make  $\mathcal{M} + \omega_j^{(0)}$  one to one, then  $\mathcal{L}_j$  is the inverse of  $\mathcal{M} + \omega_j^{(0)}$ .

By applying  $\mathcal{L}_j$  on equation (A.2), the multipole functions can be generated according to

$$\mathcal{P}_j \Psi_j^{(n)} = \mathcal{L}_j(\mathbf{c}\Psi_j^{(n-1)} - \sum_{m=1}^{n-1} \omega_j^{(m)}\Psi_j^{(n-m)}) \tag{A.4}$$

$$\tilde{\mathcal{P}}_j \Phi_j^{(n)} = \tilde{\mathcal{L}}_j(\mathbf{c} \Phi_j^{(n-1)} - \sum_{m=1}^{n-1} \omega_j^{(m)} \Phi_j^{(n-m)}).$$

Or expressed in the zeroth order basis for  $\omega_j^{(0)} \neq \omega_k^{(0)}$ ,

$$\mathbf{A}_{jk}^{(n)} = \sum_{l \in \sigma} \mathbf{c}_{lk} \mathbf{A}_{jl}^{(n-1)} \Delta_{jk} - \sum_{m=1}^{n-1} \omega_j^{(m)} \mathbf{A}_{jk}^{(n-m)} \Delta_{jk}$$

$$\mathbf{B}_{jk}^{(n)} = \sum_{l \in \sigma} \mathbf{c}_{kl} \mathbf{B}_{jl}^{(n-1)} \Delta_{jk} - \sum_{m=1}^{n-1} \omega_j^{(m)} \mathbf{B}_{jk}^{(n-m)} \Delta_{jk}$$

where  $\mathbf{c}_{jk} = \int \Psi_j^{(0)}(\mathbf{c}) \mathbf{c} \Phi_k^{(0)}(\mathbf{c}) d\mathbf{c}$  are the matrix elements of the operator  $\mathbf{c}$ , and

$$\Delta_{jk} = \begin{cases} 0 & \text{if } \omega_j^{(0)} = \omega_k^{(0)} \\ [\omega_j^{(0)} - \omega_k^{(0)}]^{-1} & \text{otherwise} \end{cases}$$

are the eigenvalues of  $\mathcal{L}_j$ .

These relations will generate the multipole functions from the seeds  $\mathbf{A}_{jk}^{(0)} = \mathbf{B}_{jk}^{(0)} = \delta_{jk}$ . If  $\omega_j^{(0)} = \omega_k^{(0)}$  then  $\mathbf{A}_{jk}^{(n)}$  and  $\mathbf{B}_{jk}^{(n)}$  may be chosen arbitrarily subject to

$$\mathbf{A}_{jk}^{(n)} + \mathbf{B}_{kj}^{(n)} = - \sum_{m=1}^{n-1} \sum_{l \in \sigma} \mathbf{A}_{jl}^{(m)} \mathbf{B}_{kl}^{(n-m)}$$

To complete the prescription, we need a formula for calculating the  $\omega_j^{(n)}$ , and we also need to check that the biorthonormality condition (A.3) is satisfied in the case  $\omega_j^{(0)} \neq \omega_k^{(0)}$ . For convenience of notation, we will define  $\Psi_j^{(n)} = \Phi_j^{(n)} = 0$  for every  $n$  less than zero. This means that all the power series expansions hold for every integer  $n$ .

From (2.8),

$$\omega_j(i\mathbf{k}) = - \int \Psi_j(\mathbf{c}, i\mathbf{k}) (\mathbf{c} \cdot \mathbf{k} + \tilde{\mathcal{M}}) \Phi_j(\mathbf{c}, i\mathbf{k}) d\mathbf{c}.$$

Expanding this in powers of  $\mathbf{k}$ , one gets

$$\omega_j^{(n)} = - \sum_{m=0}^n \int \Psi_j^{(m)}(\mathbf{c}) \left( -\mathbf{c} \Phi_j^{(n-m-1)}(\mathbf{c}) + \tilde{\mathcal{M}} \Phi_j^{(n-m)}(\mathbf{c}) \right) d\mathbf{c}.$$

The second term can be expressed as

$$\begin{aligned} \sum_{m=0}^n \int \Psi_j^{(k)}(\mathbf{c}) \tilde{\mathcal{M}} \Phi_j^{(n-m)}(\mathbf{c}) d\mathbf{c} &= \sum_{m=1}^n \int \Psi_j^{(m)}(\mathbf{c}) (\tilde{\mathcal{M}} + \omega_j^{(0)}) \Phi_j^{(n-m)}(\mathbf{c}) d\mathbf{c} + \\ &\int (\mathcal{M} + \omega_j^{(0)}) \Psi_j^{(0)}(\mathbf{c}) \Phi_j^{(n)}(\mathbf{c}) d\mathbf{c} - \omega_j^{(0)} \sum_{m=0}^n \int \Psi_j^{(m)}(\mathbf{c}) \Phi_j^{(n-m)}(\mathbf{c}) d\mathbf{c}. \end{aligned}$$

The second two terms vanish because of the biorthonormality condition (A.3) and the eigenvalue equation (2.8). The final step is to evaluate this equation by the recursion equation (A.2):

$$\begin{aligned} \omega_j^{(n)} &= \sum_{m=0}^n \int \Psi_j^{(m)}(\mathbf{c}) \mathbf{c} \Phi_j^{(n-m-1)}(\mathbf{c}) d\mathbf{c} - \\ &\sum_{m=1}^n \int \Psi_j^{(m)} \left( \mathbf{c} \Phi_j^{(n-m-1)}(\mathbf{c}) - \sum_{l=0}^{n-k} \omega_j^{(l)} \Phi_j^{(n-m-l)}(\mathbf{c}) \right) d\mathbf{c} \\ &= \int \Psi_j^{(0)} \mathbf{c} \Phi_j^{(n-1)}(\mathbf{c}) d\mathbf{c} + \sum_{l=1}^{n-1} \sum_{m=1}^{n-l} \omega_j^{(l)} \int \Psi_j^{(m)}(\mathbf{c}) \Phi_j^{(n-m-l)}(\mathbf{c}) d\mathbf{c} \\ &= \int \Psi_j^{(0)}(\mathbf{c}) \mathbf{c} \Phi_j^{(n-1)}(\mathbf{c}) d\mathbf{c} - \sum_{l=1}^{n-1} \omega_j^{(l)} \int \Psi_j^{(0)}(\mathbf{c}) \Phi_j^{(n-l)} d\mathbf{c} \\ &= \sum_{k \in \sigma} \mathbf{c}_{jk} \mathbf{B}_{jk}^{(n-1)} - \sum_{l=1}^{n-1} \omega_j^{(l)} \mathbf{B}_{jj}^{(n-l)}. \end{aligned}$$

A similar calculation using the adjoint equation gives an alternative formula for  $\omega_j^{(n)}$ .

$$\omega_j^{(n)} = \sum_{k \in \sigma} \mathbf{c}_{kj} \mathbf{A}_{jk}^{(n-1)} - \sum_{l=1}^{n-1} \omega_j^{(l)} \mathbf{A}_{jj}^{(n-l)}.$$

Thus the problem has been reduced to evaluating the matrix element  $\mathbf{c}_{jk}$ .

For example, if the spectrum of  $\mathcal{M}$  is non-degenerate, the first few coefficients of the recursion series are

$$\begin{aligned} \omega_j^{(1)} &= \mathbf{c}_{jj}; \quad \mathbf{A}_{jk}^{(1)} = \mathbf{c}_{jk} \Delta_{jk} + \delta_{jk} \boldsymbol{\eta}_j^{(1)}; \quad \mathbf{B}_{jk}^{(1)} = \mathbf{c}_{kj} \Delta_{jk} - \delta_{jk} \boldsymbol{\eta}_j^{(1)}; \quad (\text{A.5}) \\ \omega_j^{(2)} &= \sum_{k \in \sigma} \mathbf{c}_{kj} \mathbf{c}_{jk} \Delta_{jk}; \quad \omega_j^{(3)} = \sum_{k, l \in \sigma} \mathbf{c}_{jk} \mathbf{c}_{lj} \mathbf{c}_{kl} \Delta_{jl} \Delta_{jk} - \mathbf{c}_{jj} \sum_{k \in \sigma} \mathbf{c}_{kj} \mathbf{c}_{jk} \Delta_{jk}^2; \end{aligned}$$

$$\mathbf{A}_{jk}^{(2)} = \mathbf{c}_{jk}\Delta_{jk}\boldsymbol{\eta}_j^{(1)} - \mathbf{c}_{jj}\mathbf{c}_{jk}\Delta_{jk}^2 + \sum_{l \in \sigma} \mathbf{c}_{lk}\mathbf{c}_{jl}\Delta_{jl}\Delta_{jk} + \delta_{jk}\boldsymbol{\eta}_j^{(2)};$$

$$\mathbf{B}_{jk}^{(2)} = \mathbf{c}_{jk}\Delta_{jk}\boldsymbol{\eta}_j^{(1)} - \mathbf{c}_{jj}\mathbf{c}_{jk}\Delta_{jk}^2 + \sum_{l \in \sigma} \mathbf{c}_{lj}\mathbf{c}_{kl}\Delta_{jl}\Delta_{jk} + \sum_{l \in \sigma} \mathbf{c}_{lj}\mathbf{c}_{jl}\Delta_{jl}^2\delta_{jk} - \delta_{jk}\boldsymbol{\eta}_j^{(2)} - \delta_{jk}(\boldsymbol{\eta}_j^{(1)})^2.$$

In this case, the arbitrary additive terms are proportional to  $\Psi_j^{(0)}$ . The rank  $n$  tensors  $\boldsymbol{\eta}_j^{(n)}$  are the coefficients of these terms, and may be chosen to be zero.

## A.2 Consistency with Biorthonormality

For  $\omega_j^{(0)} = \omega_k^{(0)}$ , the arbitrary term from the kernel of  $\mathcal{M} + \omega_j^{(0)}$  can be chosen so as to satisfy the biorthonormality condition (A.3). For  $\omega_j^{(0)} \neq \omega_k^{(0)}$ , it is necessary to show that the multipole functions generated by the the recursion relations (A.2) are consistent with the biorthonormality condition. This is done inductively from the zeroth order biorthonormality condition.

Using the identity

$$\begin{aligned} \int (\mathcal{M} + \omega_j^{(0)})\Psi_j^{(n)}(\mathbf{c})\Phi_k^{(l)}(\mathbf{c})d\mathbf{c} &= \int \Psi_j^{(n)}(\mathbf{c})(\tilde{\mathcal{M}} + \omega_j^{(0)})\Phi_k^{(l)}(\mathbf{c})d\mathbf{c} = \\ &= \int \Psi_j^{(n)}(\mathbf{c})(\tilde{\mathcal{M}} + \omega_k^{(0)})\Phi_k^{(l)}(\mathbf{c})d\mathbf{c} + (\omega_j^{(0)} - \omega_k^{(0)}) \int \Psi_j^{(n)}(\mathbf{c})\Phi_k^{(l)}(\mathbf{c})d\mathbf{c}, \end{aligned}$$

we have for  $n > 0$ ,

$$\begin{aligned} \sum_{l=0}^n \int \Psi_j^{(l)}(\mathbf{c})\Phi_k^{(n-l)}(\mathbf{c})d\mathbf{c} &= \\ &= (\omega_j^{(0)} - \omega_k^{(0)})^{-1} \sum_{l=0}^n \left[ \int \Psi_j^{(l-1)}(\mathbf{c})\mathbf{c}\Phi_k^{(n-l)}(\mathbf{c})d\mathbf{c} - \int \Psi_j^{(l)}(\mathbf{c})\mathbf{c}\Phi_k^{(n-l-1)}(\mathbf{c})d\mathbf{c} - \right. \\ &\quad \left. \sum_{m=1}^l \omega_j^{(m)} \int \Psi_j^{(l-m)}(\mathbf{c})\Phi_k^{(n-l)}(\mathbf{c})d\mathbf{c} + \sum_{m=1}^l \omega_j^{(l)} \int \Psi_j^{(l)}(\mathbf{c})\Phi_k^{(n-l-m)}(\mathbf{c})d\mathbf{c} \right]. \end{aligned}$$

Consider the first two terms of this sum:

$$\begin{aligned} \sum_{l=1}^n \int \Psi_j^{(l-1)}(\mathbf{c})\mathbf{c}\Phi_k^{(n-l)}(\mathbf{c})d\mathbf{c} - \sum_{l=0}^{n-1} \int \Psi_j^{(l)}(\mathbf{c})\mathbf{c}\Phi_k^{(n-l-1)}(\mathbf{c})d\mathbf{c} &= \\ \sum_{l=0}^{n-1} \left[ \int \Psi_j^{(l)}(\mathbf{c})\mathbf{c}\Phi_k^{(n-l-1)}(\mathbf{c})d\mathbf{c} - \int \Psi_j^{(l)}(\mathbf{c})\mathbf{c}\Phi_k^{(n-l-1)}(\mathbf{c})d\mathbf{c} \right] &= 0. \end{aligned}$$

Here we have used the convention established earlier that  $\Psi_j^{(-1)} = 0$ . The second two terms can be arranged in the following way:

$$\begin{aligned} \sum_{l=0}^n \sum_{m=1}^l \omega_j^{(m)} \int \Psi_j^{(l-m)}(\mathbf{c}) \Phi_k^{(n-l)}(\mathbf{c}) d\mathbf{c} = \\ \sum_{l=1}^n \sum_{m=0}^{n-l} \omega_j^{(l)} \int \Psi_j^{(m)}(\mathbf{c}) \Phi_k^{(n-l-m)}(\mathbf{c}) d\mathbf{c} = 0 \end{aligned}$$

by the inductive hypothesis, and so  $\sum_{l=0}^{\infty} \int \Psi_j^{(l)}(\mathbf{c}) \Phi_k^{(n-l)}(\mathbf{c}) d\mathbf{c} = 0$  for all  $n > 0$ .  $\square$

### A.3 Invariance of $\Psi_j(\mathbf{c}, i\mathbf{k})\Phi_j(\mathbf{c}', i\mathbf{k})$

From (A.5), one can see that  $\Psi_j^{(1)}(\mathbf{c})$  and hence  $\Psi_j(\mathbf{c}, i\mathbf{k})$  is dependent on the choice of an arbitrary term  $\eta_j^{(1)}$ . However, the product  $\Psi_j(\mathbf{c}, i\mathbf{k})\Phi_j(\mathbf{c}', i\mathbf{k})$  is invariant under choice of any of the arbitrary terms  $\eta_j^{(n)}$ , which we will now demonstrate by induction for the non-degenerate case. The extension to the degenerate case is straightforward.

We need to prove that the Taylor series coefficients of the product are invariant, *i.e.* that  $\sum_{l=0}^n \Psi_j^{(n-l)}(\mathbf{c})\Phi_j^{(l)}(\mathbf{c}')$  is invariant for every  $n$ . This is clearly true for  $n = 0$ . Assume that this is true for all  $n$  less than some whole number  $N$ . Then we find

$$\begin{aligned} \sum_{l=0}^N \Psi_j^{(N-l)}(\mathbf{c})\Phi_j^{(l)}(\mathbf{c}') = \\ \mathcal{L}_j \left( \mathbf{c} \sum_{l=0}^{N-1} \Psi_j^{(N-l-1)}(\mathbf{c})\Phi_j^{(l)}(\mathbf{c}') + \sum_{m=1}^{N-l} \omega_j^{(m)} \sum_{l=0}^{N-m} \Psi_j^{(N-l-m)}(\mathbf{c})\Phi_j^{(l)}(\mathbf{c}') \right) \\ + \Psi_j^{(0)}(\mathbf{c}) \sum_{l=0}^N \mathbf{A}_{jj}^{(N-l)} \Phi_j^{(l)}(\mathbf{c}') \end{aligned}$$

by use of (A.4). The first term on the right hand side is invariant by hypothesis. Now consider the second term, and suppose that  $\sum_{l=0}^n \mathbf{A}_{jj}^{(n-l)} \Phi_j^{(l)}(\mathbf{c}')$  is

invariant for all  $n$  less than  $N$ , as it is clearly true for  $n = 0$ . Then

$$\begin{aligned} \sum_{l=0}^N \mathbf{A}_{jj}^{(l)} \Phi_j^{(N-l)}(\mathbf{c}') &= \\ & \tilde{\mathcal{L}}_j \sum_{l=0}^{N-1} \mathbf{A}_{jj}^{(l)} \left\{ \mathbf{c} \Phi_j^{(N-l-1)}(\mathbf{c}') + \sum_{m=1}^{N-l} \omega_j^{(m)} \Phi_j^{(N-l-m)}(\mathbf{c}') \right\} \\ & + \sum_{l=0}^N \mathbf{A}_{jj}^{(l)} \mathbf{B}_{jj}^{(N-l)}. \end{aligned}$$

The first term of the right hand side is invariant by hypothesis, so we only need consider the second term

$$\begin{aligned} \sum_{l=0}^N \mathbf{A}_{jj}^{(l)} \mathbf{B}_{jj}^{(N-l)} &= \\ \delta_{N0} - \sum_{l=1}^{N-1} \sum_{\substack{k \in \sigma \\ k \neq j}} \mathbf{A}_{jk}^{(l)} \mathbf{B}_{jk}^{(N-l)} &= \\ \delta_{N0} - \sum_{l=1}^{N-1} \int \Psi_j^{(l)}(\mathbf{c}) \tilde{\mathcal{P}}_j \Phi_j^{(N-l)}(\mathbf{c}) d\mathbf{c} &= \\ \delta_{N0} - \sum_{l=1}^{N-1} \int \Psi_{jm}^{(l)}(\mathbf{c}) \tilde{\mathcal{L}}_j \left( \mathbf{c} \Phi_j^{(N-l-1)}(\mathbf{c}) + \sum_{m=1}^{N-l} \omega_j^{(m)} \Phi_j^{(N-l-m)}(\mathbf{c}) \right) d\mathbf{c}. \end{aligned}$$

Clearly, this term is invariant by hypothesis, so  $\sum_{l=0}^N \Psi_j^{(N-l)}(\mathbf{c}) \Phi_j^{(l)}(\mathbf{c}')$  is invariant.  $\square$

# Appendix B

## Calculation of the end-effects due to peak collector current measurements

Equations (3.11) and (3.12) were calculated by means of computer algebra. The language used for this is SMP [see Wolfram *et. al.* (1983)].

```
rho : (z - w[1] t + x[1]) / 2 / (w[2] t - x[2]) ^ (1/2)
```

```
expr[ $lmax ]:: \
  Sum[ \
    ( Sum[ w[m] w[1-m+1], {m,1,1} ] + \
      Sum[ \
        Sum[ \
          Sum[ w[n] w[1-j*k-m+1], {m,1,1-j*k} ] * \
            (w[j] t - x[j]) ^ k / k!, \
            {j, 3, Floor[ (1-1) / k ]} \
          ] \
        {k, 1, Floor[ (1-1) / 3 ]} \
      ] \
    ) * \
    2 ^ (-1) (w[2] t - x[2]) ^ (-1/2) Her[1,rho], \
    {1,1,$lmax} \
  ]
```

```
/* substitution rules for t and z, zz == 1/z */
```

```
r: {t -> 1/(w[1] zz + a2 zz^2 + a3 zz^3), z -> 1/zz}
```

```

/* we only need the first two terms for this calculation */

Her[ $1 _= Evenp[$1], $x ]::\
  $1! (-1)^($1/2) (1 / ($1/2)! - (2 $x)^2 / 2 / ($1/2 - 1)! )

Her[ $1 _= Oddp[$1] & $1 > 1, $x ]::\
  $1! (-1)^(( $1-1) / 2 ) ( 2 $x / (($1-1) / 2)! - \
  (2 $x)^3 / 3 / (($1-3) / 2)! )

Her[1,$x]: 2 $x

/* and now for the actual calculation */

run:: \
  Lcl[ %ps ];          /* declare %ps local */ \
  expr[10];           /* for a2 and a3, we need up to l=10 */\
  S[ %, r ];          /* substitute for z and t */ \
  %ps: Ps[%, zz, 0, 3]; /* form a power series in 1/z about */\
                      /* 0 to 3 terms */ \
  Sol[ %[5,1]=0, a2 ]; /* solve for a2 */ \
  Pr[ "a2=", \
      a2: Rat[ %[1,2] ] \
      ];              /* output a2 */ \
  Sol[ %ps[5,2]=0, a3 ]; /* solve for a3 */ \
  Pr[ "a3=", \
      a3: Rat[ %[1,2] ] \
      ];              /* output a3 */

```

Wolfram is no longer supporting SMP, but has a new product on the market called Mathematica. It is expected that this language, which is similar in a lot of respects to SMP, will become quite popular in the future. To allow non-SMP people to interpret the above code, I give the following notes:

- `:` is an assignment operator, whereby the right hand side is evaluated and assigned to the left hand side.
- `::` is an assignment operator in which the right hand side is assigned verbatim to the left hand side.
- `Floor[x] = [x]`.
- `Her[j,x] = Hj(x)`

- `Sum[ x[i], {i,1,n} ] =  $\sum_i^n x(i)$`
- `S[ x, a -> b ]` means replace a by b everywhere in the expression x.
- `\` is the continuation character.
- `$l _= Evenp[$l]` means “all  $l$  such that  $l$  is even”. Similarly with `Oddp`.
- `%%` = previous result. Parts of the expression may be extracted out by means of projections. For example, `Ps[Exp[x],x,0,3]` returns a Taylor series of  $\exp x$  about  $x = 0$  to third order expressed in the form:

`Ps[1,x,0,{0,6},{[0]:1,[1]:1,[2]:1/2,[3]:1/6}]`

So to extract the second Taylor coefficient, you need the fifth part of this expression, which is a list of the coefficients, and then you need the second coefficient in this list, hence `%%[5,2]`. Similarly, the output of the solve is a list of substitutions, *i.e.* `Sol[expr, x]` returns `{x -> x0}`. This allows the possibility for more than one solution. To get the real answer, you need the second part (*i.e.* the right hand side of the substitution) of the first component of the list, *i.e.* `%%[1,2]`

# Appendix C

## Numerical Studies of the Klein-Kramers Model

The code used in the numerical studies reported in section 4.3 is reported here. Figures 4.3 to 4.6 were produced by the following code:

```
C compute the steady point source delta(x)delta(c-cp) density function,
C n(r,t) for several different times t

PROGRAM SteadyPointSource
implicit none

double precision t,r,cp,a,rmin,rscale,nu
double precision result, error, integrand, scaleFactor
double precision res2,res4,res8,res16,res32,scale
integer N, dummy, ifail, ir, FNLen, iAcc !accumulate ifail results here
character*255 VaxFName
external integrand
parameter(N=100)
real f(6,0:N-1)
common /field/ a, nu, scaleFactor
common /Gparams/ cp,r
C workspace for integration
integer LW, LIW
parameter( LW=2000, LIW=LW/8+2 )
double precision WS(LW)
integer IW(LIW)
C parameters for precision of integration
double precision absErr, relErr
```

```

        parameter( absErr=1D-35, relErr=1D-3 )
C  ascii tab
        character tab
        parameter(tab=char(9))

C  read run parameters
        accept *,a,nu,t,cp
        accept *, rmin, rscale ! in this case, rscale temp. stores rmax
        accept *,scaleFactor
        VaxFName=' '
        accept 10,FNLen,(VaxFName(ir:ir),ir=1,FNLen)
        open (unit=10,file=VaxFName,status='NEW')
10      format(Q,64A1)

        rscale = ( rscale-rmin) / N

        Do 2 ir=0,N-1
            r = rmin + rScale * ir

C          /t /oo
C          | | G(c,r,t,cp) dc dt
C          /0 /-oo

        ifail = 1
        call D01AJF( integrand, ODO, t, absErr, relErr,
&                result, error, WS, LW, IW, LIW, ifail )
        iacc = ifail

        ifail = 1
        call D01AJF( integrand, ODO, t/2, absErr, relErr,
&                res2, error, WS, LW, IW, LIW, ifail )
        iacc = iacc + ifail

        ifail = 1
        call D01AJF( integrand, ODO, t/4, absErr, relErr,
&                res4, error, WS, LW, IW, LIW, ifail )
        iacc = iacc + ifail

        ifail = 1
        call D01AJF( integrand, ODO, t/8, absErr, relErr,
&                res8, error, WS, LW, IW, LIW, ifail )
        iacc = iacc + ifail

        ifail = 1

```

```

    call D01AJF( integrand, OD0, t/16, absErr, relErr,
&             res16, error, WS, LW, IW, LIW, ifail )
    iacc = iacc + ifail

    ifail = 1
    call D01AJF( integrand, OD0, t/32, absErr, relErr,
&             res32, error, WS, LW, IW, LIW, ifail )
    iacc = iacc + ifail

    if (iacc.ne.0) then
        print *, 'integral didn't converge, r=', r
    else
        write (10,3) r, tab, result, tab, res2, tab, res4,
&             tab, res8, tab, res16, tab, res32
3       format(1x,7(E11.4,A1))
        ENDIF
2       CONTINUE

    stop
    END

double precision FUNCTION integrand( t )
implicit none
double precision t, r, cp, IntofGwrtc
common /Gparams/ cp,r
integrand = IntofGwrtc(cp,r,t)
return
END

```

The colour plates of the phase space distribution function was produced by the following code:

C compute the steady point source  $\delta(x)\delta(c-c_p)$  distribution function,  
C f(c,r,t)

```

PROGRAM SteadyPointSource
implicit none
double precision c,t,r,cp,a,cmin,cscale,rmin,rscale,nu
double precision result, error, integrand, scaleFactor
integer N, dummy, ifail, ic, ir, FNLen
character*255 VaxFName
external integrand
parameter(N=100)
parameter (cmin=-1.0,cscale=0.04)

```

```

        common /field/ a, nu, scaleFactor
        common /Gparams/ c, cp, r
C workspace for integration
        integer LW, LIW
        parameter( LW=2000, LIW=LW/8+2 )
        double precision WS(LW)
        integer IW(LIW)

        accept *,a,nu,t,cp
        accept *,rmin,rscale !rscale temporarily holds rmax
        rscale = (rscale-rmin)/N
        accept *,scaleFactor
        VaxFName=' '
10      accept 10,FNLen,(VaxFName(ic:ic),ic=1,FNLen)
        format(Q,64A1)
        open (unit=10, file=VaxFName, status='NEW')
        write (10,*) N, rmin, rScale, cmin, cScale

        Do 1 ic=0,N-1
            Do 2 ir=0,N-1
                c = cmin + cScale * ic
                r = rmin + rScale * ir

C          /t
C          | G(c,r,t,cp) dt
C          /0

        ifail = 1
        call D01AJF( integrand, ODO, t, 1D-10, 1D-3, result, error,
&            WS, LW, IW, LIW, ifail )

        if (ifail.ne.0) then
            if (ifail.ne.6) then
                print *,'integral didn''t converge'
            else
                print *,'ifail= ',ifail
            ENDIF

        write (10,*) 999.999 !give it some value that can be ignored
C                                by Uniras

        else
            write (10,*) result
        ENDIF

```

```

2          CONTINUE
1          CONTINUE

```

```

stop
END

```

```

double precision FUNCTION integrand( t )
implicit none
double precision t, r, c, cp, G
common /Gparams/ c, cp, r
integrand = G(c, cp, r, t)
return
END

```

Both of the programs call the Greens function, which is encoded as:

C Free space Green's function for the 1-D Klein Kramers model

```

double precision FUNCTION G( c, cp, r, t)
implicit none
double precision a, c, cp, r, t, AA, BB, CC, nu, scaleFactor, z, th
common /field/ a, nu, scaleFactor
double precision lnMaxReal, expArg, sqrtFactor
parameter( lnMaxReal = 80)

If (t.eq.0) then !is equal to delta(r)delta(c-cp)
  If (r.eq.0.and.c.eq.cp) then
    G = exp( lnMaxReal)
  else
    G = 0
  ENDIF
return
ENDIF

th = tanh(t/2)
z = exp(-t)
AA = 0.5*t - th
BB = r-a*t-(c+cp-2*a)*th
CC = -2*(c-a-(cp-a)*z)**2/(1-z**2)

SqrtFactor = 1/Sqrt((1-z**2)*AA)
expArg = nu * t - scaleFactor + CC - BB**2 / 4 / AA
If (expArg + log(SqrtFactor).gt.lnMaxReal) then !trap possible overflows
  G = exp( lnMaxReal )
elseif (expArg.lt.-lnMaxReal) then

```

```

        G = 0
    else
        G = SqrtFactor * exp( expArg )
    ENDIF

    return
END

```

C integral of G with respect to c over the real line

```

double precision FUNCTION IntOfGwrtc( cp, r, t )
implicit none
double precision a,c,cp,r,t,AA, nu, scaleFactor, z, th
double precision AAA,BBB,CCC, expArg, lnMaxReal, SqrtFactor
parameter( lnMaxReal = 80)
common /field/ a, nu, scaleFactor

If (t.eq.0) then !is equal to delta(r)
    If (r.eq.0) then
        IntOfGwrtc = exp( lnMaxReal)
    else
        IntOfGwrtc = 0
    ENDIF
    return
ENDIF

th = tanh(t/2)
z = exp(-t)
AA = 0.5*t - th
AAA = 2 / (1-z**2) + th**2 / 4 / AA
BBB = (4*a*(1-z) + 4*cp*z) / (1-z**2) +
& ((2*a-cp)*th**2 + (r-a*t)*th) / 2 / AA
CCC = - 2 * ( a - z * ( a - cp ) ) ** 2 / (1-z**2) +
& (
& -( 2 * a - cp ) * th + r ) ** 2
& + 2 * a * t * ( r + ( 2 * a - cp ) * th )
& - ( a * t ) ** 2
& )
& / 4/ AA

expArg = nu * t - scaleFactor + CCC + BBB**2 / 4 / AAA
SqrtFactor = 1/Sqrt((1-z**2)*AA*AAA)
If (expArg + log(SqrtFactor).gt.lnMaxReal) then !trap possible overflows
    IntOfGwrtc = exp( lnMaxReal )

```

```
elseif (expArg.lt.-lnMaxReal) then
  IntOfGwrtc = 0
else
  IntOfGwrtc = SqrtFactor * exp( expArg )
ENDIF
return
END
```

# Appendix D

## Isotropic Tensors

In a fluid, there is no preferred direction, and consequently any property of the fluid with tensorial character must be isotropic, *i.e.* the components of the tensor have the same value regardless of the coordinate system used, provided that the same metric is used. Isotropic tensors up to rank four are given in the little monograph by Temple (1960). Eu (1979) give the complete set of isotropic six rank tensors. Other than these, there appears to be no generally available source of isotropic tensors. One approach to generating isotropic tensors of arbitrary rank in three dimensions is to note that any even rank isotropic tensor must be expressed as a linear combination of products of the unit tensor ( $\delta_{\mu\nu}$ ), and odd tensors as a linear combination of products of the unit tensor and the Levi-Cevita, or determinant tensor ( $\epsilon_{\lambda\mu\nu}$ ). This result is based on Weyl's theory of invariant polynomials [see Temple (1960) for a discussion]. In practice, this means finding every possible way of writing products of inner products between pairs of vectors, so that for example, the space of isotropic rank four tensors will be spanned by:

$$\begin{aligned} \mathbf{l}_1(\mathbf{u}, \mathbf{v}, \mathbf{w}, \mathbf{x}) &= (\mathbf{u} \cdot \mathbf{v})(\mathbf{w} \cdot \mathbf{x}), \\ \mathbf{l}_2(\mathbf{u}, \mathbf{v}, \mathbf{w}, \mathbf{x}) &= (\mathbf{u} \cdot \mathbf{w})(\mathbf{v} \cdot \mathbf{x}), \\ \mathbf{l}_3(\mathbf{u}, \mathbf{v}, \mathbf{w}, \mathbf{x}) &= (\mathbf{u} \cdot \mathbf{x})(\mathbf{v} \cdot \mathbf{w}), \end{aligned}$$

and that the space of rank five isotropic tensors is spanned by:

$$\begin{aligned}
\mathbf{l}_1(\mathbf{u}, \mathbf{v}, \mathbf{w}, \mathbf{x}, \mathbf{y}) &= (\mathbf{u} \cdot \mathbf{v})(\mathbf{w} \cdot \mathbf{x} \times \mathbf{y}), \\
\mathbf{l}_2(\mathbf{u}, \mathbf{v}, \mathbf{w}, \mathbf{x}, \mathbf{y}) &= (\mathbf{u} \cdot \mathbf{w})(\mathbf{v} \cdot \mathbf{x} \times \mathbf{y}), \\
\mathbf{l}_3(\mathbf{u}, \mathbf{v}, \mathbf{w}, \mathbf{x}, \mathbf{y}) &= (\mathbf{u} \cdot \mathbf{x})(\mathbf{v} \cdot \mathbf{w} \times \mathbf{y}), \\
\mathbf{l}_4(\mathbf{u}, \mathbf{v}, \mathbf{w}, \mathbf{x}, \mathbf{y}) &= (\mathbf{u} \cdot \mathbf{y})(\mathbf{v} \cdot \mathbf{w} \times \mathbf{x}), \\
\mathbf{l}_5(\mathbf{u}, \mathbf{v}, \mathbf{w}, \mathbf{x}, \mathbf{y}) &= (\mathbf{v} \cdot \mathbf{w})(\mathbf{u} \cdot \mathbf{x} \times \mathbf{y}), \\
\mathbf{l}_6(\mathbf{u}, \mathbf{v}, \mathbf{w}, \mathbf{x}, \mathbf{y}) &= (\mathbf{v} \cdot \mathbf{x})(\mathbf{u} \cdot \mathbf{w} \times \mathbf{y}), \\
\mathbf{l}_7(\mathbf{u}, \mathbf{v}, \mathbf{w}, \mathbf{x}, \mathbf{y}) &= (\mathbf{v} \cdot \mathbf{y})(\mathbf{u} \cdot \mathbf{w} \times \mathbf{x}), \\
\mathbf{l}_8(\mathbf{u}, \mathbf{v}, \mathbf{w}, \mathbf{x}, \mathbf{y}) &= (\mathbf{w} \cdot \mathbf{x})(\mathbf{u} \cdot \mathbf{v} \times \mathbf{y}), \\
\mathbf{l}_9(\mathbf{u}, \mathbf{v}, \mathbf{w}, \mathbf{x}, \mathbf{y}) &= (\mathbf{w} \cdot \mathbf{y})(\mathbf{u} \cdot \mathbf{v} \times \mathbf{x}), \\
\mathbf{l}_{10}(\mathbf{u}, \mathbf{v}, \mathbf{w}, \mathbf{x}, \mathbf{y}) &= (\mathbf{x} \cdot \mathbf{y})(\mathbf{u} \cdot \mathbf{v} \times \mathbf{w}).
\end{aligned}$$

Because the generalized constitutive relation (1.8) must be symmetric with respect to changes in sign of the thermodynamic force and flux, we are only interested in even rank tensors. I have written a program that generates the isotropic tensors of arbitrary even rank, and then proceeds to apply symmetrization operations to the tensors to produce the final set of independent tensors. Modifying it to produce odd rank tensors should not be too difficult a task. An example of its use, may be found in finding the number of transport coefficients used to describe the second order Burnett coefficient between stress and strain. This coefficient connects a second rank stress tensor  $\mathbf{\Pi}$  with the square of a second rank strain tensor. The coefficient is thus of sixth rank. There are fifteen sixth rank isotropic tensors, but not all of them are valid candidates because the only non-vanishing components must be symmetric with respect to interchanges of the third and fifth argument, as well as the fourth and the sixth. This is the case because in the expression  $\mathbf{L} :: \nabla \mathbf{u} \nabla \mathbf{u}$ , interchanging the two  $\nabla$ s produces no effect, neither the two  $\mathbf{u}$ s. In the program, this is performed by the lines

```

Symmetrize(LinComb[i], 3, 5);
Symmetrize(LinComb[i], 4, 6);

```

In the case of a monatomic fluid, we may further expect that the tensor should be symmetric with respect to the first two indices.

The program listing following can be used for arbitrary rank by changing the constants rank, NoComp and NoCompp1. Rank is fairly obviously the tensorial rank of the tensor under study. NoComp is the number of independent isotropic tensors of that rank, given by  $\prod_{i=1}^{\text{rank}/2-1} (1 + 2i)$ .

In the program, the basis tensors are represented as an array with rank components of type integer, which contain the sequence of vectors involved in the inner products. For example,  $\mathbf{l}_3$  in the rank four case would be represented by the integer sequence 1423. The complete basis is generated in the calcTensors procedure, and stored in Tensors. It does this by generating all possible permutations of the rank vectors, then expressing them all in a canonical form in which each pair is ordered so that the lowest index comes first within the pairs, and the pairs are then ordered according to the first index in each pair. When the canonical form is found, it is checked against a list of all previous canonical tensors found, and only added to the list if it is found to be distinct.

To generate the symmetrized tensors, we store the coefficients of a linear combination of the basis tensors in variables of type LinType. The algorithm proceeds by taking every basis tensor corresponding to non-zero coefficients, swapping the indices to be symmetrized, placing the tensor in canonical form, comparing this result against the basis list to find which tensor it corresponds to, then adding the original non-zero coefficient to the slot corresponding to the swapped basis tensor.

```

program tensors;
{even rank version}
  const
    rank = 6;
    NoComp = 15;    {NoComp = (rank-1)(rank-3)...3}
    NoCompp1 = 16; {NoComp+1}
  type
    jvalType = set of 2..rank;
    TensorType = array[1..rank] of integer;
    LinType = array[1..NoComp] of integer;
  var
    tensor: array[1..NoCompp1] of TensorType;
    i, j: integer;
    TensorIndex: integer;
    zero: LinType;
    LinComb: array[1..NoComp] of LinType;
    out: text;

```

```

procedure swap (var x, y: integer);
  var
    t: integer;
begin
  t := x;
  x := y;
  y := t;
end;

procedure Sort (left, right: integer; var Tensor: TensorType);
{Yep, the good old Qsort routine copied from ATPUG issue 1}
  var
    II, JJ, temp: integer;
    Pivot: integer;
    IIisGTright, JJisLTleft, IIgreatThan: boolean;

begin
  II := left;
  JJ := right;
  pivot := Tensor[pred(2 * ((II + JJ) div 2))];
  repeat
    while Tensor[pred(2 * II)] < pivot do
      II := succ(II);
    while Tensor[pred(2 * JJ)] > pivot do
      JJ := pred(JJ);
    if II <= JJ then
      begin
        swap(Tensor[2 * II - 1], Tensor[2 * JJ - 1]);
        swap(Tensor[2 * II], Tensor[2 * JJ]);
        II := succ(II);
        JJ := pred(JJ);
      end;
    until II > JJ;
    if JJ > left then
      Sort(left, JJ, Tensor);
    if II < right then
      Sort(II, right, Tensor)
  end;

function eq (x, y: tensorType): boolean;
  var
    i: integer;
    result: boolean;

```

```

begin
  result := true;
  for i := 1 to rank do
    result := result and (x[i] = y[i]);
  eq := result;
end;

function eqL (x, y: LinType): boolean;
var
  i: integer;
  result: boolean;
begin
  result := true;
  for i := 1 to NoComp do
    result := result and (x[i] = y[i]);
  eqL := result;
end;

procedure canonical (var tensor: tensortype);
var
  j: integer;
begin
{order each pair}
  for j := 1 to rank div 2 do
    if tensor[2 * j - 1] > tensor[2 * j] then
      swap(Tensor[2 * j - 1], Tensor[2 * j]);
    sort(1, rank div 2, Tensor);
  end;

procedure calcTensors;
var
  TTensor: TensorType;
{TensorIndex: integer;}

  procedure GenerLoop (nest: integer; jvals: jvaltype; TTensor: tensorType);
  var
    j, k: integer;
  begin
    for j := (nest + 2) div 2 to rank do
      if not (j in jvals) then
        begin
          TTensor[nest] := j;
          if nest < rank then
            GenerLoop(succ(nest), jvals + [j], TTensor)

```

```

else
  begin
    canonical(TTensor);
    k := 1;
    while not eq(TTensor, Tensor[k]) and (k < TensorIndex) do
      k := succ(k);
    if k = TensorIndex then
      begin
        if TensorIndex > NoComp then
          writeln('Either I stuffed up,',
            ' or you guessed the wrong value for NoComp');
          tensor[k] := TTensor;
          TensorIndex := succ(TensorIndex);
        end;
      end; {of else}
    end; {of if not (j in jval)}
  end; {of GenerLoop}

begin
  TensorIndex := 1;
  TTensor[1] := 1;
  GenerLoop(2, [], TTensor);
end;

procedure symmetrizePairs (var LinComb: LinType; pr1, pr2: integer);
{Symmetrize tensor with respect to two pairs of indices}
var
  NewLin: LinType;
  i, j: integer;
  TTensor: TensorType;
begin
  NewLin := zero;
  for i := 1 to NoComp do
    if LinComb[i] > 0 then
      begin
{get representation of component}
        TTensor := Tensor[i];
{swap pairs 1 and 2}
        for j := 1 to rank do
          if TTensor[j] = 2 * pr1 then
            TTensor[j] := 2 * pr2
          else if TTensor[j] = pred(2 * pr1) then
            TTensor[j] := pred(2 * pr2)
          else if TTensor[j] = 2 * pr2 then

```

```

        TTensor[j] := 2 * pr1
    else if TTensor[j] = pred(2 * pr2) then
        TTensor[j] := pred(2 * pr1);
    canonical(TTensor);
{find TTensor in the list}
    j := 0;
    repeat
        j := j + 1
    until eq(TTensor, Tensor[j]);
{add the swapped part to make it symmetric}
    NewLin[j] := NewLin[j] + LinComb[i];
    end; {of for i:=1 to NoComp}
{add NewLin to LinComb}
    for i := 1 to NoComp do
        LinComb[i] := LinComb[i] + NewLin[i];
    end; {of symmetrizePairs}

procedure symmetrize (var LinComb: LinType; Index1, Index2: integer);
{Symmetrize tensor with respect to two indices}
var
    NewLin: LinType;
    i, j: integer;
    TTensor: TensorType;
begin
    NewLin := zero;
    for i := 1 to NoComp do
        if LinComb[i] > 0 then
            begin
{get representation of component}
                TTensor := Tensor[i];
{swap pairs 1 and 2}
                for j := 1 to rank do
                    if TTensor[j] = Index1 then
                        TTensor[j] := Index2
                    else if TTensor[j] = Index2 then
                        TTensor[j] := Index1;
                    canonical(TTensor);
{find TTensor in the list}
                    j := 0;
                    repeat
                        j := j + 1
                    until eq(TTensor, Tensor[j]);
{add the swapped part to make it symmetric}
                    NewLin[j] := NewLin[j] + LinComb[i];
            end;
        end;
    end;
end;

```

```

        end; {of for i:=1 to NoComp}
{add NewLin to LinComb}
    for i := 1 to NoComp do
        LinComb[i] := LinComb[i] + NewLin[i];
    end; {of symmetrize}

begin
    CalcTensors;
    for i := 1 to NoComp do
        zero[i] := 0;
    for i := 1 to NoComp do
        begin
            LinComb[i] := zero;
            LinComb[i][i] := 1;
            Symmetrize(LinComb[i], 1, 2);
            Symmetrize(LinComb[i], 3, 5);
            Symmetrize(LinComb[i], 4, 6);
            j := 0;
            repeat
                j := succ(j)
            until eqL(LinComb[j], LinComb[i]);
            if i = j then {the linear combination is unique, so output it}
                begin
                    for j := 1 to NoComp do
                        if LinComb[i][j] <> 0 then
                            write(LinComb[i][j] : 1, '*I(', j : 3, ')+');
                        writeln;
                    end;
                end;
            end;
        end.
end.

```

# Appendix E

## System Size Dependence of a Product of Intensive Phase Variables

In this appendix, we show that the phase average of a product of intensive phase variables  $\prod_{i=1}^n A_i$  is of order  $N^{1-n}$ , with  $N$  being the number of particles in the system.

Let us begin by noting that the phase variable  $A_i$  can be written as an average over individual particles:

$$A_i = \frac{1}{N} \sum_{j=1}^N A_{ij}.$$

Then we find that

$$\begin{aligned} \left\langle \prod_{i=1}^n A_i \right\rangle &= \frac{1}{N^n} \left\langle \prod_{i=1}^n \sum_{j=1}^N A_{ij} \right\rangle \\ &= \frac{1}{N^n} \sum_{j=1}^N \left\langle \prod_{i=1}^n A_{ij} \right\rangle + \frac{1}{N^n} \sum_{k=1}^N \sum_{i=1}^n \left\langle A_{ik} \prod_{\substack{j \neq i \\ l \neq k}} A_{jl} \right\rangle. \end{aligned} \quad (\text{E.1})$$

In a system where the order is short range (for example a fluid far from its critical point), we would expect that correlations of the form  $\sum_{l \neq k} \langle A_{ik} A_{jl} \rangle$  only picks up contributions from its nearest neighbours, and is consequently

intensive. More generally, we can say that  $\langle A_{ik} \prod_{j \neq i} \sum_{l \neq k} A_{jl} \rangle$  is intensive. The first term on the right hand side of (E.1) is clearly intensive, so we find

$$\left\langle \prod_{i=1}^n A_i \right\rangle = o(N^{1-n}).$$

□

# Appendix F

## Nonlinear Burnett Coefficients Calculation

### F.1 Design Considerations

This chapter lists and describes the code employed in the calculation of nonlinear Burnett coefficients. The program was initially designed for a canonical ensemble to be produced, using a standard Nosé-Hoover thermostat. Each member of this canonical ensemble was then used as a starting point for a computation at constant current, with both current and temperature fixed by a Gaussian feedback mechanism, as initially suggested by Evans and Lynden-Bell (1988). Because we required the computation to accurately reflect the initial condition for each of the constant flux evolutions, we needed to use a self-starting differential equation solver, such as the fourth order Runge-Kutta method. Later on, we realised that a single equilibrium trajectory was all that was required.

Instead of modifying an existing molecular dynamics program, I decided to code from scratch a set of modules that can be mixed and matched to obtain the desired algorithm. The idea was to have a subroutine that integrates differential equations, and to pass to it a function that implements the equations of motion. So a typical subroutine call to the integrator will be (for example a Runge-Kutta algorithm)

```
CALL RK( X, F, N, H, NTSTEP )
```

This subroutine integrates a first order differential equation of the form  $\dot{\mathbf{x}} =$

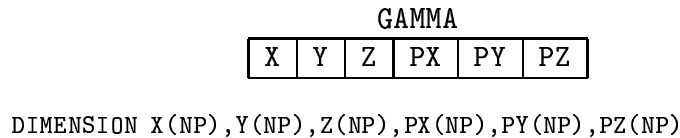


Figure F.1: Internal format of **GAMMA**

$\mathbf{f}(\mathbf{x})$ . In the above subroutine call,  $\mathbf{X}$  is a one dimensional array,  $F(I, \mathbf{X})$  is a function returning the  $i$ th component of  $\mathbf{f}(\mathbf{x})$ ,  $N$  is the number of components of  $\mathbf{X}$ ,  $H$  is the stepsize, and  $NTSTEPS$  is the number of timesteps to be evolved. The result of the computation is returned in  $\mathbf{X}$ .

In molecular dynamics simulations, the  $\mathbf{X}$  to be integrated is just the phase-space position  $\Gamma$ . From the perspective of the integrator, it does not matter in which order the components of  $\Gamma$  occur, but practically it works best to organize the  $x$ -components of the positions of all the particles, followed by the  $y$ -components and  $z$ -components, then the three momentum components are similarly arranged, as in fig F.1. This allows one to declare arrays containing only the  $x$ -components of position for example, by means of **EQUIVALENCE** statements, or common blocks.

## F.2 Parameters

In this program, all parameters are encoded as compile time constants. This approach has slightly greater efficiency and readability over reading the parameters in at run-time. The disadvantage of this method over the other is the requirement to recompile all modules of the program whenever one of the parameters change. This doesn't prove onerous, since run lengths are typically hundreds of hours compared with minutes of compile time. The following is a list of compile time parameters:

```
C Turn off default typing. This is not a standard Fortran77 construct.
C Replacing it by implicit character (a-z) produces almost as good type
  IMPLICIT CHARACTER (A-Z)

C NP = number of particles
```

```

C DIMPS = Dimension of phase space = 2 * D * NP
C D = dimension of physical space
C CUBSIZ = length of side of cube containing the particles
C TEMP = temperature
C THERMO = a switch determining whether thermostating is on
C RCUT = cut of radius for soft sphere interaction
C VO = parameter controlling the strength of the potential
C TAU = timescale for fluctuations in kinetic energy about the steady
C state mean value D * NP * TEMP
C Q = D * NP * TEMP * TAU ** 2 see Evans & Holian (1985), J Chem Phys, v83
C COLOUR = a switch determining if the colour field is on
C CURRNT = a switch determining if FCC sets up an initial colour current
C H = STEP SIZE
C NNHSTP = NUMBER OF TIMESTEPS OF NOSE HOOVER EVOLUTION BETWEEN SPURS
C NGPTS = NUMBER OF POINTS ALONG SPUR THAT ARE SAMPLED
C MAXJ = MAXIMUM VALUE OF THE COLOUR CURRENT ACCEPTED FOR THE SPUR
C EPSCUR = maximum relative variation allowed in the current
C   before a spur is rejected
C MAXRUN = maximum number of job resubmissions before termination
C MAXLAM = maximum value of lambda accepted
C TSTEP = time in milliseconds for one time origin to be executed
C QL = Nose-Hoover coupling constant for lambda
C SEEDO = initial random generator seed
      INTEGER DIMPS, D, NP
      DOUBLE PRECISION CUBSIZ, TEMP, RCUT, VO, TAU, Q, JO
      LOGICAL THERMO, COLOUR, CURRNT
      INTEGER NNHSTP, NGPTS, MAXKB, MAXRUN, MAXLAM, TSTEP, SEEDO
      DOUBLE PRECISION STPSIZ, MAXJ, EPSCUR, QL
      PARAMETER( D=3, NP=108, DIMPS = 2*D*NP, CUBSIZ=5.03, TEMP=1.08)
      PARAMETER( THERMO=.TRUE., RCUT=1.5, VO = 1, TAU = 0.09622 )
      PARAMETER( Q = D * NP * TEMP * TAU ** 2, QL=2 )
      PARAMETER( COLOUR=.TRUE., CURRNT=.TRUE. )
      PARAMETER( STPSIZ=4E-3, NNHSTP=10, NGPTS=2000)
      PARAMETER( MAXKB=1900, MAXJ = 0.2, EPSCUR=0.1, MAXLAM=20)
      PARAMETER( JO=0.0, MAXRUN=100, TSTEP=30000)
      PARAMETER( SEEDO= 14)

```

## F.3 Equations of Motion

As an example of how equations of motion are coded as a function, here is the function implementing the current-statting dynamics in equation (6.1).

```

C Equations of motions for the Norton ensemble, with Nose-Hoover

```

```

C thermostat and current statting mechanisms in the form
C (d/dt) GAMMA(I) = NORTON(I).

      DOUBLE PRECISION FUNCTION NORTON( I,GAMMA)
      INCLUDE (PARAM)
      DOUBLE PRECISION GAMMA(DIMPS+2), F(D*NP)
      DOUBLE PRECISION V, K, CALJ
      COMMON /FORCE/ F,V
      INTEGER I , ALPHA, LAMBDA, P
C Offsets into GAMMA
      PARAMETER (ALPHA=DIMPS+1,LAMBDA=DIMPS+2,P=DIMPS/2)
      INCLUDE (STFUN)

*VOCL STMT,IF(0)
      IF (I.LE.DIMPS/2) THEN
          NORTON = GAMMA(P+I)
*VOCL STMT,IF(100)
      ELSE IF (THERMO) THEN
*VOCL STMT,IF(33)
          IF (COLOUR.AND.I.LE.P+NP) THEN
              NORTON = F(I-P) - GAMMA(ALPHA) * GAMMA(I) -
&              GAMMA(LAMBDA) * E(I)
          ELSE IF (I.EQ.ALPHA) THEN
C equation of motion for alpha
              NORTON = ( K( GAMMA( P+1 ) ) / (1.5*NP*TEMP) - 1 ) /
&              TAU ** 2
          ELSE IF (COLOUR.AND.I.EQ.LAMBDA) THEN
C equation of motion for lambda
              NORTON = NP/QL * (CALJ( GAMMA( P+1 ) ) - JO)
          ELSE
              NORTON = F(I-P) - GAMMA(ALPHA) * GAMMA(I)
          ENDIF
      ELSE
          NORTON = F( I - P)
      ENDIF
      RETURN
      END

```

There are two things to note in this listing. The first is that there is generally some preprocessing to be done independently of the component number I. If Fortran allowed vector valued functions, this would be no problem, as we could do this preprocessing, and then return all components of F at once. Instead, we must use a kludge in which a call to F with I set to 0 is performed

before the individual components are returned. The second thing to note is that Fortran does not allow the equivalencing of subroutine parameters. Instead, to make thing a little more readable, I have defined the constants ALPHA, LAMBDA and P as indexes to GAMMA, so for example GAMMA(ALPHA) is the thermostating multiplier, and GAMMA(P+1) is  $p_{1x}$ .

## F.4 The Integrator

A far more efficient algorithm (by a factor of four) than the Runge-Kutta algorithm is due to Gear (1970). This is a multistep method, requiring higher order derivatives of  $\mathbf{x}$  to be known. As a consequence, a second order Runge-Kutta algorithm must be used to evaluate the higher order derivatives at time  $t = 0$ . This was tried for Gaussian systems, and was found to give the correct trajectory 99.5% of the time. The cause of the erroneous trajectories was never resolved. It was thought that the error involved in neglecting was statistically insignificant, however, the value calculated for colour conductivity disagreed with the accepted value by about 10%, or 2 standard errors. When the theory based on a single equilibrium trajectory was developed, it no longer mattered what the initial condition of the system are, so a self-starting method was no longer required.

A listing of the Gear integrator which is 4<sup>th</sup> order in  $h$  follows. The 1 in the name refers to the fact that a first order differential equation is being solved. Algorithms are listed in Gear's book for second and higher order equation. The Z refers to the equations of motion being integrated as the current and thermo-statted system listed as NORTON. It was found that in order to efficiently vectorize the code on the Fujitsu VP100, each subroutine had to be expanded inline at the compilation stage in order to avoid any recursive data dependencies (procedure integration). Unfortunately, procedure integration could not be performed on functional parameters, so the name of the equations of motion function had to be hard coded into the routine. For similar reasons, the phase space vector  $\mathbf{X}$  is now passed as a common block, so the only parameters left are H and NTSTEP. To alter this routine to do anything else only requires the strings NORTON, GAMMAG and DIMPS+2 to be globally changed with a text editor.

```
C Solve the equations of motion by the 4th order Gear predictor-  
C corrector method. Gear, C.W. (1971) Numerical Initial Value Problems
```

C in Differential Equations. (Prentice Hall: Englewood Cliffs, N.J.)  
 C This subroutine treats the equations of motion as a 1st order d.e.

```

SUBROUTINE GEAR1Z( H, NTSTEP )
  INCLUDE (PARAM)

```

```

C XT = x(t) = final state after time t = H*NTSTEP.
C H = step size
C NTSTEP = Number of time steps
C      n
C      H      n      n
C Xn = -- (d /dt ) XT
C      n!
C
C XnPRED = the predicted values of the above using a truncated Taylor
C series

```

```

      INTEGER NTSTEP, I, T
      DOUBLE PRECISION H, CORR, NORTON
      DOUBLE PRECISION XT(DIMPS+2), XTPRED(DIMPS+2), X3PRED(DIMPS+2)
      DOUBLE PRECISION X2(DIMPS+2), X2PRED(DIMPS+2), X3(DIMPS+2)
      DOUBLE PRECISION X4(DIMPS+2)
      DOUBLE PRECISION X1(DIMPS+2), X1PRED(DIMPS+2)
C Local storage is shared with SETGEG, GEARN, SETGEN
      COMMON /GSTORE/ XTPRED,X1PRED,X2PRED,X3PRED
C Derivatives filled of SETGEG
      COMMON /GSTORZ/ X1,X2,X3,X4
      COMMON /GAMMAG/ XT

```

```

C Gear coefficients
      DOUBLE PRECISION F0,F1,F2,F3,F4
      PARAMETER( F0=251./720, F1=1, F2=11./12, F3=1./3, F4=1./24)

```

```

C These statements are required for Procedure Integration on the FACOM
      DOUBLE PRECISION F(D*NP),V
      COMMON /FORCE/F,V

```

```

C Calculation loop
      DO 2 T=1,NTSTEP

```

```

C Predictor loop
      *VOCL LOOP,NOVREC(XTPRED)
      DO 3 I=1,DIMPS+2

```

```

XTPRED(I) = X1(I) + XT(I)+X2(I)+X3(I)+X4(I)
X1PRED(I) = X1(I) +
&      2 * X2(I) + 3 * X3(I) + 4 * X4(I)
X2PRED(I) = X2(I) + 3*X3(I) + 6*X4(I)
X3PRED(I) = X3(I) + 4*X4(I)
3      CONTINUE

```

```

C Evaluation step
      CALL FORCES(XTPRED)

```

```

C Corrector loop
*VOCL LOOP,NOVREC(XT)
      DO 4 I=1,DIMPS+2
          CORR = NORTON(I,XTPRED) * H - X1PRED(I)
          XT(I) = XTPRED(I) + FO * CORR
          X1(I) = X1PRED(I) + F1 * CORR
          X2(I) = X2PRED(I) + F2 * CORR
          X3(I) = X3PRED(I) + F3 * CORR
          X4(I) = X4(I) + F4 * CORR
4      CONTINUE

```

```

2      CONTINUE

```

```

      CALL CUBE( XT)
      RETURN
      END

```

## F.5 Periodic Boundary Conditions

The subroutine CUBE performs the periodic boundary conditions. It can be readily modified to perform Lees-Edwards boundary conditions if this was required.

C Retract positions to within cube

```

      SUBROUTINE CUBE( GAMMA )
      INCLUDE (PARAM)
      DOUBLE PRECISION GAMMA(DIMPS)
      INTEGER I
      DO 1 I=1,D*NP
          GAMMA(I) = GAMMA(I)-CUBSIZ*INT( GAMMA(I)/ CUBSIZ)
          IF (GAMMA(I).LT.0) GAMMA(I) = GAMMA(I)+CUBSIZ
1      CONTINUE

```

```
RETURN
END
```

## F.6 Forces

The forces routine, which is the most CPU intensive routine, was originally written for arbitrary dimension. It was found that the routine could not be vectorized properly without coding it explicitly in three dimensions. This is the only part of the code that is dimension dependent, apart from the initialization routine FCC. It is also desirable to perform potential and pressure calculations at this stage.

```
C Compute the forces on all the particles due to all the other particles
C as a function of the position in phase space GAMMA,
C and store the result in an array F(i)
```

```
      SUBROUTINE FORCES( X )
      INCLUDE (PARAM)
```

```
C R = displacement between two particles (vector quantity)
C RIJSQ = |R|**2
C FIJ = SCALF(RIJSQ) = scalar part of force term
C FKIJ = Kth component of the force between two particles
```

```
C Three dimensional version
```

```
      DOUBLE PRECISION F(NP*D), X(DIMPS)
      DOUBLE PRECISION FIJ, FKIJ, SCALF, RIJSQ
      DOUBLE PRECISION R1,R2,R3, RSI, R6, V
C F$ in front of the index variables are used to get PI to interact
C correctly with *VOCL
      INTEGER F$I,F$J
      COMMON /FORCE/ F, V

      DOUBLE PRECISION STEP,Z
      STEP(Z) = 0.5 + SIGN(0.5D0,Z)

      DO 6 F$I=1,D*NP
          F(F$I)=0
6          CONTINUE

      V = 0
```

```

*VOCL LOOP,TEMP(R1,R2,R3,RIJSQ,FIJ,FKIJ)
*VOCL LOOP,VI(F$I)
*VOCL LOOP,NOVREC(F)
*VOCL LOOP,F$I.LE.NP
*VOCL LOOP,F$J.LT.NP
*VOCL LOOP,F$J.LT.F$I

      DO 1 F$I=2,NP
        DO 2 F$J=1,F$I-1
          R1 = X(F$I) - X(F$J)
          R2 = X(F$I+NP) - X(F$J+NP)
          R3 = X(F$I+2*NP) - X(F$J+2*NP)

C Perform image particle correction
*VOCL STMT,IF(60)
      IF (ABS(R1).GT.CUBSIZ/2) R1 = R1 - SIGN(CUBSIZ,R1)
*VOCL STMT,IF(60)
      IF (ABS(R2).GT.CUBSIZ/2) R2 = R2 - SIGN(CUBSIZ,R2)
*VOCL STMT,IF(60)
      IF (ABS(R3).GT.CUBSIZ/2) R3 = R3 - SIGN(CUBSIZ,R3)

      RIJSQ = R1 ** 2 + R2 ** 2 + R3 ** 2

      RSI = 1/RIJSQ
      R6 = RSI ** 3
      V = V + 4 * (R6 * (R6-1) - RCUT ** (-6) * (RCUT**(-6)-1))
&    * STEP(RCUT**2-RIJSQ)
      FIJ = 4 * 6 * RSI * R6 *(2*R6-1) * STEP(RCUT**2-RIJSQ)

      FKIJ = R1 * FIJ
      F(F$I) = F(F$I) + FKIJ
      F(F$J) = F(F$J) - FKIJ
      FKIJ = R2 * FIJ
      F(F$I+NP) = F(F$I+NP) + FKIJ
      F(F$J+NP) = F(F$J+NP) - FKIJ
      FKIJ = R3 * FIJ
      F(F$I+2*NP) = F(F$I+2*NP) + FKIJ
      F(F$J+2*NP) = F(F$J+2*NP) - FKIJ
2    CONTINUE
1    CONTINUE
      RETURN
      END

```

## F.7 Miscellany

Statement functions which make use of system dependent features such as bit manipulation.

```
INTEGER*4 DUMARG, E
LOGICAL ODD
E( DUMARG ) = SIGN( 1, ISHFT( DUMARG, 31))
ODD( DUMARG ) = BTEST( DUMARG, 0 )
```

C set up a phase space point that corresponds to a face centred cubic  
C crystal with random velocities constrained by the temperature and zero  
C drift. 3 dimensional version

```
SUBROUTINE FCC
INCLUDE (PARAM)
```

```
DOUBLE PRECISION X(NP),Y(NP),Z(NP),PX(NP), PY(NP), PZ(NP), LATSIZ
DOUBLE PRECISION SUMPX, SUMPY, SUMPZ, SUMPSQ
INTEGER SEED, I,J,K,M, IJ, NCCC
COMMON /GAMMAG/ X,Y,Z,PX,PY,PZ
```

C These parameters are used if an initial colour current=J0 is required  
DOUBLE PRECISION C, CALJ, SCALE

```
INCLUDE (STFUN)
```

```
LATSIZ = CUBSIZ * (NP/4) ** (-1/3.)
NCCC = (NP/4) ** (1./3) + 0.1
```

C make primitive cell

C 1st particle

```
X(1) = 0.25 * LATSIZ
Y(1) = 0.25 * LATSIZ
Z(1) = 0.25 * LATSIZ
```

C 2nd particle

```
X(2) = 0.75 * LATSIZ
Y(2) = 0.75 * LATSIZ
Z(2) = 0.25 * LATSIZ
```

C 3rd particle

```
X(3) = 0.25 * LATSIZ
Y(3) = 0.75 * LATSIZ
Z(3) = 0.75 * LATSIZ
```

C 4th particle

```
X(4) = 0.75 * LATSIZ
```

```
Y(4) = 0.25 * LATSIZ
Z(4) = 0.75 * LATSIZ
```

```
C Replicate primitive cell
```

```
C M = 6 * the number of the cell generated. I,J,K run through the cube i
```

```
C different dimensions, and IJ runs through the four particles in each c
```

```
C The first run through the loop is redundant
```

```
      M = 0
      DO 1 I=1,NCCC
        DO 2 J=1,NCCC
          DO 3 K=1,NCCC
            DO 4 IJ = 1,4
              X(IJ+M) = X(IJ) + (K-1) * LATSIZ
              Y(IJ+M) = Y(IJ) + (J-1) * LATSIZ
              Z(IJ+M) = Z(IJ) + (I-1) * LATSIZ
            4      CONTINUE
              M = M + 4
          3      CONTINUE
        2      CONTINUE
      1      CONTINUE
```

```
C Generate random momenta
```

```
      SUMPX = 0
      SUMPY = 0
      SUMPZ = 0
      SUMPSQ = 0
      SEED = 10101
      DO 10 I=1,SEEDO
        CALL RAND(SEED,PX(1))
      10     CONTINUE
      DO 5 I=1,NP
        CALL RAND( SEED, PX(I) )
        CALL RAND( SEED, PY(I) )
        CALL RAND( SEED, PZ(I) )
        SUMPX = SUMPX + PX(I)

        SUMPY = SUMPY + PY(I)

        SUMPZ = SUMPZ + PZ(I)
        SUMPSQ = SUMPSQ + PX(I)**2 + PY(I)**2 + PZ(I)**2
```

```

5      CONTINUE

C calculate centre of mass kinetic energy
      SUMPSQ = SUMPSQ - 1./NP * (SUMPX**2 + SUMPY**2 + SUMPZ**2)

C Renormalize so that drift is zero and the kinetic energy is equal to t
C temperature
      DO 6 I=1,NP
        PX(I) = (PX(I) - SUMPX / NP) *
&          Sqrt( 3 * NP * TEMP / SUMPSQ)
        PY(I) = (PY(I) - SUMPY / NP) *
&          Sqrt( 3 * NP * TEMP / SUMPSQ)
        PZ(I) = (PZ(I) - SUMPZ / NP) *
&          Sqrt( 3 * NP * TEMP / SUMPSQ)
6      CONTINUE

C If an initial current is required, then adjust the momenta, and rescal
C adjust the kinetic energy
      IF (CURRNT) THEN
C Compute initial colour current
        C = CALJ(PX)
        SCALE = Sqrt( (J0**2-3*TEMP)/(C**2-3*TEMP))

C set up initial colour current
        DO 7 I=1,NP
          PX(I) = (PX(I) - E(I) * C) * SCALE + E(I) * J0
          PY(I) = PY(I) * SCALE
          PZ(I) = PZ(I) * SCALE
7      CONTINUE
        ENDIF

      RETURN
      END

      SUBROUTINE RAND(ISEED,R)
      DOUBLE PRECISION DSEED,D2P31M, D2P31, R
      DATA D2P31M/2147483647.DO/
      DATA D2P31/2147483648.DO/
      DSEED=ISEED
      DSEED=DMOD(16807.DO*DSEED,D2P31M)
      R=DSEED/D2P31
      ISEED=INT(DSEED)
      RETURN
      END

```

```

DOUBLE PRECISION FUNCTION CALJ(PX)
INCLUDE (PARAM)
DOUBLE PRECISION PX(NP), J
INTEGER I
INCLUDE (STFUN)
J = 0
DO 1 I= 1,NP
  J = J + PX(I) * E(I)
1  CONTINUE
CALJ = J / NP
RETURN
END

```

C return the kinetic energy as a function of phase space

```

DOUBLE PRECISION FUNCTION K(P)
INCLUDE (PARAM)
DOUBLE PRECISION SUMPSQ, P( D*NP )
INTEGER I
SUMPSQ = 0

DO 1 I=1,D*NP
  SUMPSQ = SUMPSQ + P(I)**2
1  CONTINUE

K = SUMPSQ / 2
RETURN
END

```

## F.8 Analysis of Data

At this stage the ideal form of the calculation would be to run the simulation saving the state vector at each step, then analysing the data with a post-processing program. Unfortunately, the run lengths involved in this project prohibited this method of operation, as gigabytes of data are produced. The only alternative was to analyse the data on the fly. The subroutine `OUTPUT` generates a sum of transient responses, and stores the results in a buffer, which is defined in the following include file:

```

DOUBLE PRECISION SLTLOJ(NGPTS), SUMJ(NGPTS)
DOUBLE PRECISION SUMLT(NGPTS), SLTLO(NGPTS)

```

```

DOUBLE PRECISION LTLOJ2(NGPTS)
COMMON /BUFFER/SUMLT,SUMJ,SLTLO,SLTLOJ,LTLOJ2

```

Output maintains a shift register, in which  $\lambda$ ,  $\lambda J$  and  $\lambda J^2$  are cycled through. The transient response function is then generated as a function of the time difference between the current value of  $\lambda$  and the previous remembered values.

```

SUBROUTINE OUTPUT
INCLUDE (PARAM)
INTEGER STEP
DOUBLE PRECISION ALPHA, LAMBDA, CALJ
INCLUDE (BUFFER)
DOUBLE PRECISION XZ(D*NP), PZ(D*NP), P
COMMON /GAMMAG/ XZ,PZ,ALPHA,LAMBDA
DOUBLE PRECISION SHIFT(NGPTS), SHFTJ(NGPTS), SHFTJ2(NGPTS)
COMMON /SHIFTR/ SHIFT, SHFTJ, SHFTJ2
DOUBLE PRECISION PRESS
CALL SHFTIN(LAMBDA, CALJ(PZ))
P = PRESS()
DO 1 STEP=1,NGPTS
  SLTLO(STEP) = SLTLO(STEP) + LAMBDA * SHIFT(STEP)
  SLTLOJ(STEP) = SLTLOJ(STEP) + P * SHFTJ(STEP)
  LTLOJ2(STEP) = LTLOJ2(STEP) + LAMBDA * SHFTJ2(STEP)
1  CONTINUE
RETURN
END

SUBROUTINE SHFTIN(L,J)
INCLUDE (PARAM)
INTEGER I
DOUBLE PRECISION L,J,SHIFT(NGPTS),SHFTJ(NGPTS), SHFTJ2(NGPTS)
COMMON /SHIFTR/ SHIFT, SHFTJ, SHFTJ2
DO 1 I=NGPTS-1,1,-1
  SHIFT(I+1)=SHIFT(I)
  SHFTJ(I+1)=SHFTJ(I)
  SHFTJ2(I+1)=SHFTJ2(I)
1  CONTINUE
SHIFT(1)=L
SHFTJ(1)=L*J
SHFTJ2(1)=L*J**2
RETURN
END

BLOCK DATA BUFNIT

```

```

INCLUDE(PARAM)
DOUBLE PRECISION SUMLT(NGPTS), SLTLO(NGPTS)
DOUBLE PRECISION SLTLOJ(NGPTS), SUMJ(NGPTS)
DOUBLE PRECISION LTLOJ2(NGPTS)
COMMON /BUFFER/SUMLT,SUMJ,SLTLO,SLTLOJ,LTLOJ2
DATA SLTLO/NGPTS*0.0/
DATA SUMLT/NGPTS*0.0/
DATA SUMJ/NGPTS*0.0/
DATA SLTLOJ/NGPTS*0.0/
DATA LTLOJ2/NGPTS*0.0/
END

```

## F.9 Putting it all Together

The program is run as a series of batch jobs, each lasting about an hour. When the program starts up, it reads the file on unit 10 to obtain the run number. If it is the first run, it will generate a face-centred cubic crystal lattice, which will then be melted to provide the fluid. After that, it will read in the current state of the system on unit 11 and the contents of the shift register on unit 13. Then it performs a loop in which the system is evolved and the TTCF calculated. Every now and then, output data is written out as a check point. When the time limit has expired, all the files are updated, and the partial sum of the TTCFs is appended to unit 12.

```

PROGRAM TTCF
C calculate the burnett coefficients using the new Nose-Hoover algorithm
C Z indicates in the Nose Current-stat
INCLUDE (PARAM)
INTEGER J,KB
INTEGER START, ERR, IOPEN, TLIMIT, TUSED, TLEFT
DOUBLE PRECISION GZ(DIMPS+2),XZ(D*NP),PZ(D*NP), CALJ
DOUBLE PRECISION G2(DIMPS+2),G3(DIMPS+2),G4(DIMPS+2)
DOUBLE PRECISION G1(DIMPS+2),LAMBDA
EQUIVALENCE (GZ,XZ),(GZ(D*NP+1),PZ),(GZ(DIMPS+2),LAMBDA)
COMMON /GAMMAG/GZ
COMMON /GSTORZ/G1,G2,G3,G4
INCLUDE (BUFFER)
DOUBLE PRECISION SHIFT(NGPTS), SHIFTJ(NGPTS), SHFTJ2(NGPTS)
COMMON /SHIFTR/ SHIFT, SHIFTJ, SHFTJ2

C GZ = NOSE-HOOVER PHASE SPACE POINT

```

```

C G2..G5 = 2ND TO 5TH DERIVATIVE OF POSITION OF NOSE-HOOVER PS POINT
C XZ, PZ =POSITION & MOMENTUM OF N.H. PHASE SPACE POINT
C KB = time step counter for NoseHoover

      READ (10,*) START
      IF (START.EQ.0) THEN
C Initialize Nose-Hoover Phase Space
      CALL FCC
      DO 100 KB=1,2000
      CALL GEAR1Z(STPSIZ,5)
      CALL SHFTIN(LAMBDA,CALJ(PZ))
100    CONTINUE
      ELSE IF (START.EQ.MAXRUN) THEN
      STOP 999
      ELSE
C read in previous check point
      READ(11) GZ,G1,G2,G3,G4
      READ(13) SHIFT,SHIFTJ,SHFTJ2
      ENDIF

      KB=0
C   WHILE CPU TIME LEFT > TIME ORIGIN TIME
20    CONTINUE
      CALL CPUTME(TLIMIT,TUSED,TLEFT)
      IF (TLEFT.LE.TSTEP) GOTO 1
      IF (MOD(KB,100000).EQ.99999) THEN
      OPEN(UNIT=14,FILE='RKS105.TTCFSAVE.DATA',STATUS='OLD')
      CALL FLUSH(KB)
      CLOSE (14)
      ENDIF
      KB = KB+1
      CALL GEAR1Z(STPSIZ, 5)
      CALL OUTPUT
      GOTO 20
1     CONTINUE
      ERR=IOPEN('UNIT=12,FILE=RKS105.TTCF.OUTPUT.DATA,STATUS=MOD')
      IF (ERR.NE.0) GOTO 11
C Error code returns to this point
13    CONTINUE
      REWIND 10
      WRITE (10,*) START+1
      REWIND 11
      WRITE (11) GZ,G1,G2,G3,G4
C Flush output buffer

```

```

WRITE (12,ERR=11) KB,NGPTS
WRITE (12,ERR=11) SLTLO
WRITE (12,ERR=11) SLTLOJ
WRITE (12,ERR=11) LTLOJ2
REWIND 13
WRITE (13) SHIFT,SHIFTJ,SHFTJ2
STOP
C Error control code - this just seemed the best place to put it
11      J=0
C      REPEAT UNTIL a file can be opened
10      CONTINUE
        CLOSE (12,ERR=12)
12      ERR=IOPEN('UNIT=12,FILE=RKS105.OUTSAVE'//CHAR(J+ICHAR('0'))//
&        '.DATA,STATUS=NEW')
        J=J+1
        PRINT *,'ERR=',ERR
        IF (ERR.NE.0) GOTO 10
        GOTO 13
END

SUBROUTINE FLUSH(KB)
INCLUDE (PARAM)
INTEGER J,KB
INTEGER START, ERR, IOPEN, TLIMIT, TUSED, TLEFT
DOUBLE PRECISION GZ(DIMPS+2),XZ(D*NP),PZ(D*NP), CALJ
DOUBLE PRECISION G2(DIMPS+2),G3(DIMPS+2),G4(DIMPS+2)
DOUBLE PRECISION G1(DIMPS+2),LAMBDA
EQUIVALENCE (GZ,XZ),(GZ(D*NP+1),PZ),(GZ(DIMPS+2),LAMBDA)
COMMON /GAMMAG/GZ
COMMON /GSTORZ/G1,G2,G3,G4
INCLUDE (BUFFER)
DOUBLE PRECISION SHIFT(NGPTS), SHIFTJ(NGPTS), SHFTJ2(NGPTS)
COMMON /SHIFTR/ SHIFT, SHIFTJ, SHFTJ2

13      CONTINUE
        REWIND 11
        WRITE (11) GZ,G1,G2,G3,G4
C Flush output buffer
        WRITE (14,ERR=11) KB,NGPTS
        WRITE (14,ERR=11) SLTLO
        WRITE (14,ERR=11) SLTLOJ
        WRITE (14,ERR=11) LTLOJ2
        REWIND 13
        WRITE (13) SHIFT,SHIFTJ,SHFTJ2

```

```
      RETURN
C Error control code - this just seemed the best place to put it
11      J=0
C      REPEAT UNTIL a file can be opened
10      CONTINUE
          CLOSE (12,ERR=12)
12      ERR=IOPEN('UNIT=12,FILE=RKS105.OUTSAVE'//CHAR(J+ICHAR('0'))//
&          '.DATA,STATUS=NEW')
          J=J+1
          PRINT *, 'ERR=', ERR
          IF (ERR.NE.0) GOTO 10
          GOTO 13
      END
```



# Bibliography

- Abramowitz, M. and Stegun, I. A. (1965). 'Handbook of Mathematical Functions'. (Dover: New York).
- Alder, B. J. and Wainwright, T. E. (1970). *Phys. Rev. A* **1**, 18.
- Allen, M. P. and Tildesley, D. (1987). 'Computer Simulation of Liquids'. (Clarendon: Oxford).
- Blevin, H. A. and Fletcher, J. (1984). *Aust. J. Phys.* **37**, 593.
- Braglia, G. L. (1980). *La Revista Del Nuovo Cimento* **3**, No. 5, 1.
- Brown, D. and Clarke, J. H. R. (1986). *Phys. Rev. A* **34**, 2093–2099.
- Burnett, D. (1935). *Proc. Lond. Math. Soc.* **40**, 382.
- Cassidy, R. A. and Elford, M. T. (1985). *Aust. J. Phys.* **38**, 587.
- Cavalleri, G. and Pavari-Fontana, S. L. (1972). *Phys. Rev. A* **5**, 327.
- Chapman, S. and Cowling, T. G. (1970). 'The Mathematical Theory of Non-Uniform Gases' 3rd ed.. (Cambridge UP: London).
- Cohen, E. G. D. (1962). *In* 'Fundamental Problems in Statistical Mechanics' (Ed. Cohen, E. G. D.),. (North Holland: Amsterdam).
- Cohen, E. G. D. (1983). *Physica A* **118**, 17–42.
- de Groot, S. R. and Mazur, P. (1962). 'Non-Equilibrium Thermodynamics'. (North Holland: Amsterdam).
- Dorfman, J. R. (1963). *Proc. Nat. Acad. Sci.* **50**, 804.

- Dorfman, J. R. and van Beijeren, H. (1977). *In* ‘Statistical Mechanics, Part B’ (Ed. Berne, J.), pp. 65–179. (Plenum: New York).
- England, J. P. and Elford, M. T. (1987). *Aust. J. Phys.* **40**, 355.
- Erdélyi, A. (1954). ‘Higher Transcendental Functions’ vol 2. (McGraw-Hill: New York).
- Ernst, M. H., Cichocki, B., Dorfman, J. R., Sharma, J., and van Beijeren, H. (1978). *J. Stat. Phys.* **18**, 237–270.
- Erpenbeck, J. J. (1987). *Phys. Rev. A* **35**, 218.
- Eu, B. C. (1979). *Can. J. Phys.* **58**, 931.
- Evans, D. J. (1983). *J. Chem. Phys.* **78**, 3297.
- Evans, D. J. and Holian, B. L. (1985). *J. Chem. Phys.* **83**, 4069.
- Evans, D. J., Hoover, W. J., Failor, B. H., Moran, B., and Ladd, A. J. C. (1983). *Phys. Rev. A* **28**, 1016.
- Evans, D. J. and Lynden-Bell, R. M. (1988). *Phys. Rev. A* **38**, 5249.
- Evans, D. J. and Morriss, G. P. (1984). *Chem. Phys.* **87**, 451.
- Evans, D. J. and Morriss, G. P. (1985). *Phys. Rev. A* **31**, 3817.
- Evans, D. J. and Morriss, G. P. (1986). *Phys. Rev. Lett.* **56**, 2172.
- Evans, D. J. and Morriss, G. P. (1988). *Mol. Phys.* **64**, 521.
- Evans, D. J. and Standish, R. K. (1990). *In* ‘Computer Modelling of Fluids, Polymers and Solids’ (Eds. Catlow, C. et al.), pp. 125–154. (Kluwer: Dordrecht).
- Gatland, I. R., Morrison, W. R., Ellis, H. W., Thackston, M. G., McDaniel, E. W., Alexander, M. H., Viehland, L. A., and Mason, E. A. (1977). *J. Chem. Phys.* **66**, 5121.
- Gear, C. W. (1970). ‘Numerical Initial Value Problems in Differential Equations’. (Prentice Hall: Englewood Cliffs, N.J.).

- Grad, H. (1963). In 'Rarefied Gas Dynamics' (Ed. Laurmann, J. A.), (Academic Press: New York).
- Hamm, H. (1977). *Proceedings of Symposia in Pure Mathematics* **30**, 31.
- Harris, S. (1981). *J. Chem. Phys.* **75**, 3037.
- Hood, L. M. (1989). 'Computer Simulations of Shear Flow in Simple Fluids' PhD thesis Australian National University GPO Box 4 Canberra 2601 Australia.
- Hood, L. M., Evans, D. J., and Morriss, G. P. (1987). *Molec. Phys.* **62**, 419–428.
- Hoover, W. G. (1985). *Phys. Rev. A* **31**, 1695.
- Hoover, W. G., Ladd, A. J. C., and Moran, B. (1982). *Phys. Rev. Lett.* **48**, 1818.
- Howorka, F., Fehsenfeld, F. C., and Albritton, D. L. (1979). *J. Phys. B* **12**, 4189.
- Huxley, L. G. and Crompton, R. W. (1974). 'The Diffusion and Drift of Electrons in Gases'. (Wiley: New York).
- Knopp, K. (1951). 'Theory and Application of Infinite Series'. (Blackie and Son: London).
- Kondo, K. (1987). *Aust. J. Phys.* **40**, 367.
- Kumar, K. (1980). *Aust. J. Phys.* **33**, 449–468.
- Kumar, K. (1981). *J. Phys. D* **14**, 2199.
- Kumar, K. (1984). *Phys. Rep.* **112**, 321.
- Kumar, K. and Robson, R. E. (1973). *Aust. J. Phys.* **26**, 157.
- Kumar, K., Skullerud, H. R., and Robson, R. (1980). *Aust. J. Phys.* **33**, 343.
- Kuščer, I. and Williams, N. M. R. (1967). *Phys. Fluids* **10**, 1922.

- Lees, Q. W. and Edwards, S. F. (1972). *J. Phys. C* **5**, 1921.
- Lovaas, T. H., Skullerud, H. R., Kristensen, O. H., and Linhjell, D. (1988). *J. Phys. D* **20**, 11.
- MacIntosh, A. I. (1974). *Aust. J. Phys.* **27**, 59.
- Malgrange, B. K. (1974). *Annales Scientifique Ecole Normale Superieure 4e Serie* **7**, 405.
- Marchesoni, F. and Grigolini, P. (1985). *Adv. Chem. Phys.* **62**, 29.
- Marshall, T. W. and Watson, E. J. (1987). *J. Phys. A* **20**, 1345.
- Morriss, G. P. and Evans, D. J. (1985). *Molec. Phys.* **54**, 629.
- Morruzzi, J. L. and Kondo, Y. (1980). *Jap. J. App. Phys.* **19**, 1411.
- Nosé, S. (1984a). *Mol. Phys.* **52**, 255.
- Nosé, S. (1984b). *J. Chem. Phys.* **81**, 511.
- Pao, Y. (1974). *Comm. Pure Appl. Math.* **27**, 407.
- Risken, H. (1984). 'The Fokker Planck Equation'. (Springer: Berlin).
- Robson, R. E. (1975). *Aust. J. Phys.* **28**, 523.
- Selinger, J. V. and Titulaer, U. M. (1984). *J. Stat. Phys.* **36**, 293.
- Senff, U. E. and Burton, P. G. (1986). *Mol. Phys.* **58**, 637–645.
- Serra, R., Andretta, M., Compiani, M., and Zanarini, G. (1986). 'Introduction to the Physics of Complex Systems: The Mesoscopic Approach To Fluctuations, Nonlinearity and Self-organization'. (Pergamon: Oxford).
- Skullerud, H. R. (1974). *Aust. J. Phys.* **27**, 195.
- Skullerud, H. R. (1977). In 'Proc. 13th International Conference on Phenomena in Ionised Gases, Part III' pp. 303–319. (GDR Physical Society: Berlin).
- Skullerud, H. R., Eide, T., and Stefansson, T. (1986). *J. Phys. D* **19**, 197.

- Standish, R. (1987). *Aust. J. Phys.* **40**, 519.
- Standish, R. K. (1989). *Aust. J. Phys.* **42**, 223.
- Standish, R. K. and Evans, D. J. (1990). On the Nonlinear Burnett Coefficients *Phys. Rev. A* (in press).
- Standish, R. K. and Kumar, K. (1987). End Effects in Time of Flight Swarm Experiments *Proc 5th Int. Swarm Seminar* (in press).
- Tagashira, H. (1981). In 'Proc 15th International Conference on Phenomena in Ionized Gases' p. 377. ).
- Tagashira, H., Sakai, Y., and Sakamoto, S. (1977). *J. Phys. D* **10**, 1051.
- Takata, N. (1975). *J. Phys. B* **8**, 2390–2392.
- Temple, G. I. (1960). 'Cartesian Tensors'. (Methuen: London).
- Thomas, W. R. (1969). *J. Phys. B* **2**, 551.
- Titulaer, U. M. (1983). *J. Chem. Phys.* **78**, 1004.
- Tolman, R. C. (1962). 'The Principles of Statistical Mechanics'. (Dover: New York).
- Viehland, L. A. (1982). *Chem. Phys.* **70**, 149.
- Viehland, L. A. (1983). *Chem. Phys.* **78**, 279.
- Wagner, E. B., Davis, F. J., and Hurst, G. S. (1967). *J. Chem. Phys.* **47**, 3138.
- Waldman, M. and Mason, E. A. (1981). *Chem. Phys. Lett.* **83**, 369–371.
- Whealton, J. H. (1974). *J. Phys. B* **7**, 1602.
- Wolfram, S., Kong, M., and Grief, J. (1983). 'SMP: a Symbolic Manipulation Program'. (Inference: Mass.).
- Yamada, T. and Kawasaki, K. (1967). *Prog. Theo. Phys.* **38**, 1030.
- Yan, C. C. and Wannier, G. H. (1968). *Bull. Am. Phys. Soc.* **13**, 899.

Zwanzig, R. (1965). *Ann. Rev. Phys. Chem.* **16**, 67.

# Mathematical Notation

This section presents mathematical notation that is widespread throughout the thesis. Symbols that are used only in specific locations will be defined at that point.

## Conventions

### Vectors and Tensors

Vector quantities are written in bold typeface, e.g.  $\mathbf{x}$ , and tensors are written in a bold sans serif typeface, e.g.  $\mathbf{x}$ . Unit vectors are indicated by a caret placed over the symbol, e.g.  $\hat{\mathbf{a}}$  is the unit vector parallel to  $\mathbf{a}$ . This convention is extended in the usual fashion so that  $\hat{x}$  is the unit vector in the direction of the coordinate  $x$ . When two vectors or tensors are written sequentially, as in  $\mathbf{xy}$ , it is implied that the tensor or outer product is to be taken. This convention is extended so that  $\mathbf{x}^k$  means that  $\mathbf{x}$  is to be raised to the  $k$ th power with respect to the tensor product. To indicate the square of the length of a vector, the symbol is written in a plain type style, i.e.  $x^2$  is a rank two tensor (or dyad), whereas  $x^2$  is the square of the length of  $\mathbf{x}$ . Moments of functions are written with a superscript in parentheses, e.g.  $\mathbf{f}^{(l)} = \int \mathbf{r}^l f(\mathbf{r}) d\mathbf{r}$ . These are  $l$ th rank tensor quantities that may also be considered as the Taylor coefficients of the Fourier transform,  $\mathbf{f}^{(l)} = \Omega^{(l)} \tilde{f}(\mathbf{k})$ .

### Differentiation and Integration

The derivative operator will usually be written as  $\partial_x$  irrespective of whether  $x$  is a vector or scalar. If  $x$  is a vector, then the whole symbol is written as bold, e.g.  $\partial_{\mathbf{x}}$ . Exceptions occur to this convention when the derivative is with

respect to  $\mathbf{r}$  (position), in which case the symbol  $\nabla$  is often used, and when the derivative is with respect to time, when Newton's convention of placing a dot over the symbol is often used. With integrals, a volume integral will be written as  $\int f(\mathbf{r})d\mathbf{r}$ . This is sometimes written as  $\int f(\mathbf{r})d^3\mathbf{r}$  by other authors.

## Other Conventions

The Fourier transform of a function will be represented by a tilde placed over the function. The precise definition adopted here is:

$$\tilde{f}(\mathbf{k}) = \int \exp(i\mathbf{k} \cdot \mathbf{r})f(\mathbf{r})d\mathbf{r}$$

where the integration is over the whole of space ( $\mathbb{R}^3$ ). The tilde is also used to denote the adjoint of an operator.

## List of Symbols

$\cdot$	inner product	$\eta$	shear viscosity
$:$	double inner product (contraction over 2 indices)	$\eta_V$	bulk viscosity
$::$	quadruple inner product (contraction over 4 indices)	$\Theta(x)$	Heaviside step function ( $\Theta(x < 1) = 0, \Theta(x > 1) = 1$ )
$\odot$	$n$ -fold inner product (contraction over $n$ indices)	$\Lambda$	phase space compression factor
$\nabla$	derivative with respect to position	$\mu$	mobility
$\langle \dots \rangle$	phase average	$\nu$	reaction rate
$[x]$	greatest integer less than or equal to $x$ .	$\nu_c$	collision frequency
$\mathbf{1}$	unit tensor, second rank tensor with the Kronecker delta for components ( $1_{ij} = \delta_{ij}$ )	$\nu(c)$	velocity dependent collision frequency
$\alpha_T$	first Townsend ionization coefficient	$\xi_{2i,j}$	cylindrically symmetric components of $\Omega^{(2i+j)} \ln(1 + x(\mathbf{k}, 0))$
$\beta$	$1/k_B T$	$\Pi$	viscous pressure tensor
$\gamma$	strain rate in Planar Couette systems	$\rho$	mass density
$\Gamma$	$6N$ -dimensional phase space vector	$\rho_{\perp}, \rho_z$	see page 28
$\delta(x)$	Dirac delta function	$\sigma$	width parameter of a Gaussian source
$\delta = (v_{\text{dr}}^2/4D_L - \nu)^{\frac{1}{2}}$		$\tau$	non-hydrodynamic relaxation time $= \{\min_j \text{Re}(\omega_0(0) - \omega_j(0))\}^{-1}$
$\Delta J = J - J_0$		$\Phi$	potential energy
		$\Phi_j(\mathbf{c}, \mathbf{k})$	eigenfunctions of $i\mathbf{c} \cdot \mathbf{k} + \tilde{\mathcal{M}}$
		$\Psi_j(\mathbf{c}, \mathbf{k})$	eigenfunctions of $i\mathbf{c} \cdot \mathbf{k} + \mathcal{M}$
		$\omega^{(l)}$	$l$ th order transport coefficient (swarms)
		$\omega^{(0)}$	reaction rate

$\omega^{(1)}$ drift velocity	$\dot{H}^{\text{ad}}$ adiabatic rate of change of internal energy
$\omega^{(2)}$ diffusion coefficient	$H_j(x)$ $j$ th order Hermite polynomial
$[\omega^{(2)}]^{-1}$ inverse of $\omega^{(2)}$ considered as a matrix, $= D_L^{-1} \hat{\mathbf{z}}\hat{\mathbf{z}} + D_T^{-1}(\hat{\mathbf{x}}\hat{\mathbf{x}} + \hat{\mathbf{y}}\hat{\mathbf{y}})$ .	$J$ thermodynamic flux
$\omega_j(\mathbf{k})$ $j$ th eigenvalue of $i\mathbf{c} \cdot \mathbf{k} + \mathcal{M}$	$J_0 = \langle J \rangle$
$\omega_{2i,j}$ components of $\omega^{(2i+j)}$ satisfying cylindrical symmetry	$\mathcal{J}$ collision operator
$\Omega^{(l)} = \lim_{k \rightarrow 0} \frac{(i\partial_{\mathbf{k}})^l}{l!}$	$\mathbf{k}$ coordinate of Fourier transform
$\mathbf{a}$ acceleration of swarm particle due to field	$k_B$ Boltzmann's constant
$\mathcal{B}$ boundary, or field inhomogeneity operator	$K$ kinetic energy
$\mathbf{c}$ velocity (as in mesoscopic picture)	$L$ p-Liouvillean
$\det(\omega^{(2)})$ determinant of $\omega^{(2)}$ considered as a matrix $= D_T^2 D_L$	$\mathcal{L}$ f-Liouvillean
$D_L$ longitudinal diffusion	$\mathcal{M} = \mathbf{a} \cdot \partial_{\mathbf{c}} + \mathcal{J}$
$D_T$ transverse diffusion	$N$ average number density (swarms), number of particles (statistical mechanics)
$\text{erfc}(x)$ complementary error function	$n(\mathbf{r}, t)$ number density
$E$ electric field	$\mathbf{p}_i$ momentum of the $i$ th particle
$F_e$ external thermodynamic force	$\mathbf{P}$ pressure tensor
$G$ Greens function	$\mathbf{q}_i$ co-ordinate of the $i$ th particle
$H$ internal energy of the system $= K(\mathbf{\Gamma}) + \Phi(\mathbf{\Gamma})$	$q_n^r$ the $r$ th root of $\omega_n(k)$
	$Q_n$ saddle point of $\omega_n(k)$
	$\mathbf{r}$ position
	$\text{Res}(f(z), z_0)$ residue of $f$ at $z_0$

$S$  source function

$t$  time

$t_m$  time at which the swarm peak arrives at the collector

$T$  temperature

$\mathbf{u}$  streaming velocity

$v_{\text{dr}}$  drift velocity

$x(\mathbf{k}, t)$  non-hydrodynamic part of the density



# Index

- adiabatic incomp. of phase space,
  - 71, 81
- adjoint, 98
- AIF, 81, 71
- arrival time spectrum, 28
- asymptotic, 61, 63, 64
  
- Bessel functions, 45
- biorthonormality, 96
- Boltzmann equation, 7, 9, 10, 13,
  - 46, 59
  - linear, 8, 14
- Boltzmann operator,
  - inhomogeneous, 63
- boundary, 13, 40
- Bradbury-Nielson method, 27
- Brownian motion, 22
- Burnett, 7
  - coefficients,
    - non-linear, 7, 10, 78, 128
  - functions, 24
  - hydrodynamics, 8, 11
  - Super-, hydrodynamics, 8, 11
  
- canonical ensemble, 84, 128
- Cauchy's residue theorem, 61
- Chapman-Enskog, 7, 10, 12, 94
- collision frequency, 13, 23, 33
  - velocity dependent, 21
- collision operator, 9, 20, 38, 94
  - linearized, 12
- colour conductivity, 77, 86
- computer algebra, 102
- constitutive relation, 79
  - Newtonian, 5, 7
- contact potentials, 40
- continuity equation, 3, 35
- cross section, 1, 21, 23, 33
- current-statting, 131
- cylindrical symmetry, 6, 34
  
- derived thermodynamic quantities,
  - 67
- determinant, 115
- diffusion, 38, 44
  - coefficient, 6, 14
  - equation, 6, 14, 30, 45, 58
  - higher-order, 40
  - lateral, 43
  - transverse, 29
- dissipative flux, 72
- $\Delta J$ -ensemble, 84
- drift velocity, 6, 14, 21, 32, 36
- Dyson equation, 41, 71, 85
  
- eigenfunction, 17, 23, 63, 94
- eigenvalue, 18, 38, 63, 94
- eigenvector, 38
- end-effect, 30, 39, 40
- end-effects, 102

equations of motion, 131  
 Euler,  
     hydrodynamics, 11  
  
 field inhomogeneity, 13, 40  
 field interpenetration, 40  
 flux-statted, 80, 84  
     Liouvillean, 85  
     propagator, 81, 85  
 Fokker-Planck equation, 22  
 free space solution, 34, 41  
  
 Gaussian thermostat, 67, 70, 72,  
     75, 128  
 Gear integrator, 134  
 Green-Kubo, 10, 65, 78, 85  
 Greens function, 23, 41, 47, 95, 111  
  
 Hamilton's equations, 65  
 hard sphere potential, 20  
 harmonic oscillator, 23  
 Heisenberg picture, 70  
 helium, 29, 33  
 Hermite polynomials, 24, 30, 36, 37  
 hydrodynamic, 8, 10, 18, 20  
     regime, 11  
  
 intensive, 126  
 isokinetic distribution, 67  
 isotropic tensors, 115  
  
 Kawasaki, 81  
     distribution function, 72  
 Klein-Kramers, 106  
     equation, 22, 41  
     model, 32, 46, 60, 61  
 Kramers-Moyal expansion, 22  
  
 Lees-Edwards boundary conditions,  
     74, 76, 137  
 Lennard-Jones, 86  
 Lennard-Jones force, 77  
 Levi-Cevita, 115  
 Liouville's,  
     equation, 9, 68  
     theorem, 69, 71  
 Liouvillean,  
     f-, 68  
     p-, 68  
 lithium, 29, 33  
 long time tails, 78  
  
 macroscopic, 8  
 Maxwell molecules, 20  
 Maxwellian,  
     local, 11  
 mesoscopic, 8  
 mesoscopic, 10  
 method of steepest descent, 60  
 microscopic, 8  
 mobility, 6, 29, 40  
 mode-coupling theories, 78  
 molecular dynamics simulation, 84  
 Monte Carlo, 84  
 Morriss's lemma, 71  
 multipole, 95  
  
 Navier-Stokes,  
     equation, 5  
     hydrodynamics, 7, 11  
     transport, 74  
 Newton's laws of motion, 9  
 non-hydrodynamic, 15, 18, 25, 37,  
     40, 44, 51, 63  
 nonhydrodynamic effects, 94

Norton ensemble, 79  
 Nosé-Hoover, 80  
 Nosé-Hoover thermostat, 67, 70, 75, 128  
  
 parallel plane, 43  
 peculiar, 66  
 peculiar momenta, 71  
 peculiar velocities, 75  
 perturbation, 94  
 phase average, 126  
 phase averages, 69  
 phase space, 65  
 phase space compressibility, 71  
 planar couette flow, 74, 83  
 planar Couette flow, 87  
 pressure dependence, 38  
 pressure tensor, 3  
     viscous, 4, 7  
 procedure integration, 134  
 projection, 96  
 propagator, 67, 69, 85  
     constant current, 79  
 Pulsed Townsend, 45  
  
 Rayleigh gas, 22  
 reaction rate, 14, 22  
 Rodrigues' formula, 36  
 runaway, 13, 21  
 Runge-Kutta, 128  
  
 saddle point, 60, 63  
 Schrödinger picture, 70, 72  
 shear modulus,  
     infinite frequency, 83  
 SLLOD equations, 75  
 SMP, 102  
 spectrum, 13, 16, 18, 20, 23, 63, 98  
  
 Steady State Townsend, 45  
 strain rate, 4, 78, 83  
 stress, 78, 80, 83  
 swarm, 1, 8  
  
 Taylor series, 100  
 thermal flux, 7  
 time of flight, 27, 44  
 Townsend,  
     first ionization coefficient, 44, 47  
 Townsend-Huxley method, 44  
 transient time correlation function, 66, 73, 79, 81  
 transport,  
     coefficients, 6, 7, 21, 30, 35, 38, 43  
     higher order, 8  
     higher order, 38  
     linear, 78, 85  
     time dependent, 15, 16  
     equation, 15, 30  
     time dependent, 35  
 TTCF, 66, 79, 81  
 Tyndell-Powell method, 27  
  
 viscosity, 83  
     bulk, 5  
     shear, 5  
     vortex, 5